IRRIGATION RETURN FLOW MODELING AT SAN ACACIA, NEW MEXICO

by

Mark J. Simonett

Submitted in Partial Fulfillment
of the Requirements for the Degree of
Master of Science in Hydrology

New Mexico Institute of Mining and Technology

Socorro, New Mexico

May 1981

ABSTRACT

Two modeling approaches were used to determine the nature of important hydrologic parameters influencing the return flow quality from an irrigated farm in San Acacia, New Mexico. The first approach employed multiple celled lumped parameter models, and the second consisted of a steady-state finite element flow model coupled with the U. S. Bureau of Reclamation chemistry model.

Steady-state and transient lumped parameter model simulations of drain chloride concentrations indicated a transient regional flow of poor quality enters the study area at a rate similar to the average irrigation recharge rate during the period of 1978 through 1980. A steady-state finite element flow model was then used to construct a flow net for a vertical section of the layered aquifer receiving equal regional and irrigation recharge. The aquifer was divided into separate regional and irrigation flow systems as defined by the flow net, and the Bureau of Reclamation chemistry model was used to simulate outflow concentrations from the irrigation system. Drain concentrations were simulated by mixing the predicted irrigation system outflow concentrations with regional inflow concentrations which were assumed equal to those observed in three deep wells at the farm. Steady-state simulation results obtained by excluding soil-water chemical reactions indicate the observed deep well concentrations are representative of the regional inflow. Due to the transient interaction of the regional and irrigation flow systems, it was determined that this modeling approach could not be used to assess the importance of possible chemical reactions occurring at the farm.

TABLE OF CONTENTS

	Page
ABSTRACT	ii
LIST OF FIGURES	v
LIST OF TABLES	vii
ACKNOWLEDGEMENTS	viii
1. INTRODUCTION	
1.1.1 Objective	1
1.1.2 Study Location and General Information	1
2. GENERAL HYDROGEOLOGIC INFORMATION	
2.1.1 Shallow Lithology	4
2.1.2 Effective Porosity and Hydraulic Conductivity	7
2.1.3 Regional Flow	12
3. MULTICELLED LUMPED PARAMETER MODELS	
3.1 INTRODUCTION	15
3.2 STEADY-STATE MODELS	17
3.2.1 The Two Cell Model	17
3.2.2 The Three Cell Model	22
3.2.3 The Two Cell Model with Separating Aquitard	25
3.2.4 Applications and Conclusions	30
3.3 THE TRANSIENT TWO CELL LUMPED PARAMETER MODEL	36
3.3.1 Model Development	36
3.3.2 Model Application	41
Parameter Assignment	41
Finite Difference Representation and Programming Algorith	48
Simulation	54
3.3.3 Discussion	59
4. THE COUPLED U.S. BUREAU OF RECLAMATION CHEMISTRY - FINITE ELEMENT FLOW MODEL	
4.1 INTRODUCTION	62
4.2 THE FLOW MODEL	64
4.2.1 Flow Model Development	64
4.2.2 Flow Model Application	70

Page

4.3 COUPLED MODEL APPLICATION 75
4.3.1 Steady-State Simulation 75
4.3.2 Transient Simulation 84

4.4 DISCUSSION 100

5. SUMMARY AND CONCLUSIONS 103

APPENDIX 105

REFERENCES 111

LIST OF FIGURES

Figure		Page
1.1.1	Farm layout.	2
3.2.1	(a) Two cell aquifer representation, and (b) Idealized two layered Dupuit aquifer	18
3.2.2	(a) Three cell aquifer representation, and (b) Idealized three layered Dupuit aquifer	23
3.2.3	Aquifer representation for two cell model with separating aquitard	26
3.3.1	(a) Transient two cell aquifer representation, and (b) Two layered Dupuit aquifer	37
3.3.2	Thiessen polygons and aquifer area	43
3.3.3	Observed and tailwater adjusted drain concentrations	50
3.3.4	Simulated and tailwater adjusted drain concentrations . . .	56
3.3.5	Simulated and observed mass outflow rates without tailwater effects	58
4.2.1	(a) Vertical section of middle drain aquifer, and (b) Representation of a typical element	65
4.2.2	Simulated steady-state flow net	74
4.3.1	Simulated drain calcium and sodium concentrations for soil analysis and deep well concentration initial conditions; observed drain concentrations; and, irrigation water concentrations	79
4.3.2	Simulated drain sulfate and bicarbonate concentrations for soil analysis and deep well concentration initial conditions; observed drain concentrations; and, irrigation water concentrations	80
4.3.3	Simulated drain chloride and TDS concentrations for soil analysis and deep well concentration initial conditions; observed drain concentrations; and, irrigation water concentrations	81
4.3.4	Simulated drain calcium and sodium concentrations with and without chemical reactions; observed drain concentrations; and, irrigation water concentrations	82
4.3.5	Simulated drain bicarbonate and TDS concentrations with and without chemical reactions; observed drain concentrations; and, irrigation water concentrations	83

Figure		Page
4.3.6	Simulated drain calcium and sodium concentrations with and without chemical reactions	88
4.3.7	Simulated drain bicarbonate and TDS concentrations with and without chemical reactions	89
4.3.8	Simulated and observed drain calcium and sodium concentrations	91
4.3.9	Simulated and observed drain sulfate and bicarbonate concentrations	92
4.3.10	Simulated and observed drain chloride and TDS concentrations	93
4.3.11	Simulated and observed mass output of calcium and sodium . .	94
4.3.12	Simulated and observed mass output of sulfate and bicarbonate	95
4.3.13	Simulated and observed mass output of chloride and TDS . . .	96
4.3.14	Observed and simulated chloride concentration and mass output histories with lateral winter month regional inflow	98
4.3.15	Observed and simulated TDS concentration and mass output histories with lateral winter month regional inflow . .	99
A1	Effective porosity test apparatus	107
A2	Conductivity breakthrough curve for sample 3	110

LIST OF TABLES

Table		Page
2.2.1	Borehole logs	5
2.1.2	Grain size analyses from borehole 1	8
2.1.3	Effective porosities used in groundwater contaminant modeling studies	10
2.1.4	Effective and total porosities, bulk densities and hydraulic conductivities of San Acacia samples	11
2.1.5	Observed winter middle drain discharges	13
2.1.6	Average irrigation water, middle drain, and deep well concentrations	14
3.2.1	Steady-state two cell model applications	32
3.2.2	Steady-state three cell model applications	33
3.2.3	Applications of the steady-state two cell model with separating aquitard	34
3.3.1	Polygon areas and percentage area	44
3.3.2	Applied water and chloride concentration, drain outflow rate and chloride concentration, and upper layer saturated thickness for each four week period	46
3.3.3	Irrigation recharge and chloride concentration, tailwater adjusted drain flow and chloride concentration, and tailwater coefficients for each four week period	49
3.3.4	Simulated regional and interlayer flow rates, layer chloride concentrations, and drain chloride concentrations	57
4.2.1	Irrigation stream tube travel times and pore volumes	73
4.3.1	Steady-state coupled model input data	76
4.3.2	Transient coupled model input data	85
4.3.3	Specific surface application data	87
A1	Effective porosity test data for sample 3	109

ACKNOWLEDGEMENTS

Financial support for this study was provided by the U. S. Environmental Protection Agency.

The study site is located on the farm of Gordon Herkenhoff, Jr. whose cooperation is appreciated. Much of the data used in this investigation was collected by Warren Strong, Albert Bustamante and Mallery Austin, and was coordinated and interpreted by Chris Duffy and Ken Rehfeldt. Dr. Marvin J. Shaffer with the University of Minnesota (formerly with the U. S. Bureau of Reclamation in Denver) provided helpful suggestions regarding the implementation of the Bureau of Reclamation model. Frequent assistance with the application of this model was received from Tian-Chyi Yeh. Finally, the advise and guidance provided by Dr. Lynn W. Gelhar throughout the course of this study is most gratefully acknowledged.

1. INTRODUCTION

1.1.1 Objective

The objective of this study is the identification and determination of important hydrologic parameters influencing the return flow quality of an irrigated farm in San Acacia, New Mexico. Two different approaches to modeling irrigation return flow are used for this purpose. The first is a multiple celled lumped parameter model based on linear reservoir theory. The second is a modified version of the U. S. Bureau of Reclamation return flow profile model. A comparison of the modeling approaches will be made, and the feasibility of applying each model to the San Acacia site will be evaluated.

1.1.2 Study Location and General Information

The study site is located on a 250 acre farm in San Acacia, New Mexico owned by Mr. Gordon Herkenhoff. Figure 1.1.1 shows the layout of the farm which is bordered on the west by Interstate 25 and on the east by the Rio Grande Main Conveyance Channel. The area to the north of the farm increases in elevation and is noncultivated semi-desert rangeland. To the south the farm is bordered by noncultivated bosque largely covered with saltcedar. Irrigation water is delivered to the farm from a large irrigation canal running parallel to the main conveyance channel. The drainage system consists of a main drain largely encompassing the farm and an east-west trending middle drain which discharges into the main drain.

The farm has been intensely monitored and studied since early in 1977 (Wierenga et al., 1979; Gelhar et al., 1980). A network of observation wells was installed to monitor water table elevations and groundwater quality on a weekly sampling basis. The irrigation water and effluent of both drains were also sampled on a weekly basis. All samples were

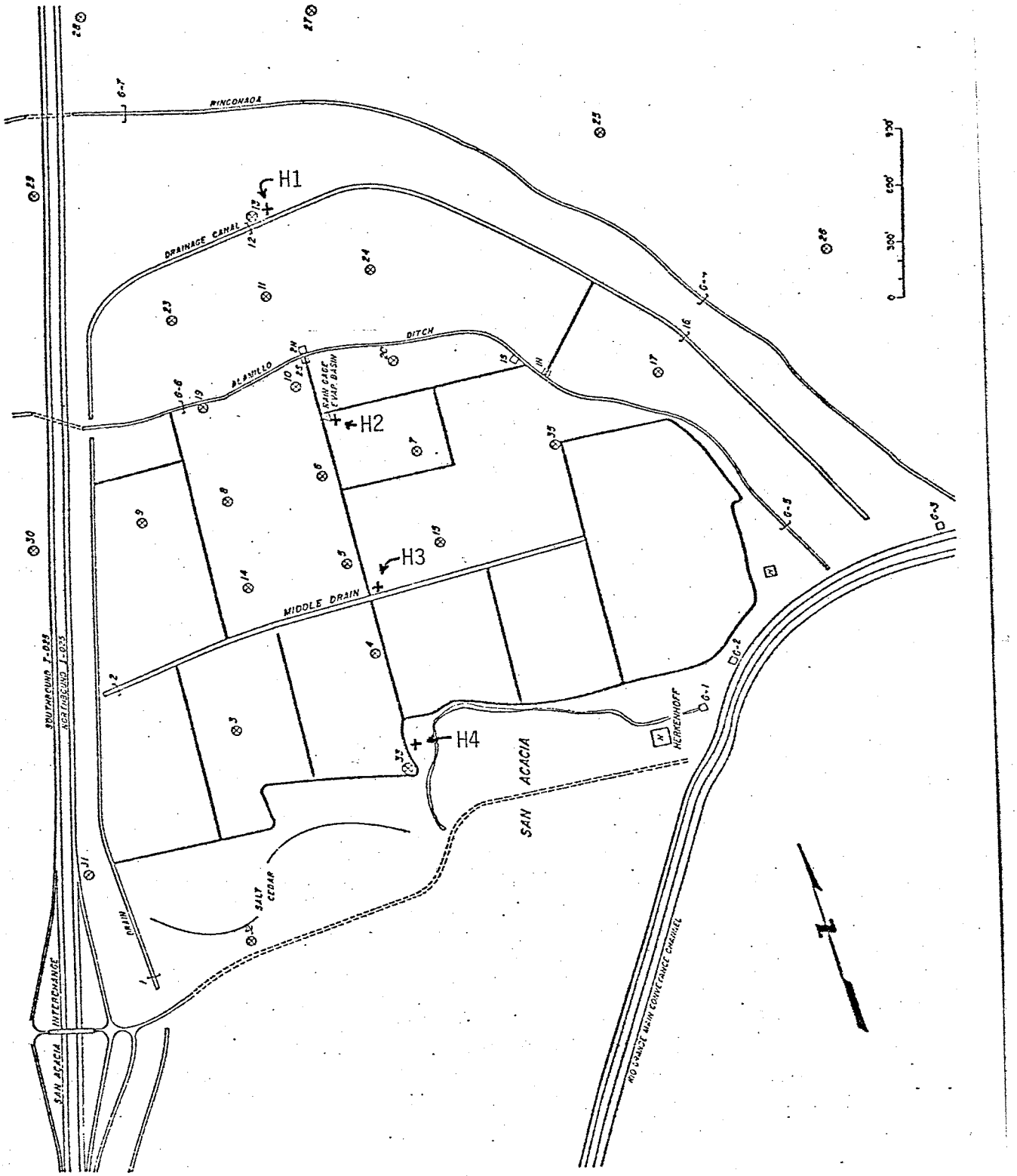

Figure 1.1.1: Farm Layout

analyzed for electrical conductivity, pH, and chloride concentration. Once each month, samples were also analyzed for dissolved anions and cations (Ca, Mg, Na, K, Cl, HCO_3, CO_3, and SO_4) and nutrients (NO_3-N, NH_4-N, Total P, and ortho-P). Continuous stage recorders were installed to measure irrigation diversion volumes and discharges of both drains. A rain gage and class A evaporation pan were placed in the center of the farm to obtain precipitation and evaporation data.

The focus of this study is on the middle drain flow system. This system was chosen based on the following considerations:

(1) It is representative of the major portion of the farm;

(2) It is the area most intensely monitored; and,

(3) It represents a symmetric flow system.

2. GENERAL HYDROGEOLOGIC INFORMATION

2.1.1 Shallow Lithology

Four boreholes have been drilled in a north-south transect of the middle drain. The locations of the boreholes (labelled H1, H2, H3 and H4) are shown in Figure 1.1.1. All boreholes were drilled using four inch diameter flight auger with the exception of borehole 2 which was rotary drilled. The augered holes were logged by taking samples off the auger in one foot intervals as the drill stem was retrieved. Table 2.1.1 provides a coarse description of the subsurface lithology based on the borehole logs.

The logs of boreholes 2, 3 and 4 display the general layering structure present in the middle drain area. The reddish clay present at approximately 68 feet below the surface in holes 2 and 3 marks the division between Tertiary and Quaternary sediments. This clay is believed to underlie the entire middle drain area since reddish clay material also appears in the southern borehole (H4) at the same depth as in boreholes 2 and 3. The shallow grayish clay occupying the 25 to 35 feet depth interval in borehole 2 may also be continuous in the middle drain area since similar material is noted in boreholes 3 and 4. Between these two clays are layers composed of various mixtures of medium to coarse sand, gravel and pebbles. The deposits above the shallow clay consist predominantly of sand.

The layering structure observed in the northern most borehole (H1) does not match that of the middle drain area. The gray clay appears over the intervals of 20-27 and 40-44 feet and the deeper red clay lies about 88 feet below the surface. This site is of interest, however, since

Table 2.1.1: Borehole Logs

Depth (ft)	Material
Borehole 1 (H1)	
0 - 1	soil
1 - 20	medium to very coarse sand, pebbles
20 - 27	gray clay
27 - 40	medium sand
40 - 44	gray clay
44 - 88	sand, gravel
88 - 90	red clay
90 - 95	sand, gravel
Borehole 2 (H2)	
0 - 5	soil
5 - 23	fine sand, minor gravel
23 - 35	gray-brown clay
35 - 52	medium sand, gravel
52 - 68	gravel, cobbles, sand
68 - 100	red clay mixed with some sand and gravel (Sierra Ladrones formation)
Borehole 3 (H3)	
0 - 4	soil
4 - 18	sand
18 - 25	sand, minor gravel
25 - 35	sand, minor clay lenses, sandy clay
35 - 43	sand, pebbles, some gravel

Depth (ft)	Material
Borehole 3 (cont.)	
43 - 67	sand, gravel, conglomeritic material
67 - 72	reddish brown clay, minor sand (Sierra Ladrones formation)
Borehole 4 (H4)	
0 - 10	fine to medium sand
10 - 26	medium to coarse sand, minor pebbles
26 - 30	gray silt-clay mud and sandy mud
30 - 68	fine to very coarse sand, pebbles
68 - 70	reddish brown mud and sandy mud mixed with sand and pebbles
70 - 90	fine to very coarse sand, pebbles

grain size analyses have been performed on some of the borehole samples. The representative grain sizes d_{10} and d_{50} obtained from these analyses are listed in Table 2.1.2.

2.1.2 Effective Porosity and Hydraulic Conductivity

Effective porosity is defined here as the portion of total porosity which contributes to groundwater flow. Total porosity is defined as the ratio of volume of the void space to the bulk volume of a macroscopic porous medium (Bear, 1972, p. 43). Effective porosity is less than total porosity due to the adhesion and cohesion of water to the matrix surface and the possible presence of noninterconnected and dead-end pores. Mathematically effective porosity is expressed as

$$n_e = \frac{q}{v}$$

where q is the specific discharge or Darcian velocity and v is the mean pore velocity of flowing groundwater.

Specific yield and effective porosity are often assumed synonymous in definition and equal in value. As defined by Meinzer (1923) specific yield is the ratio of (1) the volume of water which, after being saturated, a rock or soil will yield by gravity to (2) its own volume. Specific yield is a measure of the gravity drainage ability of a material and therefore should not be considered equivalent to effective porosity as defined here.

Effective porosity is a very important parameter in groundwater contamination studies as it directly influences the rate of contaminant movement through an aquifer and the contaminant response time or buffering ability of the aquifer. In order to obtain an estimate of effective porosity for the San Acacia farm alluvium, a literature survey of

Table 2.1.2: Grain Size Analyses from Borehole 1

Depth (ft)	d_{10} (mm)	d_{50} (mm)
3	.110	.327
4	.160	.406
5	.155	.374
6	.185	.452
7	.160	.628
8	.250	.461
9	.250	.483
10	.165	.482
11	.195	.585
12	.210	.693
13	.225	.872
14	.185	.467
15	.165	.368
16	.175	.383
17	.190	.494
18	.160	.512
19	.155	.349
20	.145	.452
51	.135	.330
52	.130	.343
53	.145	.382
55	.150	.358
57	.175	.507
58	.175	.360
59	.165	.351
60	.165	.369
62	.155	.365
63	.160	.355
64	.155	.347
65	.160	.386
67	.165	.415
68	.170	.439
69	.083	.376
70	.140	.372
71	.115	.349
72	.110	.313
73	.120	.317
75	.155	.353
77	.165	.418
78	.155	.406

contaminant transport studies in similar materials was conducted. The literature search produced a broad range of effective porosity values as summarized in Table 2.1.3. In the studies by Pinder (1973) and Robson (1978) the effective porosity was assumed equal to measured values of total porosity. These measured values (.35 and .40) are noticeably greater than the effective porosities assumed in the remaining studies.

Finding no conclusive results from the literature survey, direct measurements of effective porosity were performed on samples from the farm. Undisturbed sleeved samples from depths of 4 to 5 feet were taken at 25 feet intervals north of the middle drain in the same transect as the boreholes (Figure 1.1.1). The sleeves are 5 cm in diameter and 5.1 cm in length thus containing a sample volume of 100 cc. A 10 ml volume of tracer solution containing dissociated NaCl was displaced through each sample while the electrical conductivity of the effluent was measured in 2 ml increments (a detailed description of the tests is presented in the Appendix). The resulting conductivity breakthrough curves displayed Gaussian behavior with good agreement between the mode and expected pore volumes. The measured effective porosities, total porosities, and dry bulk densities of eight of the samples are listed in Table 2.1.4. A solid density of 2.65 g/cc was used in the total porosity computations. The average effective porosity of the samples, which consisted mostly of sand, is 0.38.

The hydraulic conductivities of fourteen of the sleeved samples (including those used for effective porosity determinations) were measured using an Eijkelkamp constant head permeameter. The values ranged from 3 to 346 ft/day (see Table 2.1.4) with the sample mean and standard deviation both equalling about 80 ft/day.

Table 2.1.3: Effective Porosities Used in Groundwater Contaminant Modeling

Material	Location	Effective Porosity	Reference
Alluvial gravel, sand, silt and clay	Southeastern Colorado	.20, .15	Konikow and Bredehoeft (1974)
Alluvial sands and gravels with some clay lenses	Lyons, France	.20	Fried (1975)
Alluvium - medium to fine sand with some clay and silt	Mobile, Alabama	.25	Papadopulos and Larson (1978)
Alluvium	Rocky Mountain Arsenal near Denver, Co.	.30	Konikow (1977)
Glacial outwash - fine to coarse sand, gravel and some silt	Long Island, New York	.35	Pinder (1973)
Alluvium	Barstow, Ca.	.40	Robson (1978)

Table 2.1.4: Effective and Total Porosities, Bulk Densities, and Hydraulic Conductivities of San Acacia Samples

Sample No.	Effective Porosity	Total Porosity	Bulk Density (g/cc)	Hydraulic Conductivity (ft/day)
1		.39	1.62	98
2	.38	.43	1.51	47
3	.39	.47	1.40	67
4		.36	1.70	3
5	.38	.41	1.57	346
6	.37	.40	1.59	44
7	.37	.39	1.61	58
8	.37	.40	1.60	88
9	.38	.41	1.56	127
10	.37	.39	1.61	69
11				40
12				37
13				25
14				91

Using time series analysis of the water level, drain flow and irrigation recharge occurring in the middle drain flow system, a transmissivity of 2120 ft^2/day was determined by Duffy (in Gelhar et al., 1980, pp. 142-159). This translates to a hydraulic conductivity of roughly 100 ft/day if the shallow clay is taken as the base of the irrigated flow system or about 30 ft/day if the deeper clay is the base. These values are in fair agreement with the average hydraulic conductivity of the small samples.

2.1.3 Regional Flow

A regional flow of poor quality water is believed to enter the farm from the north. The Rio Salado, situated about two miles north of the farm at a higher elevation, may be the source of this inflow. Perennial saline springs discharge into the Salado at an estimated 500 gallons per minute (Spiegel, 1957).

Observed water levels in observation wells and middle drain discharges support the proposition of a regional inflow. Yearly average water table elevations obtained from the shallow observation well data indicate a southward groundwater movement through the farm. The occurrence of drain flow during periods of insignificant surficial recharge also implies an external source of water is present. The ranges of middle drain discharge observed during winter months are listed in Table 2.1.5. The low winter drain flow of the 1977-1978 winter might be attributed to the dry conditions prevalent in the Rio Grande Valley during the summer and fall of 1977.

Table 2.1.5: Observed Winter Middle Drain Discharges

Winter	Drain Discharge Range (cfs)
1977-1978	.02 - .06
1978-1979	.09 - .31
1979-1980	.10 - .20
1980-1981	.22 - .31

The poor quality nature of the regional inflow is inferred from comparison of the average irrigation water, deep well and middle drain concentrations observed since the commencement of monitoring in 1977. These concentrations are listed in Table 2.1.6. A nest of three deep wells at sampling depths of roughly 50, 65 and 100 feet are located at the site of borehole 2. A fourth deep well was emplaced in borehole 3 near the middle drain and samples a depth of about 55 feet. The high concentrations observed in the three wells at depths of 50 to 65 feet are very similar and remain fairly constant. The average total dissolved solids observed in these three wells is about 2600 ppm. Groundwater below this zone is of better quality as indicated by an average total dissolved solids of 1200 ppm in the 100 foot well. The shallow groundwater would be expected to possess roughly twice the irrigation water concentrations assuming an irrigation efficiency of 50 percent. Observed drain concentrations are much greater than expected shallow groundwater concentrations and are only exceeded by the high groundwater concentrations of the 50 to 65 foot zone. Therefore, it is a necessary conclusion that high concentration groundwater from this zone comprises part of the drain discharge. Further support of the assumption that this high concentration drain flow component is due to regional inflow is presented in the following section.

Table 2.1.6: Average Irrigation Water, Middle Drain, and Deep Well Concentrations

Constituent	Irrigation Water Concentration		Drain Concentration		Deep Well Concentrations			
					50 - 65 ft.		100 ft.	
	meq/l	ppm	meq/l	ppm	meq/l	ppm	meq/l	ppm
Cl	1.5	52	9.7	345	21.6	767	10.7	381
SO_4	3.1	149	12.5	602	16.2	776	4.9	235
Ca	3.1	62	9.3	187	11.3	226	3.6	72
Na	3.6	82	14.8	341	24.2	558	13.6	313
Mg	1.0	12	4.1	50	5.0	60	2.4	29
HCO_3	3.0	186	5.1	309	3.4	205	3.0	184
TDS		543		1834		2592		1214

3. MULTICELLED LUMPED PARAMETER MODELS

3.1 INTRODUCTION

The models presented in this section are generalizations of the lumped parameter water quality model presented by Gelhar and Wilson (1974). This model is especially applicable to distributed contaminant source situations such as an irrigated system. The conceptual base of the model is a well mixed linear reservoir in which temporal variations of the mean contaminant concentration may be determined knowing the nature of the inputs. Emphasis is thus placed on aquifer-wide changes in groundwater quality rather than spatial variations.

According to Gelhar and Wilson (1974) a representation of the groundwater flow in an irrigated unconfined aquifer can be stated in terms of a water balance in the form

$$S_y \frac{dh}{dt} = \varepsilon_I + q_r - q_d$$

$$\text{or} \qquad n \frac{dh}{dt} = \left(n - S_y\right) \frac{dh}{dt} + \varepsilon_I + q_r - q_d \qquad (3.1.1)$$

where h = average saturated aquifer thickness;

n = average effective porosity;

S_y = specific yield;

ε_I = irrigation recharge rate;

q_r = regional inflow per unit area;

q_d = aquifer outflow (drain flow) per unit area; and,

t = time.

Similarly, an aquifer mass balance for a contaminant of average solute concentration $C(t)$ can be expressed as

$$n \frac{d}{dt}(hC) = \varepsilon_I C_I + q_r C_r - q_d C \qquad (3.1.2)$$

where C_I and C_r are the concentrations of the irrigation recharge and regional inflow respectively. Equation (3.1.2) is based on the assumption that the system is thoroughly mixed, thus the outflow concentration is identical to that of the aquifer. By combining (3.1.1) and (3.1.2) a more convenient form of the mass balance equation is obtained

$$nh \frac{dC}{dt} = \varepsilon_I \left[C_I - C\right] + q_r \left[C_r - C\right] + \left[n - S_y\right] C \frac{dh}{dt} \qquad (3.1.3)$$

Chloride was chosen as the contaminant in the following lumped parameter model studies due to its conservative nature and the availability of weekly chloride chemical analyses of drain flow and irrigation water.

3.2 STEADY-STATE MODELS

The steady-state models of this section are used to simulate average yearly outflow concentrations of the middle drain aquifer assuming steady irrigation recharge and a high initial groundwater concentration. Irrigation is assumed to commence during the year 1950 - the year of middle drain emplacement as indicated by aerial photographs of the farm.

The Bureau of Reclamation return flow model was employed in an earlier similar study of the farm in which the aquifer was assumed to be homogeneous (in Gelhar et al., 1980, pp. 49-66). Aquifer depths of 60, 80 and 120 feet were used in simulations of the period 1950 to 1978, and in all cases predicted drain chloride concentrations for 1977 and 1978 were less than half of those observed. One explanation for the disagreement is the presence of a regional inflow of poor quality water. The other possibility, investigated in this section, is that aquifer layering or heterogeneity produces a slower flushing of the high initial concentration groundwater than would be experienced in the homogeneous case. Due to the layering observed in the vicinity of the middle drain it is possible to view the system as consisting of two or three individual but hydrologically connected aquifers or cells. Several hypothetical flow systems could be constructed depending on the total assumed system depth and the cells to which the individual layers are assigned.

3.2.1 The Two Cell Model

A two layered system may be approached by generalizing the single cell lumped parameter model in the manner presented by McLin (1981). The layers are treated as two interacting mixing cells as depicted in Figure 3.2.1(a). The upper layer possesses effective porosity n_1, hydraulic

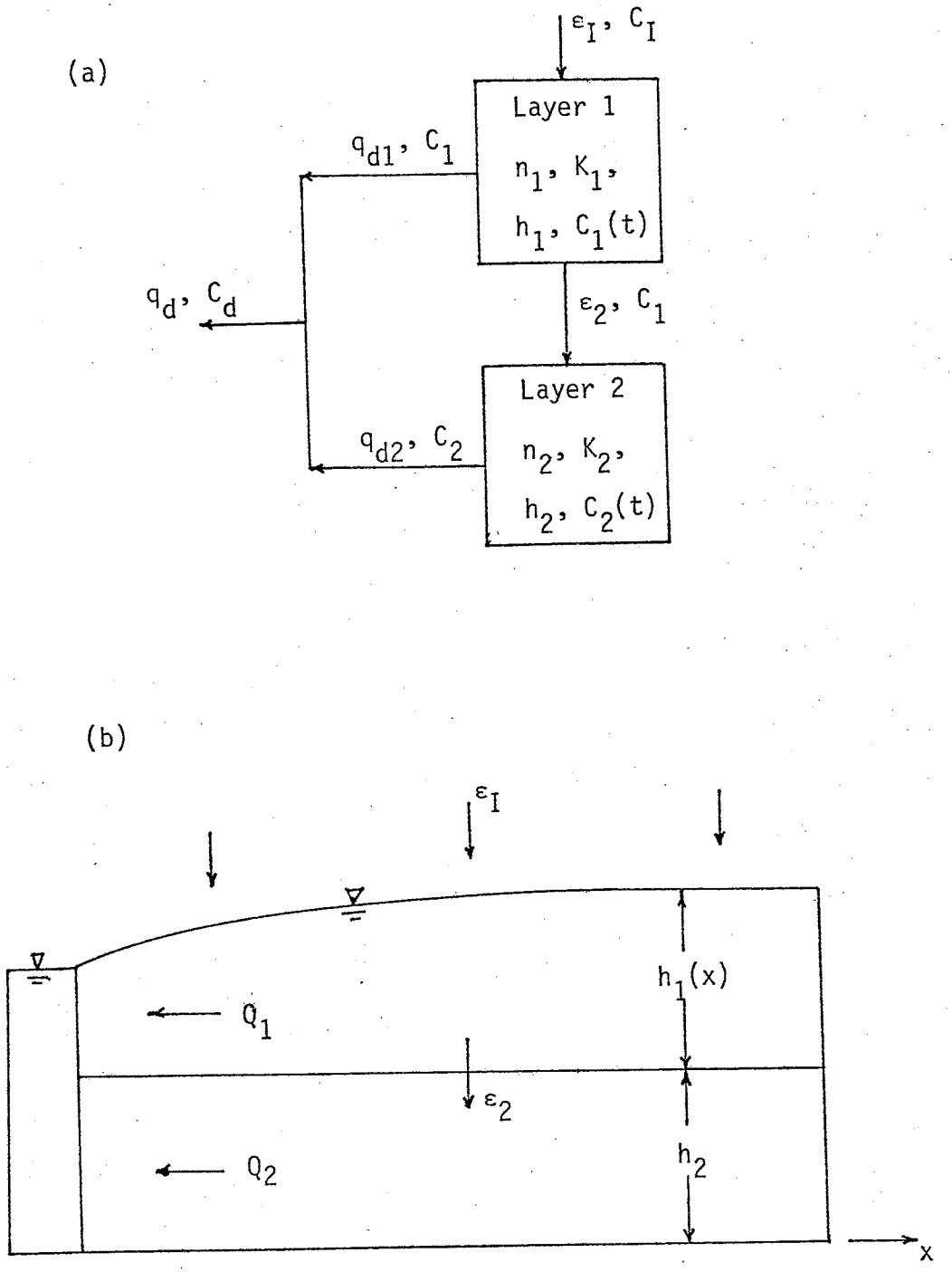

Figure 3.2.1: Two Cell Aquifer Representation,(a); and, Idealized Two Layered Dupuit Aquifer, (b).

conductivity K_1, average saturated thickness h_1 and average solute concentration $C_1(t)$. The lower layer has effective porosity n_2, hydraulic conductivity K_2, saturated thickness h_2 and average solute concentration $C_2(t)$. Irrigation water enters the upper cell at a steady rate ε_I, producing a steady flow from the upper to lower cell at the rate ε_2.

The relative magnitudes of the cell inflow rates ε_2 and ε_I may be determined by employing the Dupuit assumptions of a fully penetrating drain and negligible vertical gradients (Figure 3.2.1(b)). Under these assumptions, the steady-state drain flow contribution per unit length of drain from each layer may be written as

$$Q_1 = -K_1 h_1 \frac{dh_1}{dx} = -T_1 \frac{dh_1}{dx} \tag{3.2.1}$$

$$\text{and} \quad Q_2 = -K_2 h_2 \frac{dh_1}{dx} = -T_2 \frac{dh_1}{dx} \tag{3.2.2}$$

where T_1 is the average transmissivity of the upper layer and T_2 is the lower layer transmissivity. The change in outflow as the drain is approached can be expressed in terms of the accretion rates to or from each layer as

$$-\frac{dQ_1}{dx} = \varepsilon_I - \varepsilon_2 \tag{3.2.3}$$

$$\text{and} \quad -\frac{dQ_1}{dx} = \varepsilon_2 \tag{3.2.4}$$

Substituting equations (3.2.1) and (3.2.2) into (3.2.3) and (3.2.4) respectively, and equating second derivatives of h_1 yields

$$\varepsilon_2 = \mu \varepsilon_I \tag{3.2.5}$$

$$\text{where} \quad \mu = \frac{T_2/T_1}{1 + T_2/T_1}$$

The rate of inflow to the lower cell is thus dependent on the irrigation recharge rate and the transmissivities of the layers.

By analogy to the single cell model, the steady-state water balance equations for the two layers are

$$0 = \varepsilon_I - \varepsilon_2 - q_{d1} \tag{3.2.6}$$

$$\text{and} \quad 0 = \varepsilon_2 - q_{d2} \tag{3.2.7}$$

where q_{d1} and q_{d2} are the drain flows per unit area from the layers. Adding equations (3.2.6) and (3.2.7) the water balance for the system is

$$0 = \varepsilon_I - \left(q_{d1} + q_{d2}\right) = \varepsilon_I - q_d$$

where q_d is the drain discharge rate of the system. Assuming thorough mixing, the mass balance equations for the layers are

$$n_1 h_1 \frac{dC_1}{dt} = \varepsilon_I C_I - \varepsilon_2 C_1 - q_{d1} C_1 \tag{3.2.8}$$

$$\text{and} \quad n_2 h_2 \frac{dC_2}{dt} = \varepsilon_2 C_1 - q_{d2} C_2 \tag{3.2.9}$$

where C_I is the concentration of the irrigation recharge. Substitution of equations (3.2.6) and (3.2.7) into (3.2.8) and (3.2.9) respectively, yields the governing mass balance equations

$$\frac{dC_1}{dt} + \frac{1}{t_{c1}} C_1 = \frac{1}{t_{c1}} C_I \qquad (3.2.10)$$

and $$\frac{dC_2}{dt} + \frac{1}{t_{c2}} C_2 = \frac{1}{t_{c2}} C_1 \qquad (3.2.11)$$

where $$t_{c1} = \frac{n_1 h_1}{\varepsilon_I}$$

and $$t_{c2} = \frac{n_2 h_2}{\varepsilon_2} = \frac{n_2 h_2}{\mu \varepsilon_I}$$

The terms t_{c1} and t_{c2} are the solute response times of the layers.

For the case where the irrigation recharge rate (ε_I) and concentration (C_I) are constant in time, equation (3.2.10) has the solution

$$C_1(t) = C_I + \left(C_{o1} - C_I\right) e^{-t/t_{c1}} \qquad (3.2.12)$$

where C_{o1} is the average concentration of layer 1 at t = 0. Using this result in equation (3.2.11), the average concentration of layer 2 is given by

$$C_2(t) = C_I + \left(C_{o2} - C_I\right) e^{-t/t_{c2}} + \left(C_{o1} - C_I\right) \frac{1}{(t_{c2}/t_{c1}) - 1} \left(e^{-t/t_{c2}} - e^{-t/t_{c1}}\right) \qquad (3.2.13)$$

where C_{o2} is the average concentration of layer 2 at t = 0. The drain concentration is a mixture of the outflows from the layers given by

$$C_d(t) = \frac{q_{d1}}{qd} C_1 + \frac{q_{d2}}{qd} C_2$$

$$= (1 - \mu) C_1 + \mu C_2$$

where μ is defined in (3.2.5).

3.2.2 The Three Cell Model

To account for a three layered aquifer, the two cell model is easily generalized by adding a third mixing cell to the system as shown in Figure 3.2.2(a). Visualizing the system as an idealized Dupuit aquifer (Figure 3.2.2(b)), the drain flow contribution per unit length of drain from each layer is

$$Q_i = -K_i h_i \frac{dh_1}{dx} = -T_i \frac{dh_1}{dx} \quad , \quad i = 1,2,3 \tag{3.2.14}$$

The total drain flow per unit length of drain is

$$Q_T = Q_1 + Q_2 + Q_3$$

Expressing the change in outflow as the drain is approached in terms of the accretion rates to or from each layer yields

$$-\frac{dQ_1}{dx} = \varepsilon_I - \varepsilon_2 \tag{3.2.15}$$

$$-\frac{dQ_2}{dx} = \varepsilon_2 - \varepsilon_3 \tag{3.2.16}$$

$$-\frac{dQ_3}{dx} = \varepsilon_3 \tag{3.2.17}$$

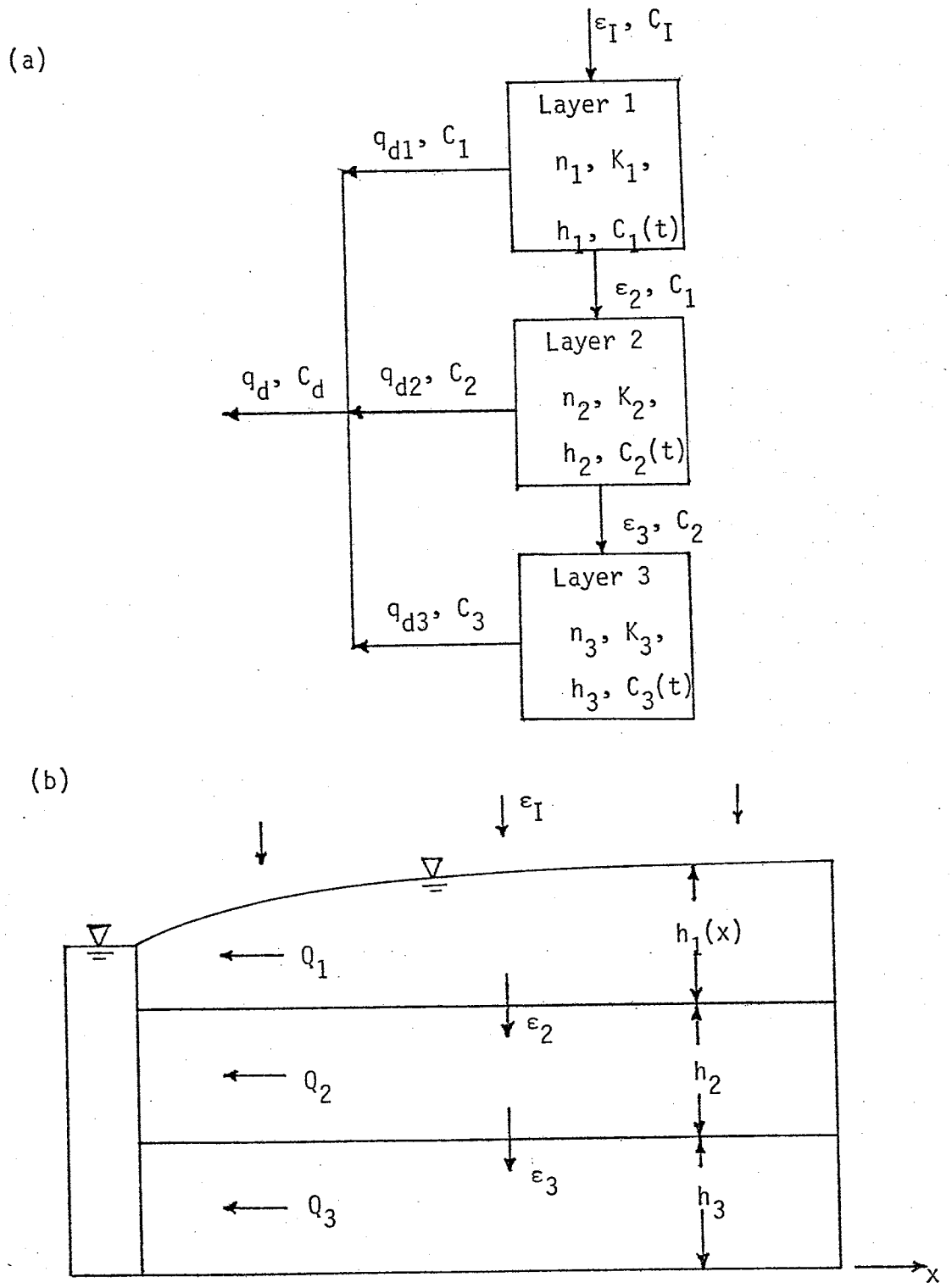

Figure 3.2.2: Three Cell Aquifer Representation, (a); and, Idealized Three Layered Dupuit Aquifer, (b).

where ε_I is the rate of irrigation recharge, ε_2 is the flow rate from the upper to middle layer, and ε_3 is the flow rate from the middle to lower layer. Combining equations (3.2.14) and (3.2.15) through (3.2.17), the flow rates between the layers are found to be

$$\varepsilon_2 = (1 - a)\, \varepsilon_I$$

$$\text{and} \qquad \varepsilon_3 = (1 - a - b)\, \varepsilon_I$$

$$\text{where} \qquad a = \frac{1}{1 + T_2/T_1 + T_3/T_1}$$

$$\text{and} \qquad b = \frac{T_2/T_1}{1 + T_2/T_1 + T_3/T_1}$$

The mass balance equations for the upper two cells are identical to (3.2.10) and (3.2.11) with the exception that the middle layer solute response time is now

$$t_{c2} = \frac{n_2 h_2}{\varepsilon_2} = \frac{n_2 h_2}{(1 - a)\, \varepsilon_I}$$

The concentrations of the two upper layers are thus given by (3.2.12) and (3.2.13), assuming the irrigation recharge rate and concentration are constant in time. The governing mass balance equation for the lower layer is

$$\frac{dC_3}{dt} + \frac{1}{t_{c3}} C_3 = \frac{1}{t_{c3}} C_2 \qquad (3.2.18)$$

$$\text{where} \quad t_{c3} = \frac{n_3 h_3}{\varepsilon_3} = \frac{n_3 h_3}{(1 - a - b)\varepsilon_I}$$

and C_2 is given by (3.2.13). The solution to (3.2.18) subject to the constant irrigation recharge rate and concentration assumption is

$$C_3(t) = C_I + \left(C_{O3} - C_I\right)e^{-t/t_{c3}} + \frac{C_{O2} - C_I}{(t_{c3}/t_{c2})-1}\left(e^{-t/t_{c3}} - e^{-t/t_{c2}}\right)$$

$$+ \frac{C_{O1} - C_I}{(t_{c2}/t_{c1})-1}\left[\frac{\left(e^{-t/t_{c3}} - e^{-t/t_{c2}}\right)}{(t_{c3}/t_{c2}) - 1} - \frac{\left(e^{-t/t_{c3}} - e^{-t/t_{c1}}\right)}{(t_{c3}/t_{c1}) - 1}\right]$$

where C_{O3} is the average lower layer concentration at t = 0.

The drain concentration is a mixture of the outflows from the three layers given by

$$C_d(t) = \frac{Q_1}{Q_T} C_1 + \frac{Q_2}{Q_T} C_2 + \frac{Q_3}{Q_T} C_3$$

$$= aC_1 + bC_2 + (1 - a - b)C_3$$

3.2.3 The Two Cell Model with Separating Aquitard

A logical way to assign the observed layering at the farm to the two or three cell structure of the previous models would be to place a clay layer at the boundary between cells. In this case the clay may behave as an aquitard making the assumption of hydrostatic head invalid. The model presented here accounts for the possibility of differing hydraulic heads in two layers separated by an aquitard of thickness b and hydraulic conductivity K_a as depicted in Figure 3.2.3. The layers separated by the aquitard are treated as the two mixing cells shown in

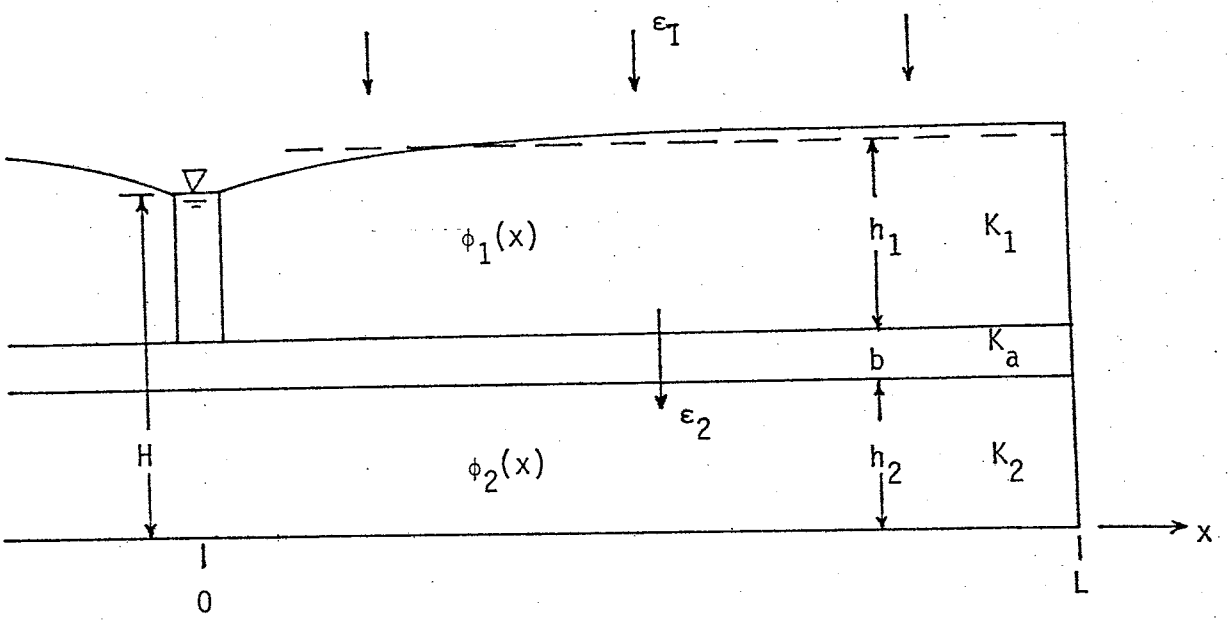

Figure 3.2.3: Aquifer Representation for Two Cell Model with Separating Aquitard.

Figure 3.2.1(a). The difference between this model and the two cell model of section 3.2.1 is the magnitude of the lower layer inflow rate, ε_2. The following assumptions are made in this model:

(1) The drain is of negligible width and fully penetrates the upper layer.

(2) Flow across the aquitard is vertical and causes no change in concentration.

(3) The upper and lower layers are well mixed.

For this system the flows per unit length of drain through the upper and lower layers are given by

$$Q_1 = -K_1 h_1 \frac{d\phi_1}{dx} = -T_1 \frac{d\phi_1}{dx} \tag{3.2.19}$$

and

$$Q_2 = -K_2 h_2 \frac{d\phi_2}{dx} = -T_2 \frac{d\phi_2}{dx} \tag{3.2.20}$$

where T_1 is the average upper layer transmissivity, T_2 is the lower layer transmissivity, and $\phi_1(x)$ and $\phi_2(x)$ are the hydraulic potential distributions of the layers. The vertical flow across the aquitard is

$$q_a = K_a \frac{(\phi_1 - \phi_2)}{b} \tag{3.2.21}$$

The horizontal change in flow through the layers may be expressed as

$$\frac{dQ_1}{dx} = \varepsilon_1 - q_a \tag{3.2.22}$$

and

$$\frac{dQ_2}{dx} = q_a \tag{3.2.23}$$

where ε_I is the irrigation recharge rate. Appropriate substitution of equations (3.2.19) through (3.2.21) into (3.2.22) and (3.2.23) produces the coupled equations

$$T_1 \frac{d^2\phi_1}{dx^2} = \frac{K_a}{b}(\phi_1 - \phi_2) - \varepsilon_I \qquad (3.2.24)$$

and

$$T_2 \frac{d^2\phi_2}{dx^2} = -\frac{K_a}{b}(\phi_1 - \phi_2) \qquad (3.2.25)$$

which define the potential distributions of the layers. Simultaneous solution of (3.2.24) and (3.2.25) subject to the boundary conditions

$$\phi_1(0) = H$$

$$\left.\frac{d\phi_1}{dx}\right|_{x=L} = \left.\frac{d\phi_2}{dx}\right|_{x=L} = \left.\frac{d\phi_2}{dx}\right|_{x=0} = 0$$

yields the hydraulic head distributions

$$\phi_1(x) = \frac{\varepsilon_I L \left[T_2\left(1+\exp\{2L\sqrt{\gamma/\eta}\}\right) - T_2\left(\exp\{\sqrt{\gamma/\eta}\,x\} + \exp\{\sqrt{\gamma/\eta}\,(2L-x)\}\right)\right]}{T_1\,\gamma\sqrt{\gamma/\eta}\left(\exp\{2L\sqrt{\gamma/\eta}\}-1\right)}$$

$$+ \frac{\varepsilon_I X}{2\gamma}(2L - x) + H \qquad (3.2.26)$$

and

$$\phi_2(x) = \frac{\varepsilon_I L \left[T_2\left(1+\exp\{2L\sqrt{\gamma/\eta}\}\right) + T_1\left(\exp\{\sqrt{\gamma/\eta}\,x\} + \exp\{\sqrt{\gamma/\eta}\,(2L-x)\}\right)\right]}{T_1\,\gamma\sqrt{\gamma/\eta}\left(\exp\{2L\sqrt{\gamma/\eta}\}-1\right)}$$

$$+ \frac{\varepsilon_I x}{2\gamma} (2L-x) - \frac{\eta}{\gamma T_1} \varepsilon_I + H \qquad (3.2.27)$$

where L is the distance from the drain to the water table divide and γ and η are constants defined as

$$\gamma = T_1 + T_2 \ ,$$

$$\eta = \frac{b}{K_a} T_1 T_2 \ .$$

At some point x_o between the drain and water table divide, the hydraulic potentials of the two layers are equal and there is no flow across the aquitard. Equating the head distributions (3.2.26) and (3.2.27) and assuming

$$\exp\left(2L\sqrt{\gamma/\eta}\right) >> 1 \ ,$$

the point of no flow across the aquitard is approximately

$$x_o \cong \sqrt{\eta/\gamma}\ \ell n \left(L\sqrt{\gamma/\eta}\right) \ .$$

The total flow per unit length of drain passing through the lower layer is thus

$$Q_2(x_o) = -T_2 \frac{d\phi_2}{dx}\Big|_{x=x_o} = \varepsilon_I L \frac{T_2}{\gamma}\left[1 - \frac{1}{L}\left(x_o + \sqrt{\eta/\gamma}\right)\right] \ .$$

The total inflow to the system is

$$Q_T = \varepsilon_I L$$

which implies the drain flow contribution per unit length of drain from the upper layer is

$$Q_1 = Q_T - Q_2(x_o) = \frac{\varepsilon_I L}{\gamma}\left[T_1 + \frac{T_2}{L}(x_o + \sqrt{\eta/\gamma})\right] .$$

Assuming a constant irrigation recharge rate and concentration, the mass balance equations and concentrations of the layers are given by equations (3.2.10) through (3.2.13) with the exception that the inflow to the lower layer is now

$$\varepsilon_2 = \frac{Q_2(x_o)}{L} = \varepsilon_I \mu\left[1 - \frac{1}{L}(x_o + \sqrt{\eta/\gamma})\right] \qquad (3.2.28)$$

where $\mu = \frac{T_2/T_1}{1+T_2/T_1}$ as defined in equation (3.2.5). Comparison of equations (3.2.28) and (3.2.5) indicates less inflow is received by the lower layer with the inclusion of the aquitard. The resulting drain flow concentration is

$$C_d(t) = \frac{Q_1}{Q_T} C_1 + \frac{Q_2(x_o)}{Q_T} C_2$$

where C_1 and C_2 are given by equations (3.2.12) and (3.2.13).

3.2.4 Applications and Conclusions

The three models presented in this section were used to predict drain chloride concentrations through 1979 for a given set of hydrologic parameters and initial condition in 1950. An initial groundwater chloride concentration of 850 ppm (24 meq/l) was assumed, and an irrigation recharge rate of 3.3 ft/year was used based on a yearly application of 6

feet and an irrigation efficiency of 45 percent. The average Rio Grande chloride concentration at San Acacia for the 30 year period is 31 ppm which implies an irrigation recharge concentration of about 56 ppm due to the irrigation loss. The distance from the drain to the water table divide required in the aquitard model was taken to be 620 feet. These parameters were also used in the earlier study employing the Bureau of Reclamation model mentioned in section 3.2. The remaining parameters - hydraulic conductivity ratios, effective porosities and layer thicknesses - were varied to simulate several different flow systems for each model type. The overall attempt was to manipulate these parameters in order to produce the highest possible predicted drain concentration for the year 1979. Increasing the effective porosities or thicknesses of the layers increases the solute response times and thus predicted drain concentrations are maintained at a higher level. For this reason, flow systems up to 125 feet in depth and effective porosities up to 40 percent were used. The hydraulic conductivities of the layers were generally assumed to decrease with depth.

The layer parameters, cell response times and predicted drain concentrations for selected applications of the two cell, three cell, and two cell with separating aquitard models are listed in Tables 3.2.1, 3.2.2, and 3.2.3 respectively. The observed drain chloride concentrations during the period of 1977 through 1980 are roughly 300 to 400 ppm. In every flow system investigated here, the predicted drain concentration for 1979, and even 1969, is well below that range. The implication of these results is that a simple flushing of high initial concentration groundwater by irrigation recharge is not the mechanism producing the high observed drain concentrations. Based on these results and the discussion in section 2.1.3

Table 3.2.1: Steady-State Two Cell Model Applications

Case	Conductivity Ratio K_1/K_2	Effective Porosity n_1	Effective Porosity n_2	Layer Thickness (ft) h_1	Layer Thickness (ft) h_2	Response Time (yrs) t_{c1}	Response Time (yrs) t_{c2}	Predicted Drain Concentration (ppm) 1959	1969	1979
1	2	.30	.25	25	30	2.3	6.1	151	73	59
2	2	.30	.40	25	75	2.3	15	348	205	133
3	3	.30	.40	25	75	2.3	18	321	207	143
4	2	.35	.40	25	75	2.7	15	359	210	135
5	3	.35	.40	25	75	2.7	18	331	210	145
6	20	.20	.40	60	35	3.6	150	126	79	75
7	10	.20	.40	60	35	3.6	77	144	94	87
8	5	.20	.40	60	35	3.6	41	172	114	99
9	5	.30	.40	60	35	5.5	41	242	132	104
10	5	.30	.40	60	50	5.5	42	265	154	122

Table 3.2.2: Steady-State Three Cell Model Applications

Case	Conductivity Ratios		Effective Porosities			Layer Thickness (ft)			Response Times (yrs)			Predicted Drain Concentration (ppm)		
	K_1/K_2	K_1/K_3	n_1	n_2	n_3	h_1	h_2	h_3	t_{c1}	t_{c2}	t_{c3}	1959	1969	1979
1	2	5	.35	.30	.40	30	30	40	3.2	6.3	32	268	161	124
2	2	5	.35	.30	.40	30	30	60	3.2	5.8	35	298	192	150
3	3	5	.35	.30	.40	30	30	40	3.2	7.3	29	267	170	130
4	3	5	.35	.30	.40	30	30	60	3.2	6.4	32	301	201	157
5	2	10	.35	.30	.40	30	30	40	3.2	7.0	59	237	137	108

Table 3.2.3: Applications of the Steady-State Two Cell Model with Separating Aquitard

Case	Conductivity Ratios		Effective Porosity		Layer Thickness (ft)			Response Time (yrs)		Predicted Drain Concentration (ppm)		
	K_1/K_a	K_2/K_a	n_1	n_2	h_1	b	h_2	t_{c1}	t_{c2}	1959	1969	1979
1	10	5	.40	.40	30	5	30	3.6	13	230	124	86
2	20	10	.40	.40	30	5	30	3.6	14	226	124	88
3	200	100	.35	.35	30	5	30	3.2	18	182	113	87
4	10	10	.40	.35	30	5	30	3.6	7.8	236	103	68
5	100	100	.35	.35	30	5	30	3.2	11	207	109	76
6	10	5	.35	.35	30	5	60	3.2	16	287	169	115
7	15	3	.35	.35	30	5	60	3.2	27	228	158	125
8	5	15	.35	.35	60	15	30	6.4	7.5	345	148	83
9	20	10	.35	.35	60	15	30	6.4	24	286	146	103
10	10	5	.40	.35	60	15	50	7.3	25	355	197	136
11	5	10	.40	.35	60	15	50	7.3	12	418	218	127
12	25	5	.35	.35	60	15	50	6.4	54	276	147	113
13	3	3	.35	.35	60	15	50	6.4	15	370	197	124

it was concluded that a regional inflow of poor quality water is contributing flow to the middle drain.

3.3 THE TRANSIENT TWO CELL LUMPED PARAMETER MODEL

The following model was used to simulate middle drain chloride concentration and chloride mass output for the years 1978 through 1980. It includes the effects of transient flow and a regional inflow component. The base of the flow system is taken as the surface of the lower clay and the cell division is marked by the upper surface of the shallow clay. In a similar study by Senn (in Gelhar et al., 1980, pp. 71-110) this system was treated as a single cell.

3.3.1 Model Development

The two cell representation of the physical system is shown in Figure 3.3.1(a). The upper layer possesses specific yield S_y, effective porosity n_1, hydraulic conductivity K_1, average saturated thickness $h_1(t)$, and average concentration $C_1(t)$. The lower layer has effective porosity n_2, hydraulic conductivity K_2, constant saturated thickness h_2, and average concentration $C_2(t)$. Regional flow is assumed to enter or exit the system through the base of the lower layer at a rate q_r. Irrigation recharge enters the upper layer at the rate ε_I and interlayer flow occurs at a rate of ε_2.

Employing the Dupuit assumptions of a fully penetrating drain and negligible vertical gradients (Figure 3.3.1(b)), for any fixed time the drain flow contribution per unit length of drain from the layers may be written as

$$Q_1 = -K_1 h_1 \frac{dh_1}{dx} = -T_1 \frac{dh_1}{dx} \qquad (3.3.1)$$

and

$$Q_2 = -K_2 h_2 \frac{dh_1}{dx} = -T_2 \frac{dh_1}{dx} \qquad (3.3.2)$$

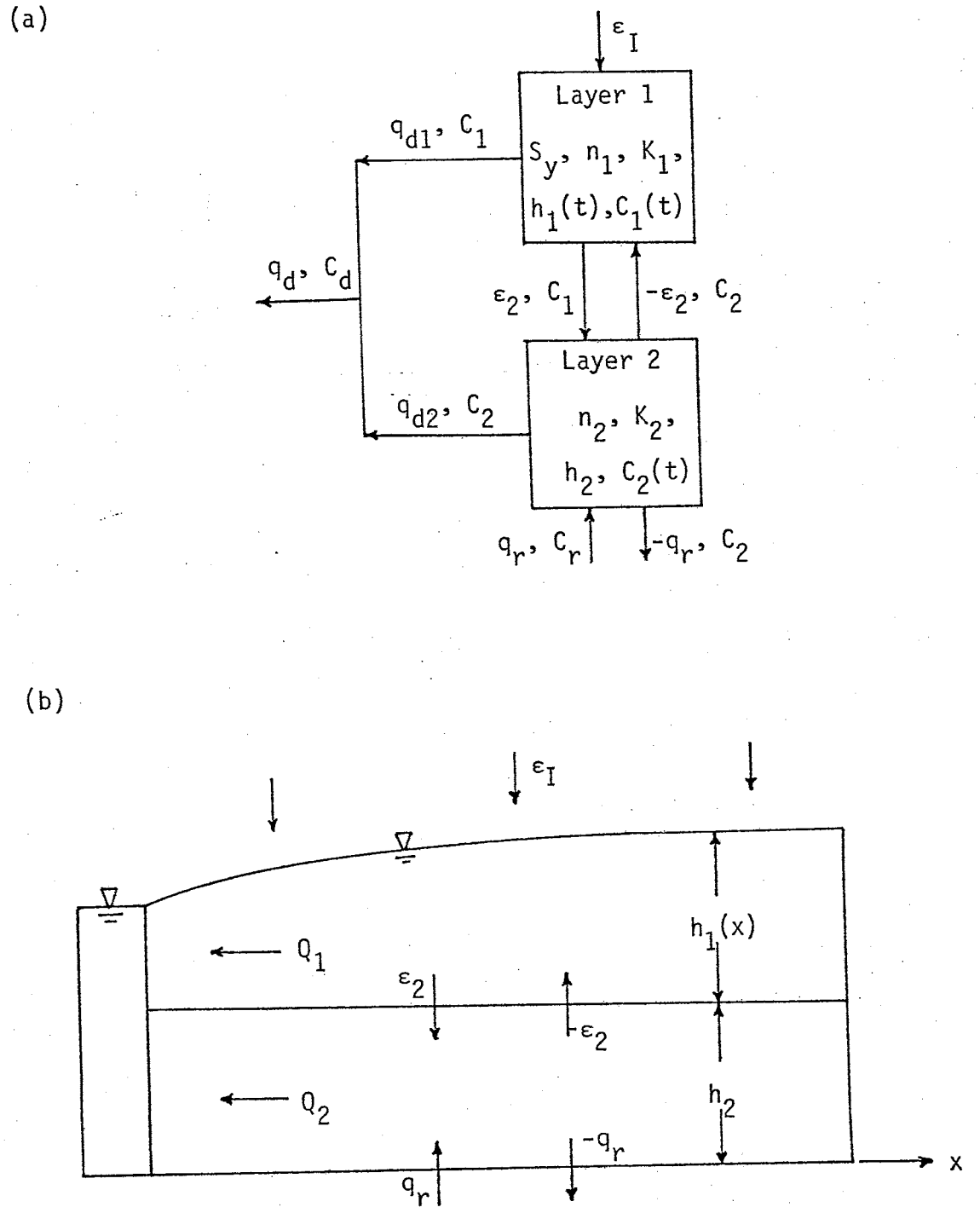

Figure 3.3.1: Transient Two Cell Aquifer Representation, (a); and, Two Layered Dupuit Aquifer, (b).

where T_1 is the average upper layer transmissivity and T_2 is the lower layer transmissivity. The change in layer outflow as the drain is approached can be expressed in terms of the accretion rates to or from each layer as

$$-\frac{dQ_1}{dx} = \varepsilon_I - \varepsilon_2 \tag{3.3.3}$$

and

$$-\frac{dQ_2}{dx} = \varepsilon_2 + q_r \tag{3.3.4}$$

Substituting equations (3.3.1) and (3.3.2) into (3.3.3) and (3.3.4) respectively, and equating second derivatives of h_1 yields

$$\varepsilon_2 = \frac{(T_2/T_1)\ \varepsilon_I - q_r}{1 + T_2/T_1} \tag{3.3.5}$$

The flow between layers is thus dependent on the transmissivity ratio and the irrigation recharge and regional flow rates. When $(T_2/T_1)\varepsilon_I$ is less than q_r, ε_2 is negative and the interlayer flow is from the lower to upper layer.

By analogy to the single cell model of Gelhar and Wilson (1974) the water balance equations for the individual layers may be stated as

$$S_y \frac{dh_1}{dt} = \varepsilon_I - \varepsilon_2 - q_{d1} \tag{3.3.6}$$

and

$$0 = \varepsilon_2 + q_r - q_{d2} \tag{3.3.7}$$

where q_{d1} and q_{d2} are the drain outflows per unit aquifer area from the two layers. Adding equations (3.3.6) and (3.3.7) yields the water balance equation for the system

$$Sy \frac{dh_1}{dt} = \varepsilon_I + q_r - q_d \qquad (3.3.8)$$

where q_d is the total drain flow rate from the system. Equation (3.3.8) may be used to determine the regional inflow rate if the specific yield is known and the total drain flow rate, irrigation recharge rate, and average upper layer saturated thickness are known functions of time. A negative value of q_r indicates flow is leaving the system through the lower layer base.

The mass balance equations for the two layers are dependent on the directions (signs) of ε_2 and q_r. Assuming the irrigation recharge rate is always nonnegative, it can be seen from equation (3.3.5) that the following three states are possible for the flow system:

(1) $\varepsilon_2, q_r > 0 \Rightarrow$ regional inflow and flow from upper to lower layer;

(2) $\varepsilon_2 > 0, q_r < 0 \Rightarrow$ regional outflow and flow from upper to lower layer; and

(3) $\varepsilon_2 < 0, q_r > 0 \Rightarrow$ regional inflow and flow from lower to upper layer.

The mass balance equations for state (1) will now be developed from which the equations for states (2) and (3) will be generalized.

For system state (1), a mass balance for a contaminant of average concentration $C_1(t)$ in the upper layer is given by

$$n_1 \frac{d}{dt}(h_1 C_1) = \varepsilon_I C_I - \varepsilon_2 C_1 - q_{d1} C1 \qquad (3.3.9)$$

where C_I is the irrigation recharge concentration. Expanding the derivative in (3.3.9) and substituting (3.3.6) in the form

$$n_1 \frac{dh_1}{dt} = (n_1 - S_y) \frac{dh_1}{dt} + \varepsilon_I - \varepsilon_2 - q_{d1}$$

yields a more convenient form of the mass balance equation

$$n_1 h_1 \frac{dC_1}{dt} + (n_1 - S_y) C_1 \frac{dh_1}{dt} = \varepsilon_I (C_I - C_1) \qquad (3.3.10)$$

Similarly, the mass balance equation for a contaminant of average solute concentration $C_2(t)$ in the lower layer is

$$n_2 h_2 \frac{dC_2}{dt} = \varepsilon_2 C_1 + q_r C_r - q_{d2} C_2 \qquad (3.3.11)$$

where C_r is the concentration of the regional inflow. Substitution of equation (3.3.7) into (3.3.11) produces the alternate form of the lower layer mass balance equation

$$n_2 h_2 \frac{dC_2}{dt} = \varepsilon_2 (C_1 - C_2) + q_r (C_r - C_2) \qquad (3.3.12)$$

In system state (2), the regional flow term of (3.3.11) becomes an outflow carrying the concentration of the lower layer. Under these conditions the lower layer mass balance equation is

$$n_2 h_2 \frac{dC_2}{dt} = \varepsilon_2 (C_1 - C_2) \qquad (3.3.13)$$

and the upper layer mass balance equation is identical to (3.3.10).

In system state (3), regional flow enters the lower layer and the interlayer flow is from the lower to upper layer. The mass balance equations for this system state are

$$n_1 h_1 \frac{dC_1}{dt} + (n_1 - S_y)\, C_1 \frac{dh_1}{dt} = \varepsilon_I (C_I - C_1) - \varepsilon_2 (C_2 - C_1) \qquad (3.3.14)$$

for the upper layer, and

$$n_2 h_2 \frac{dC_2}{dt} = q_r (C_r - C_2) \qquad (3.3.15)$$

for the lower layer.

For all system states, the drain concentration is obtained by mixing the outflows from the two layers according to

$$C_d' = \frac{q_{d1}}{q_d} C_1 + \frac{q_{d2}}{q_d} C_2 \qquad (3.3.16)$$

3.3.2 Model Application

Parameter Assignment

In order to apply the model, the time dependent parameters - q_d, ε_I, C_I, ε_2, q_r, and h_1 - must be determined as well as the constant parameters - n_1, n_2, S_y, h_2, C_r, K_1/K_2, and the simulation time increment. The time increment used in this study is a four week period, thus periods 1 through 13, 14 through 26, and 27 through 39 represent the years 1978, 1979 and 1980 respectively. The regional inflow concentration (assumed constant) and hydraulic conductivity ratio will remain as variable inputs; the optimum values of which will be determined from model runs. The assignment of the remaining parameters will now be discussed.

The upper cell is assigned to the zone composed predominantly of sand above the clay appearing at a depth of about 24 feet. The remainder of the system, consisting of the shallow clay and sand and gravel

deposits between it and the deeper clay, is assigned to the lower cell. The deeper clay is roughly 68 to 70 feet below the surface which implies a lower layer saturated thickness of about 45 feet. An effective porosity of 0.35 was assigned to the upper layer based on the measured values discussed in section 2.1.2. The lower layer effective porosity was assumed to be 0.30 based on a lithological comparison with the upper layer. A specific yield of 0.19 determined from drain flow recessions was also used as the effective porosity in the single cell study by Senn (in Gelhar et al., 1980, pp. 71-110). Laboratory tests on a column of repacked sand taken from a depth of 3 to 4 feet indicated a specific yield of 0.13. Based on these determinations a value of 0.15 was assigned to the specific yield.

Weekly depth to water measurements for 13 wells in the vicinity of the middle drain are available for the study period. The Theissen polygon method was employed by Senn to determine weekly average water table positions using these wells. The well locations and polygons constructed by Senn are shown in Figure 3.3.2, and the corresponding area percentages are listed in Table 3.3.1. Using these area percentages the average water table elevation was computed for each week. The three year mean water table elevation corresponds to a depth to water of roughly 4 feet. Therefore, the average saturated thickness of the upper layer, about which weekly fluctuations occur, is 20 feet. The three year mean water table elevation was subtracted from each weekly average elevation to obtain the weekly fluctuation. These fluctuations were then added to 20 feet to obtain the average upper layer saturated thickness for each week. Each four week period is assigned the average saturated thickness corresponding to the last week of the period. These values are listed in Table 3.3.2.

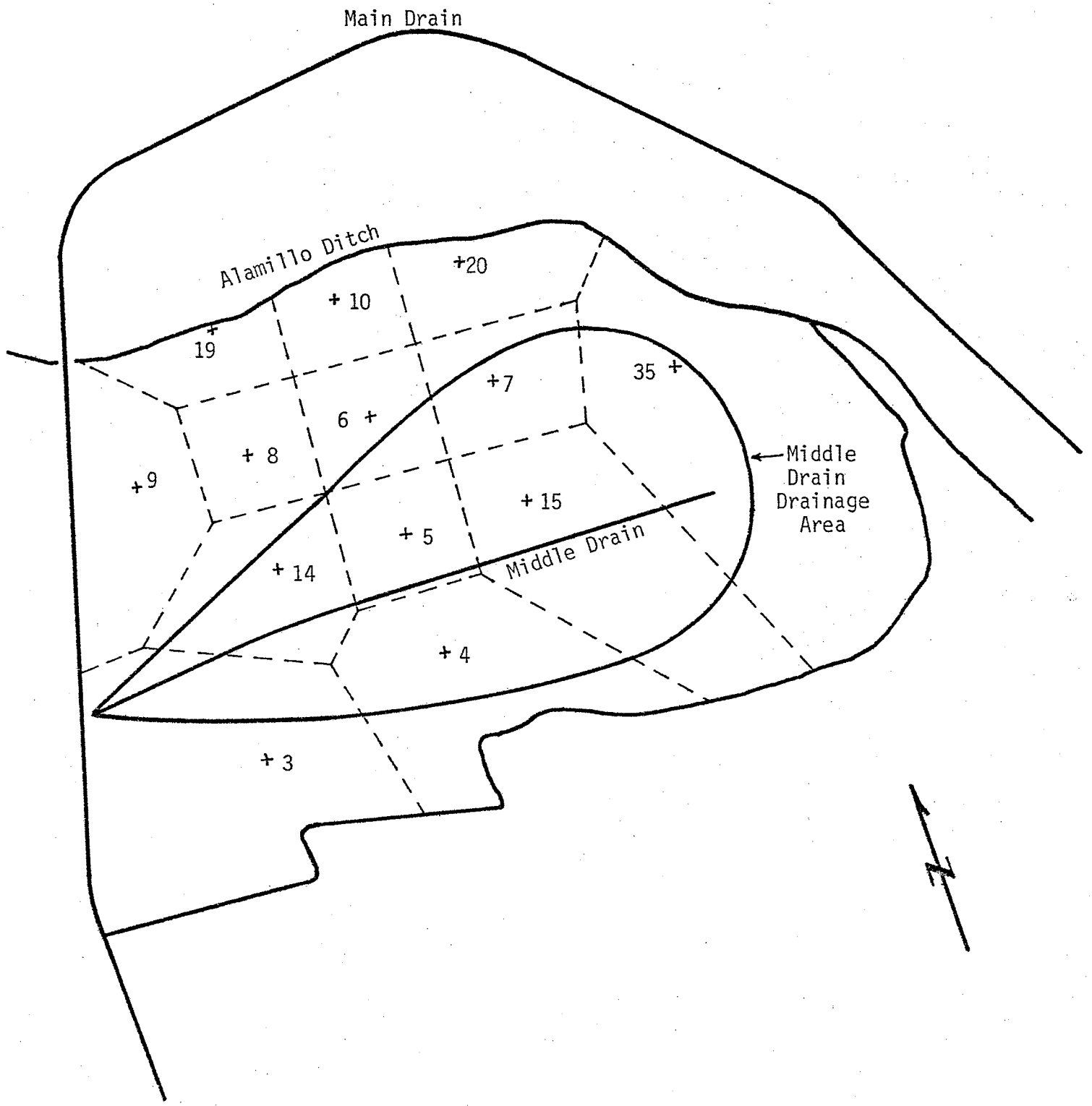

Figure 3.3.2: Thiessen Polygons and Aquifer Area.

Table 3.3.1: Polygon Areas and Percentage Area

Well Number	Area (acres)	Fraction of Total Area
3	20.35	.14724
4	15.06	.10896
5	6.14	.04443
6	5.69	.04117
7	6.98	.05050
8	5.39	.03900
9	9.82	.07105
10	4.43	.03205
14	9.73	.07040
15	19.01	.13754
19	4.16	.03010
20	5.76	.04160
35	25.69	.18588
Total	138.21	1.0

The average volumetric drain flow for each four week period was obtained from continuous discharge records. The volumetric discharge is converted to an outflow rate by dividing by the aquifer area. The aquifer area contributing flow to the middle drain is 59.5 acres as determined by Senn from a contour map of April 1978 water table elevations (Figure 3.3.2). The weekly drain chloride concentrations were arithmetically averaged for each four week period. Comparison of the arithmetically averaged concentrations to flow weighted drain concentrations for 1980 displayed a maximum disagreement of 7 percent. The arithmetically averaged concentrations were therefore assumed to be representative of the drain effluent. The drain outflow rate and concentration for each period is listed in Table 3.3.2.

The amount of applied water for each period includes the accumulative amounts of both irrigation water and precipitation. The irrigation application depths were determined from diversion and irrigated area records, and the precipitation depths were obtained from rain gage data. Weekly irrigation water concentrations were averaged for each four week period and flow weighted with zero concentration precipitation to obtain the concentration of the total applied water. The total application amounts and corresponding concentrations for each period are also listed in Table 3.3.2.

The amount and concentration of groundwater recharge resulting from each surface application is dependent on the irrigation efficiency and the amount of tailwater. The irrigation efficiency is the percentage of applied water which is evaporated or transpired by plants. The leaching fraction is the complement of the irrigation efficiency and represents the percentage of applied water which becomes groundwater recharge.

Table 3.3.2: Applied Water and Chloride Concentration, Drain Outflow Rate and Chloride Concentration, and Upper Layer Saturated Thickness for Each Four Week Period

Period No.	Applied Water $\hat{q}_I$(ft/4wk)	Applied Conc. $\hat{C}_I$(meq/l)	Drain Flow $\hat{q}_d$(ft/4wk)	Drain Conc. $\hat{C}_d$(meq/l)	Saturated Thick. h_1(ft)
1	.016	0	.023	10.73	19.04
2	.103	0	.047	11.09	19.13
3	.015	0	.054	10.41	19.19
4	.715	1.49	.208	9.72	19.61
5	.919	1.22	.420	8.22	20.72
6	.705	0.91	.549	8.74	20.70
7	.956	0.97	.630	8.55	20.22
8	.780	1.25	.569	8.09	20.34
9	.741	1.22	.315	9.76	19.54
10	.823	1.34	.250	9.54	19.48
11	.730	1.49	.191	9.22	19.91
12	.053	0	.156	9.39	19.91
13	.033	0	.222	9.88	19.73
14	.046	0	.266	9.24	19.91
15	.045	0	.243	9.97	20.07
16	0	0	.238	9.78	19.85
17	.994	1.10	.686	9.40	20.50
18	.437	1.06	.700	8.54	20.68
19	.900	1.22	.679	10.00	20.93
20	.876	0.75	.695	9.05	20.57
21	.761	1.29	.625	10.07	19.97
22	.671	0.97	.544	9.97	20.04
23	.491	0.85	.247	10.31	19.81
24	.518	1.04	.392	10.66	19.72
25	.047	0	.173	9.84	19.57
26	.035	0	.152	10.53	19.58
27	.021	0	.121	10.91	19.48
28	.072	0	.103	9.28	19.69
29	0	0	.112	11.66	19.77
30	.791	1.49	.373	10.10	20.54
31	.265	1.30	.523	8.57	20.22
32	1.193	1.45	.859	9.70	20.75
33	.711	0.85	.775	10.07	20.45
34	.933	1.24	.513	8.21	20.31
35	.709	0.92	.373	9.97	20.77
36	.363	1.11	.411	8.10	19.90
37	0	0	.224	9.09	19.98
38	.008	0	.243	9.35	19.93
39	.033	0	.233	9.00	19.92

Tailwater is the percentage of applied water which enters the drain either directly or by shallow interflow near the drain. Considering the loss due to tailwater, the portion of applied water available for consumptive use or recharge is

$$q_I = (1 - \eta)\hat{q}_I$$

where $\hat{q}_I$ is the application rate and η is the tailwater coefficient. The amount of recharge for a given application is

$$\varepsilon_I = (1 - \mu)q_I = (1 - \mu)(1 - \eta)\hat{q}_I \tag{3.3.17}$$

where μ is the irrigation efficiency. The corresponding recharge concentration is given by

$$C_I = \frac{\hat{C}_I}{(1 - \mu)} \tag{3.3.18}$$

where $\hat{C}_I$ is the applied water concentration. Senn computed an irrigation efficiency of 0.55 for the year 1978 during which the aquifer area was almost entirely covered by alfalfa. In 1979 alfalfa composed roughly two thirds of the aquifer area and the remainder was planted with corn. During 1980 over half of the aquifer area was allotted to corn. Based on these cropping patterns and the higher consumptive use of alfalfa than corn, irrigation efficiencies of 0.55 for 1978 and 1979 and 0.50 for 1980 were assumed in the model.

Tailwater also produces a greater flow and lower concentration in the drain as compared to the actual aquifer outflow and concentration. The drain flow due to aquifer outflow is given by

$$q_d = \hat{q}_d - \eta\hat{q}_I \tag{3.3.19}$$

where $\hat{q}_d$ is the measured drain flow rate. The corresponding drain concentration due to aquifer outflow is

$$C_d = (\hat{q}_d\hat{C}_d - n\hat{q}_I\hat{C}_I)/(\hat{q}_d - n\hat{q}_I) \qquad (3.3.20)$$

where $\hat{C}_d$ is the observed drain concentration. The tailwater coefficients used during the irrigation seasons of the modeled period are listed in Table 3.3.3 along with the irrigation recharge and concentration and tailwater adjusted drain flow and concentration for each period. The tailwater coefficients average 10 percent and were chosen to produce a smoothing of the sharp declines in drain concentration during the irrigation seasons as shown in Figure 3.3.3.

Finite Difference Representation and Programming Algorithm

Using the parameters assigned in the previous section it is possible to perform a model simulation by assuming values for the regional inflow concentration (C_r) and the hydraulic conductivity ratio (K_1/K_2). The regional flow rate for each period may be computed using the water balance equation (3.3.8) in the finite difference form

$$q_{ri} = q_{di} - \varepsilon_{Ii} + \frac{S_y}{\Delta t}(h_{1i} - h_{1i-1}) \qquad (3.3.21)$$

where the subscript i denotes the period number and Δt is the simulation time increment (four weeks). As previously mentioned, the upper layer saturated thickness h_i corresponds to the last week of period i, thus the storage term of (3.3.21) represents the change in storage due to inflow and outflow occurring in that period. The regional flow rates are now used to determine the interlayer flow rates from equation (3.3.5)

Table 3.3.3: Irrigation Recharge and Chloride Concentration, Tailwater Adjusted Drain Flow and Chloride Concentration, and Tailwater Coefficients for Each Four Week Period

Period No.	Irrigation Recharge ε_I(ft/4wk)	Recharge Conc. C_I(meq/l)	Adj. Drain Flow q_d(ft/4wk)	Adj. Drain Conc. C_d(meq/l)	Tailwater Coeff.
1	.007	0	.023	10.73	0
2	.046	0	.047	11.09	0
3	.007	0	.054	10.41	0
4	.322	3.31	.208	9.72	0
5	.372	2.71	.328	10.18	.10
6	.286	2.02	.478	9.89	.10
7	.387	2.16	.534	9.91	.10
8	.316	2.78	.491	9.18	.10
9	.333	2.71	.315	9.76	0
10	.370	2.98	.250	9.54	0
11	.329	3.31	.191	9.22	0
12	.024	0	.156	9.33	0
13	.015	0	.222	9.88	0
14	.021	0	.266	9.24	0
15	.020	0	.243	9.97	0
16	0	0	.238	9.78	0
17	.425	2.44	.636	10.05	.05
18	.167	2.36	.634	9.31	.15
19	.405	2.71	.679	10.00	0
20	.355	1.67	.607	10.25	.10
21	.342	2.87	.625	10.07	0
22	.302	2.16	.544	9.97	0
23	.221	1.89	.247	10.31	0
24	.233	2.31	.392	10.66	0
25	.021	0	.173	9.84	0
26	.018	0	.152	10.53	0
27	.011	0	.121	10.91	0
28	.036	0	.103	9.28	0
29	0	0	.112	11.66	0
30	.396	2.98	.373	10.10	0
31	.119	2.60	.496	8.96	.10
32	.597	2.90	.859	9.70	0
33	.356	1.70	.775	10.07	0
34	.420	2.48	.420	9.76	.10
35	.355	1.84	.373	9.97	0
36	.163	2.22	.375	8.78	.10
37	0	0	.224	9.09	0
38	.004	0	.243	9.35	0
39	.017	0	.233	9.00	0

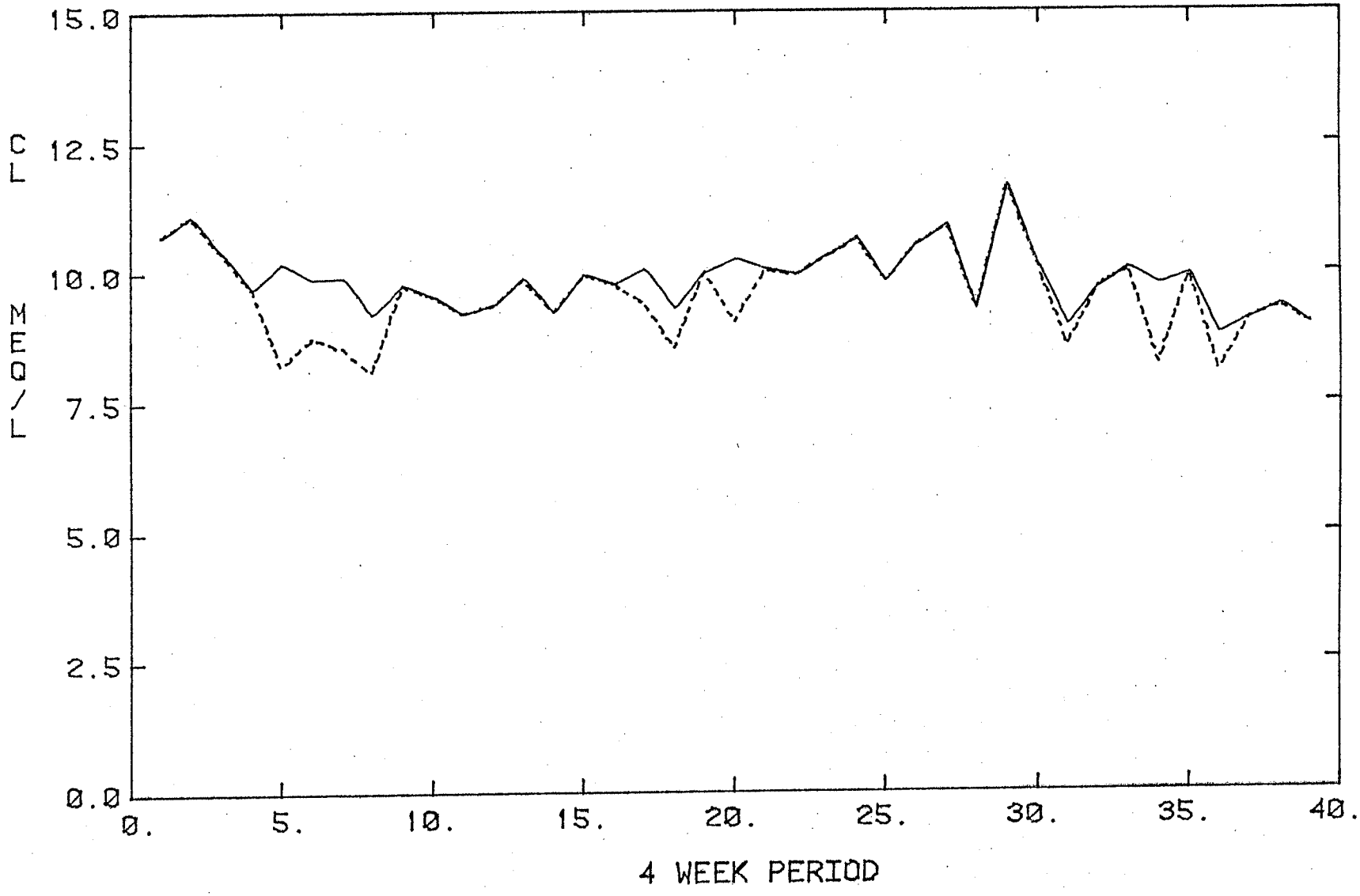

Figure 3.3.3: Observed (---) and Tailwater Adjusted (——) Drain Concentrations.

in the form

$$\varepsilon_{2i} = \frac{(K_2h_2/K_1\bar{h}_{1i})\ \varepsilon_{Ii} - q_{ri}}{1 + K_2h_2/K_1\bar{h}_{1i}} \qquad (3.3.22)$$

where $\bar{h}_{1i} = (h_{1i} + h_{1i-1})/2$,

the average upper layer saturated thickness during period i.

All inputs to the mass balance equations (3.3.10) and (3.3.12) through (3.3.15) are now either calculated or assumed. For each period the directions (signs) of the regional and interlayer flow rates determine the appropriate mass balance equations to be solved for C_{1i} and C_{2i}. The finite difference representations of the mass balance equations for the three system states are given as follows:

For $\varepsilon_{2i} > 0$

$$n_1 \frac{(h_{1i} + h_{1i-1})}{2}\frac{(C_{1i} - C_{1i-1})}{\Delta t} + (n_1 - S_y)\ \frac{(C_{1i} + C_{1i-1})}{2}\frac{(h_{1i} - h_{1i-1})}{\Delta t}$$

$$= \varepsilon_{Ii}\left[C_{Ii} - \frac{(C_{1i} + C_{1i-1})}{2}\right] \qquad (3.3.23)$$

if $q_{ri} > 0$ (system state (1))

$$n_2h_2\ \frac{(C_{2i} - C_{2i-1})}{\Delta t} = \varepsilon_{2i}\left[\frac{(C_{1i} + C_{1i-1})}{2} - \frac{(C_{2i} + C_{2i-1})}{2}\right]$$

$$+ q_{ri}\left[C_r - \frac{(C_{2i} + C_{2i-1})}{2}\right] \qquad (3.3.24)$$

if $q_{ri} < 0$ (system state (2))

$$n_2 h_2 \frac{(C_{2i} - C_{2i-1})}{\Delta t} = \varepsilon_{2i} \left[\frac{(C_{1i} + C_{1i-1})}{2} - \frac{(C_{2i} + C_{2i-1})}{2} \right] \quad (3.3.25)$$

For $\varepsilon_{2i} < 0$ and $q_{ri} > 0$ (system state (3))

$$n_2 h_2 \frac{(C_{2i} - C_{2i-1})}{\Delta t} = q_{ri} \left[C_r - \frac{(C_{2i} + C_{2i-1})}{2} \right] \quad (3.3.26)$$

$$n_1 \frac{(h_{1i} + h_{1i-1})(C_{1i} - C_{1i-1})}{2} \frac{}{\Delta t} + (n_1 - S_y) \frac{(C_{1i} + C_{1i-1})}{2} \frac{(h_{1i} - h_{1i-1})}{\Delta t}$$

$$= \varepsilon_{Ii} \left[C_{Ii} - \frac{(C_{1i} + C_{1i-1})}{2} \right] - \varepsilon_{2i} \left[\frac{(C_{2i} + C_{2i-1})}{2} - \frac{(C_{1i} + C_{1i-1})}{2} \right] \quad (3.3.27)$$

The drain discharge rates from the layers are found from the water balance equations (3.3.6) and (3.3.7) in the forms

$$q_{d1i} = \varepsilon_{Ii} - \varepsilon_{2i} - \frac{S_y}{\Delta t} (h_{1i} - h_{1i-1}) \quad (3.3.28)$$

and

$$q_{d2i} = \varepsilon_{2i} + q_{ri} \quad (3.3.29)$$

The simulated drain concentration is then computed using equation (3.3.16) as

$$C'_{di} = \frac{q_{d_1 i}}{q_{di}} C_{1i} + \frac{q_{d_2 i}}{q_{di}} C_{2i} \quad (3.3.30)$$

where $q_{di} = q_{d1i} + q_{d2i}$.

The simulation is initialized by assuming the upper layer possesses an average chloride concentration of 9 meq/l, the average chloride concentration observed in a 20 foot depth observation well during that period. The first period concentration of the lower layer is obtained by setting C'_{d1} in (3.3.30) equal to the observed drain concentration for period one and solving for C_{21}. The result is a reproduction of the observed drain concentration for the first period.

The following algorithm describes the computational process of the model:

Read: effective porosities (n_1,n_2); specific yield (S_Y); lower layer thickness (h_2); irrigation efficiency (μ); and, first period upper layer concentration (C_{11}).

Read for each period:

irrigation application amount ($\hat{q}_{Ii}$) and concentration ($\hat{C}_{Ii}$); measured drain flow rate ($\hat{q}_{di}$) and concentration ($\hat{C}_{di}$); upper layer saturated thickness (h_{1i}); regional inflow quality (C_{ri}); and, tailwater coefficient (η_i).

Compute for all periods:

tailwater adjusted drainflow (q_{di}) and concentration (C_{di}) using equations (3.3.19) and (3.3.20);

irrigation recharge (ε_{Ii}) and concentration (C_{Ii}) using equations (3.3.17) and (3.3.18);

regional flow rate (q_{ri}) from(3.3.21); and,

interlayer flow rate (ε_{2i}) from (3.3.22).

Compute C_{21} which reproduces the observed first period drain concentration using (3.3.30).

For periods 2 through 39:

If $\varepsilon_{2i} > 0$

solve (3.3.23) for upper layer concentration (C_{1i})

if $q_{ri} > 0$, solve (3.3.24) for lower layer concentration (C_{2i})

if $q_{ri} < 0$, solve (3.3.25) for lower layer concentration (C_{2i})

If $\varepsilon_{2i} < 0$

solve (3.3.26) for lower layer concentration (C_{2i})

solve (3.3.27) for upper layer concentration (C_{1i})

Compute upper layer outflow rate (q_{d1i}) from (3.3.28)

Compute lower layer outflow rate (q_{d2i}) from (3.3.29)

Compute predicted drain concentration (C'_{di}) from (3.3.30)

Simulation

Several simulations were performed using various combinations of values for the conductivity ratio and regional inflow concentration. In the study by Senn, the optimal value for the unknown regional inflow concentration was 20.5 meq/l. More information about the regional flow quality can be obtained from deep observation wells. As mentioned in section 2.1.3, the average chloride concentration observed in three wells at depths of 50 to 65 feet is about 22 meq/l. Two other wells at depths of 18 and 63 feet were installed near the main drain at borehole site H1 (Figure 1.1.1) in the summer of 1980. One set of samples taken during that summer indicated chloride concentrations of 23 meq/l in the shallow well and 28 meq/l in the deeper well. Water levels in the wells at the time of sampling indicated an upward flow. Based on the value obtained by Senn and the concentrations observed in the deep wells, regional inflow concentrations between 20 and 28 meq/l were tried in the simulations.

The conductivity ratio embodies the effects of the shallow clay. Since the hydraulic properties and lateral extent of the clay are unknown, it is difficult to ascertain a reasonable range of values for this parameter. The conductivity ratio K_1/K_2 was assumed to be greater than unity due to the assignment of the shallow clay to the lower layer.

The most favorable results were obtained with a regional inflow concentration of 23 meq/l and a conductivity ratio of 10. Figure 3.3.4 is a plot of simulated and tailwater adjusted drain concentration histories for this run. The simulated regional and interlayer flow rates, layer concentrations, and drain concentration for each period are listed in Table 3.3.4. The simulation of higher than observed drain concentrations for periods 37, 38, and 39 may be due to inaccurate drain flow measurements. In October of 1980 there appeared to be a downstream obstruction in the main drain causing unusually high stage readings at the middle drain recording station. This produced an overestimation of drain discharge for the last three periods and thus a greater simulated regional inflow rate due to the water balance assumptions. The high concentration of the regional inflow in turn caused high predicted drain concentrations.

Chloride mass output rates for the simulation were computed with and without the effect of tailwater. The simulated and observed mass outflow histories for the case of tailwater exclusion are shown in Figure 3.3.5. The inclusion of tailwater does not significantly change the mass outflow histories due to the much lower tailwater volume and concentration as compared to aquifer outflow volume and concentration.

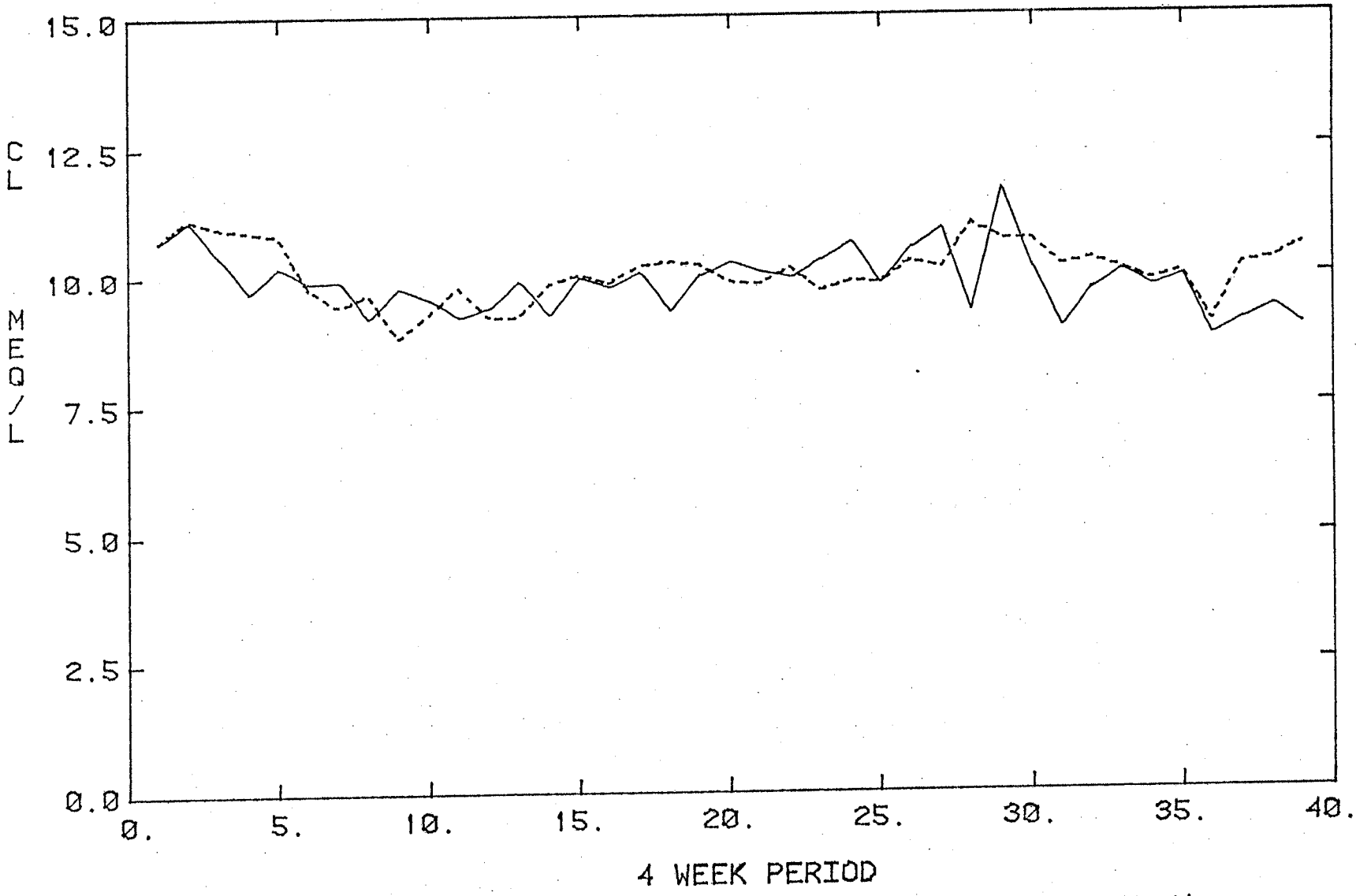

Figure 3.3.4: Simulated (---) and Tailwater Adjusted (——) Drain Concentrations.

Table 3.3.4: Simulated Regional and Interlayer Flow Rates, Layer Chloride Concentrations, and Drain Chloride Concentrations

Period No.	Regional Flow q_r(ft/4wk)	Layer Interflow ε_2(ft/4wk)	Layer Concentrations Upper C_1(meq/l)	Lower C_2(meq/l)	Drain Conc. C'_d(meq/l)
1	.016	-.012	9.00	18.05	10.73
2	.014	-.002	8.92	18.05	11.16
3	.056	-.044	8.95	18.08	10.98
4	-.051	.102	8.58	18.01	10.90
5	.122	-.032	8.07	18.05	10.82
6	.190	-.105	7.98	18.12	9.78
7	.075	.008	7.78	18.14	9.40
8	.193	-.101	7.68	18.21	9.66
9	-.138	.174	7.62	18.07	8.81
10	-.130	.175	7.39	17.94	9.30
11	-.073	.120	7.11	17.84	9.78
12	.132	-.104	7.25	17.89	9.21
13	.180	-.144	7.49	17.96	9.19
14	.272	-.218	7.75	18.06	9.85
15	.246	-.197	7.98	18.15	10.04
16	.205	-.167	8.27	18.22	9.85
17	.309	-.175	8.03	18.33	10.20
18	.494	-.376	8.39	18.50	10.28
19	.312	-.184	8.28	18.60	10.21
20	.199	-.100	8.18	18.67	9.88
21	.193	-.096	8.20	18.73	9.84
22	.252	-.150	8.15	18.81	10.15
23	-.008	.047	8.01	18.77	9.72
24	.145	-.075	7.96	18.82	9.90
25	.129	-.101	8.13	18.86	9.87
26	.136	-.107	8.27	18.90	10.28
27	.096	-.076	8.40	18.93	10.13
28	.098	-.073	8.42	18.96	10.99
29	.124	-.101	8.55	18.99	10.70
30	.093	-.004	8.08	19.02	10.69
31	.329	-.248	8.43	19.12	10.18
32	.342	-.173	8.12	19.21	10.31
33	.374	-.243	8.25	19.32	10.12
34	-.021	.093	7.95	19.24	9.89
35	.088	-.008	7.57	19.26	10.06
36	.081	-.036	7.69	19.29	9.06
37	.236	-.193	7.99	19.35	10.19
38	.231	-.188	8.30	19.41	10.28
39	.215	-.173	8.55	19.47	10.55

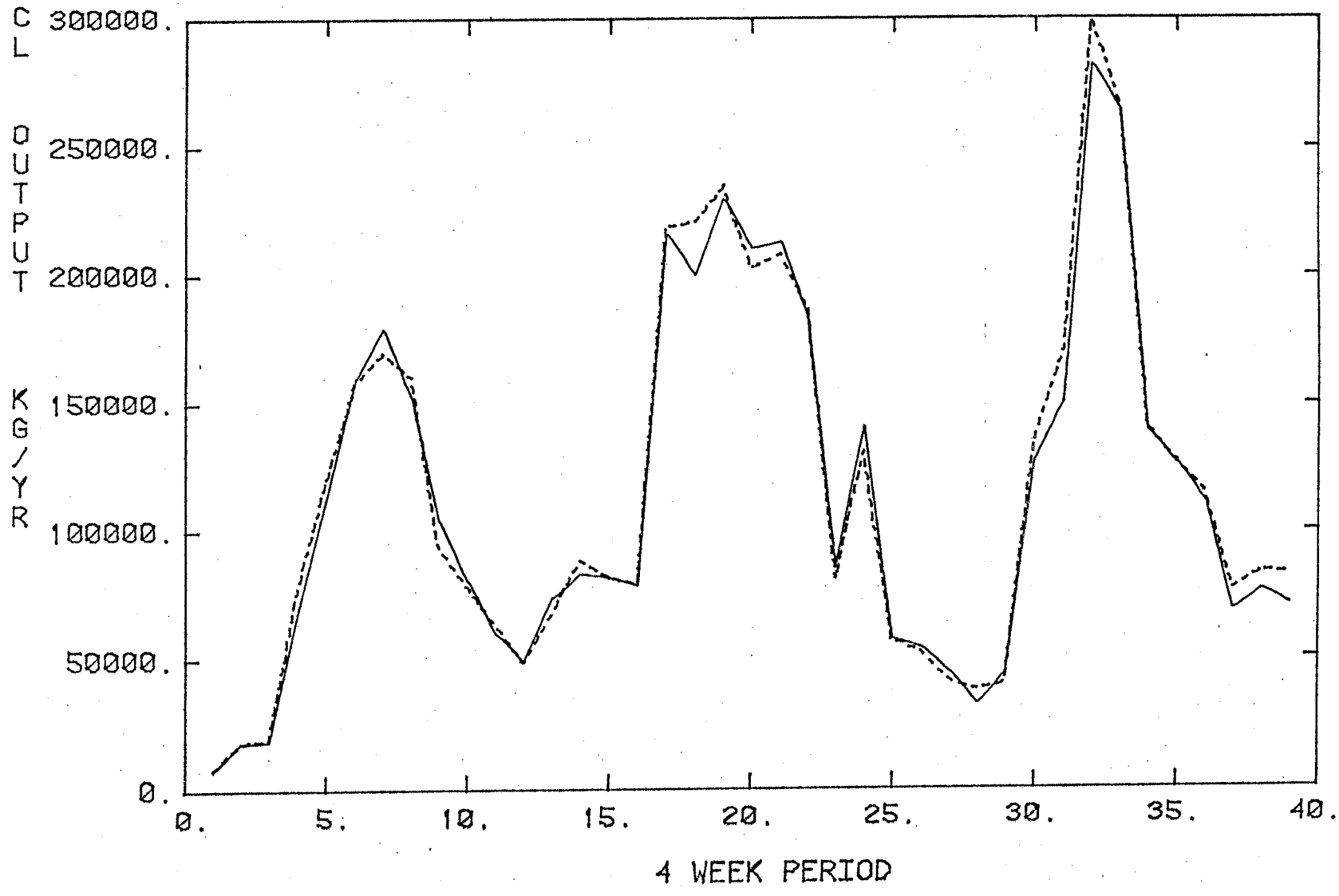

Figure 3.3.5: Simulated (---) and Observed (——) Mass Outflow Rates without Tailwater Effects.

3.3.3 Discussion

An important implication of this study is that the flow system is not one in which a simple flushing of high initial concentration groundwater occurs. Rather it is a dynamic system dominated by regional inflow. Following is a comparison of yearly regional inflow and surficial recharge rates obtained from the transient model simulation:

Year	Regional Inflow (ft/yr)	Irrigation and Precipitation Recharge (ft/yr)
1978	0.98	2.81
1979	2.81	2.53
1980	2.07	2.47

Based on these figures, regional inflow constitutes roughly 43 percent of the total inflow to the system during the three year period. The regional inflow of 1978 may not be indicative of a typical year due to the dry conditions prevalent in the Rio Grande valley during 1977. Assuming the conditions during 1979 and 1980 are representative of most years, the average regional inflow and surface recharge rates could be considered as equivalent. Most of the inflow to the system is conveyed through the more transmissive upper layer as indicated by the frequency of negative simulated interlayer flow rates. The lower layer, receiving little input from the upper layer, maintains a high concentration due to the regional inflow. Upper layer concentrations are higher than irrigation recharge concentrations due to inflow from the lower layer.

Another inference of this study deals with the magnitude of effective porosity at the farm. In the single cell study by Senn, the effective porosity was assumed equal to the specific yield of 0.19 determined from drain flow recessions. Underthis assumption the mass balance

equation for the single cell model is

$$(nh)\frac{dC}{dt} = (S_y h)\frac{dC}{dt} = \varepsilon_I(C_I - C) + q_r(C_r - C)$$

where the storage term

$$(n - S_y)\, C\, \frac{dh}{dt}$$

of equation (3.1.3) is zero. Noting that the effective porosity and saturated thickness appear as a product in the mass balance equation, this product could be treated as a single "pore thickness" parameter. The average saturated thickness in the single cell study was approximately 62 feet, implying a pore thickness of

$$nh = S_y h = (0.19)(62\ \text{ft}) = 11.8\ \text{ft}$$

under the assumption of equal effective porosity and specific yield. An equivalent pore thickness would be obtained with an average saturated thickness of 34 feet and the effective porosity of 0.35 based on measured values. The single cell model would thus be roughly analogous to the two cell model with the shallow clay assigned to the upper cell. The amount of regional inflow simulated by the two models would be approximately the same in order to preserve a water balance, and the optimal regional inflow concentration of the single cell model would be less than that of the two cell model due to mixing in the layer below the shallow clay. In support of this analogy, the average regional inflow rate for 1978 and 1979 determined by Senn is 1.95 ft/yr as compared to 1.90 ft/yr simulated here, and the optimal regional inflow concentrations were 20.5 meq/l in the single cell study and 23 meq/l in the two cell study. The

point of this comparison is that effective porosity is a parameter worthy of investigation in groundwater quality studies. An effective porosity of 0.30 to 0.35 is believed to be representative of the alluvial middle drain aquifer, a range closer to the total porosity than the specific yield.

As indicated by the results of this study, the lumped parameter model may be used to simulate a complex transient system. The simple conceptual base and ease of generalization make the model a versatile investigative tool. The model presented here has limited predictive capability due to the required input of the transient drain flow. However, it does provide estimates of important parameters and a possible description of the middle drain flow system.

4. THE COUPLED U. S. BUREAU OF RECLAMATION CHEMISTRY-FINITE ELEMENT FLOW MODEL

4.1 INTRODUCTION

The U.S. Bureau of Reclamation water quality model (Shaffer et al., 1977) is capable of modeling an irrigated aquifer from the soil surface to a tile or open drain. In general, the model consists of seven modules: Irrigation Scheduling, Unsaturated Flow, Unsaturated Chemistry, Saturated Flow, Saturated Chemistry, Drainout, and Drain Effluent Prediction. The Irrigation Scheduling module performs several functions including simulation of irrigation and precipitation amounts and timing, calculation of evapotranspiration, and determination of deep percolation water volumes. The Unsaturated Flow module simulates one dimensional unsaturated flow between the soil surface and water table including infiltration, redistribution, plant root extraction, and drainage of soil water under a growing crop. The Unsaturated Chemistry module models important biological and chemical reactions in the unsaturated zone. The Saturated Flow module simulates the average or steady-state response of a drainage system to deep percolation inputs, and the Drainout module predicts the transient response of a drainage system to deep percolation inputs. The Saturated Chemistry module handles the chemistry of the saturated soil-water system and salt movement across the base of the aquifer. Finally, the Drain Effluent Prediction module combines the outputs of the Drainout, Saturated Flow, and Saturated Chemistry modules to simulate solute concentrations in the drains.

The model versatility allows simulation of only the desired irrigation system components by using the appropriate modules. A model version bypassing the unsaturated zone simulation modules was used for

sensitivity analysis and preliminary simulations of the middle drain flow system for the period 1950 through 1978 by Simonett (in Gelhar et al., 1980, pp. 49-66). The flow modules of the U.S. Bureau of Reclamation model assume the aquifer is homogeneous, isotropic, and receives surficial recharge only. Therefore, a separate finite element flow model will be used in this study to simulate steady-state flow in the layered farm aquifer including both regional and irrigation inflow components. The simulated potential distribution will be used to construct a flow net from which stream tube pore volumes and travel times will be determined for the tubes conveying irrigation recharge. This information is required by the Saturated Chemistry and Drain Effluent Prediction programs which are used to simulate outflow concentrations of the irrigated flow system defined by these stream tubes. Drain concentrations are simulated by mixing the outflow of the irrigation system with the outflow of the regional flow system defined by the remaining stream tubes.

4.2 THE FLOW MODEL

4.2.1 Flow Model Development

The governing equation defining the hydraulic head distribution for steady flow in a vertical section of a heterogeneous isotropic aquifer is

$$L(h) = \frac{\partial}{\partial x}\left(K_x \frac{\partial h}{\partial x}\right) + \frac{\partial}{\partial y}\left(K_y \frac{\partial h}{\partial y}\right) = 0 \qquad (4.2.1)$$

where K_x and K_y are the hydraulic conductivities in the horizontal and vertical directions, and $h(x,y)$ is the total hydraulic head.

The boundaries of a vertical section of the middle drain aquifer are depicted in Figure 4.2.1(a). The upper boundary consists of the drain, road and irrigated fields. The respective boundary conditions for these segments are

$$h(x,b) = b \quad \text{for} \quad d \le x \le L\,, \qquad (4.2.2)$$

$$\left.\frac{\partial h}{\partial y}\right|_{y=b} = 0 \quad \text{for} \quad r \le x < d\,, \qquad (4.2.3)$$

and

$$\left.K_y \frac{\partial h}{\partial y}\right|_{y=b} = -\varepsilon \quad \text{for} \quad 0 \le x < r \qquad (4.2.4)$$

where ε is the rate of irrigation recharge. The lower boundary is subject to the condition

$$\left.K_y \frac{\partial h}{\partial y}\right|_{y=0} = -q_r \quad \text{for} \quad 0 \le x \le L \qquad (4.2.5)$$

where q_r is the rate of regional inflow. Assuming flow symmetry, the vertical boundaries at the water table divide and drain centerline are treated as impermeable, thus

(a)

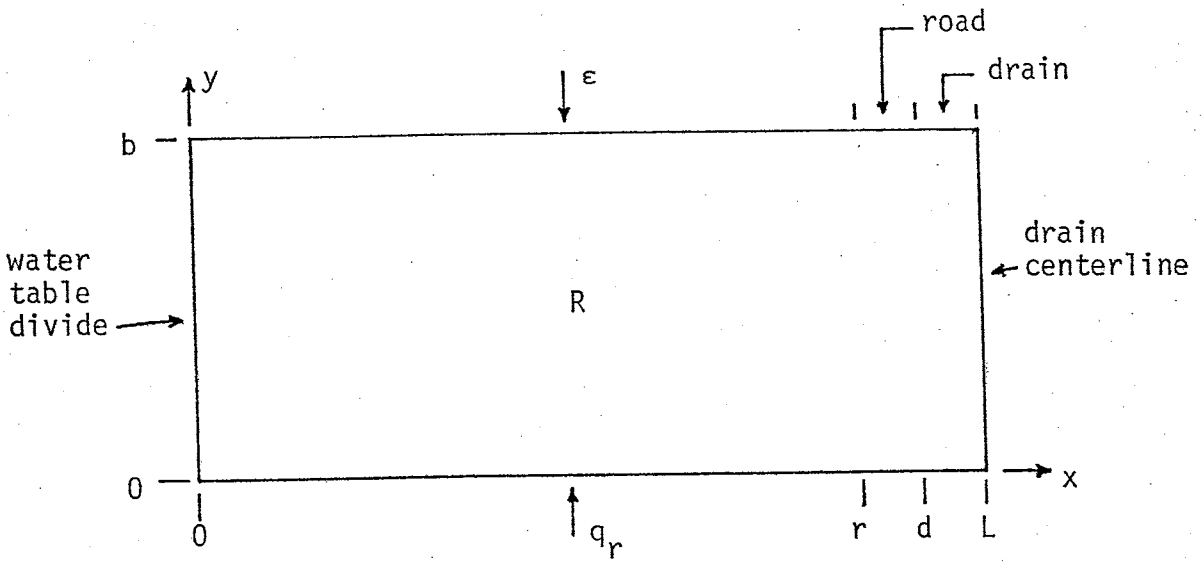

(b)

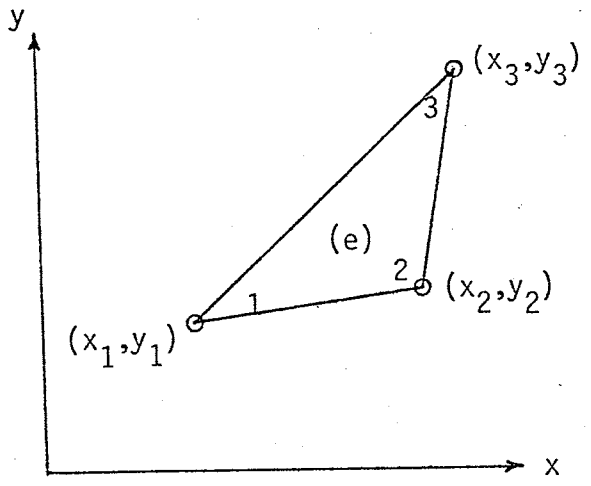

Figure 4.2.1: Vertical Section of the Middle Drain Aquifer, (a); and, Representation of a Typical Element, (b).

$$\left.\frac{\partial h}{\partial x}\right|_{x=0} = \left.\frac{\partial h}{\partial x}\right|_{x=L} = 0 \quad \text{for} \quad 0 \le x \le b \qquad (4.2.6)$$

The hydraulic head distribution described by the governing flow equation (4.2.1) and boundary conditions (4.2.2) through (4.2.6) is approximated using the Galerkin finite element approach. Linear triangular elements are used to discretize the system. For a typical element with nodes labeled 1, 2 and 3 as shown in Figure 4.2.1(b), the weighting or basis functions used to define the hydraulic head distribution and coorinate transformation are given by

$$N_p(x,y) = (a_p + b_p x + c_p y)/2A \quad , \quad p = 1,2,3 \qquad (4.2.7)$$

where A is the element area defined as

$$A = \frac{1}{2} \det \begin{bmatrix} 1 & x_1 & y_1 \\ 1 & x_2 & y_2 \\ 1 & x_3 & y_3 \end{bmatrix}$$

and the coefficients a_p, b_p and c_p are given in the following table:

p	a_p	b_p	c_p
1	$x_2y_3 - y_2x_3$	$y_2 - y_3$	$x_3 - x_2$
2	$x_3y_1 - y_3x_1$	$y_3 - y_1$	$x_1 - x_3$
3	$x_1y_2 - y_2x_1$	$y_1 - y_2$	$x_2 - x_1$

Using this definition of the weighting functions, the hydraulic head at any point (x,y) within the element is linearly approximated by

$$h(x,y) \cong \sum_{p=1}^{3} h_p N_p (x,y)$$

where h_p (p=1,2,3) are the known values of hydraulic head at the element nodes.

The head distribution for the entire discretized system is approximated with the trial function

$$\hat{h}(x,y) = \sum_{j=1}^{n} h_j N_j(x,y) \cong h(x,y) \tag{4.2.8}$$

where n is the total number of modes in the system. A residual or error introduced by substituting the trial function (4.2.8) into (4.2.1) is defined as

$$E = L(\hat{h}) \tag{4.2.9}$$

To obtain an exact solution, the residual must vanish. This is equivalent to requiring orthogonality of the residual with the weighting function, $N_i(x,y)(i=1,2....,n)$, as given by the system of equations

$$\int_R N_i \left[\frac{\partial}{\partial x} \left(K_x \frac{\partial \hat{h}}{\partial x} \right) + \frac{\partial}{\partial y} \left(K_y \frac{\partial \hat{h}}{\partial y} \right) \right] dR = 0 \quad , \quad i = 1,\ldots,n \tag{4.2.10}$$

where R is the solution domain. Using the divergence theorem, the system of equations (4.2.10) may be written as

$$\int_R \left(\frac{\partial N_i}{\partial x} K_x \frac{\partial \hat{h}}{\partial x} + \frac{\partial N_i}{\partial y} K_y \frac{\partial \hat{h}}{\partial y} \right) dR$$

$$= \int_B N_i \left(\vec{i}\, K_x \frac{\partial \hat{h}}{\partial x} + \vec{j}\, K_y \frac{\partial \hat{h}}{\partial y} \right) \cdot \vec{n}\, dB \quad , \quad i = 1,\ldots,n \tag{4.2.11}$$

where B is the boundary of the solution domain, $\vec{n}$ is the unit outward vector normal to the boundary, and $\vec{i}$ and $\vec{j}$ are the unit vectors in the x and y directions. Substituting the trial function (4.2.8) and boundary conditions (4.2.4) and (4.2.5) in the forms

$$\vec{j}\, K_y \frac{\partial h}{\partial y}\bigg|_{y=b} = \varepsilon \qquad 0 \le x < r$$

and $$\vec{j}\, K_y \frac{\partial h}{\partial y}\bigg|_{y=0} = -q_r \qquad 0 \le x \le L$$

into equation (4.2.11) yields

$$\int_R \left(K_x \frac{\partial N_i}{\partial x} \sum_{j=1}^{n} \frac{\partial N_j}{\partial x} h_j + K_y \frac{\partial N_i}{\partial y} \sum_{j=1}^{n} \frac{\partial N_j}{\partial y} h_j \right) dR$$

$$= \int_{B_1} \varepsilon N_i dB_1 + \int_{B_2} q_r N_i dB_2 \quad , \quad i = 1,\ldots,n \tag{4.2.12}$$

where the boundary B_1 is defined by $y = b$, $0 \le x < r$; and the boundary B_2 is defined by $y = 0$, $0 \le x \le L$.

The system of equations represented by (4.2.12) may be expressed in matrix form as

$$[A]\,\{h\} = \{F\} \tag{4.2.13}$$

where [A] is the global stiffness matrix (nxn), {F} is the force vector (n x 1), and {h} is the unknown hydraulic head vector (n x 1). The global stiffness matrix and force vector are defined as

$$[A] = \sum_{e=1}^{m} [a]_e \tag{4.2.14}$$

and $$\{F\} = \sum_{e=1}^{m} \{f\}_e \tag{4.2.15}$$

where $[a]_e$ is the elementary stiffness matrix (3 x 3), $\{f\}_e$ is the

elementary force vector (3 x 1), and m is the total number of elements in the system. The entries of the elementary stiffness matrix are given by

$$a_{ij} = \int_{R^e} \left(K_x \frac{\partial N_i}{\partial x} \frac{\partial N_j}{\partial x} + K_y \frac{\partial N_i}{\partial y} \frac{\partial N_j}{\partial y} \right) dR^e \qquad (4.2.16)$$

$$= \left(K_x b_i b_j + K_y c_i c_j \right) / 4A^e \quad , \qquad i,j = 1,2,3$$

where A^e is the element area and b_p, c_p ($p = 1,2,3$) are as defined in equation (4.2.7). The elementary stiffness matrix symmetry produces a symmetric global stiffness matrix. The entries of the elementary force vector are nonzero only if the element possesses a side on boundary B_1 or B_2. The elementary force vector for an element on boundary B_1 is

$$\{f\} = \int_{B_1^e} \varepsilon N_i dB^e = \frac{\varepsilon}{2} \ell_{ij} \begin{Bmatrix} 1 \\ 1 \\ 0 \end{Bmatrix} \text{ if side ij is on } B_1$$

$$= \frac{\varepsilon}{2} \ell_{ik} \begin{Bmatrix} 1 \\ 0 \\ 1 \end{Bmatrix} \text{ if side ik is on } B_1$$

$$= \frac{\varepsilon}{2} \ell_{jk} \begin{Bmatrix} 0 \\ 1 \\ 1 \end{Bmatrix} \text{ if side jk is on } B_1 \qquad (4.2.17)$$

where ℓ_{pq} is the length of the element side defined by nodes p and q (Pinder and Gray, 1977). Half of the flux received by the element is assigned to each of the two boundary nodes using this definition of the elementary force vector. The elementary force vectors for elements on the lower recharge boundary, B_2, are identical to (4.2.17) with q_r replacing ε.

Formation of the global stiffness matrix and force vector defined by equations (4.2.14) and (4.2.15) is accomplished by using two sets of subscripts for the nodes. The nodes numbered 1,2,3 for a given element are also assigned corresponding unique global node numbers p, q, r $\in \{1,\ldots,n\}$. For each element the elementary stiffness matrix entries $a_{11}, a_{12},\ldots,a_{33}$ are determined and added to the corresponding entries $A_{pp}, A_{pq},\ldots,A_{rr}$ of the global stiffness matrix. Similarly, the elementary force vector entries f_1, f_2, f_3 are calculated for each element and added to the corresponding global force vector entries F_p, F_q, F_r. After formation, the global stiffness matrix and force vector are modified to incorporate the known head values of nodes located on the drain. The system of equations defined by (4.2.13) is then solved for the nodal head distribution using a numerical matrix inversion technique.

4.2.2 Flow Model Application

The model was applied to the vertical section in which flow is perpendicular to the middle drain. This section, defined by a line normal to both the water table divide and middle drain, is roughly 800 feet in length as measured on the north side of the middle drain in Figure 3.3.2. A value of 10 feet was assigned to the road width and half-width of the drain. The drain width was slightly exaggerated to compensate for the convergence of streamlines near the drain.

The average amount of irrigation and precipitation water received by the system from 1978 through 1980 is 5.8 feet per year. Assuming half of this amount becomes recharge, a steady-state irrigation recharge rate of 2.9 feet per year was used in the model. The regional recharge rate was assumed equal to the surface recharge rate based on the results of the transient lumped parameter model discussed in section 3.3.3.

Using the surface of the deeper clay as a datum, the drain water surface elevation is about 64 feet. The shallow clay is assumed to be continuous throughout the aquifer area, composing the interval from 33 to 43 feet above the deeper clay. The aquifer is thus divided into three layers: an upper layer of mostly sand; a middle clay layer; and, a lower layer consisting predominantly of sand and gravel.

Since no direct measurements of the clay or lower layer hydraulic conductivities have been made, they will be estimated relative to the upper layer conductivity. Assuming hydraulic conductivity is proportional to the square of a representative grain size (Bear, 1972, pp. 134-135), the grain size analyses presented in section 2.1.1 (Table 2.1.2) could be used to make a conductivity comparison of the upper and lower layers. Also, the ratio of the arithmetic to harmonic mean squared representative grain size of samples from a single layer would provide an indication of the anisotropy ratio, K_x/K_y. The sampling depth intervals of 3 to 20 feet and 51 to 68 feet were used to represent the upper and lower layers and compute the following means:

Depth(ft)	Arithmetic Mean (mm^2) d_{10}^2	d_{50}^2	Harmonic Mean (mm^2) d_{10}^2	d_{50}^2
3-20	.034	.256	.029	.201
51-68	.025	.140	.024	.128

Based on these arithmetic means and the middle drain area borehole information (section 2.1.1), the lower layer was assigned one half the conductivity of the upper layer. The ratios of the arithmetic to harmonic mean d_{10}^2 and d_{50}^2 values are near unity for both layers indicating little anisotropy. A small anisotropy ratio of $K_x/K_y = 2.25$ was assumed in the

model. No grain size information was available for the intermediate clay layer. The clay was assumed to possess 1/20th of the upper layer conductivity and anisotropy equivalent to the other layers. The average sleeved sample conductivity of 80 ft/day (section 2.1.2) was assigned to the upper layer vertical conductivity. In accordance with the conductivity and anisotropy ratios just assigned, the layer conductivities used in the model are as follows:

Layer	K_x(ft/day)	K_y(ft/day)
upper	180	80
clay	9	4
lower	90	40

When used in the model, these conductivity values produced a water table elevation difference of about 0.9 feet between the divide and drain. A difference in water table elevation of one foot was indicated by the water level in a shallow well near the divide and an elevation of the drain water surface late in the summer of 1980. Although the measured surcharge may not be indicative of a steady-state condition, its proximity to the simulated surcharge suggests that the assumed conductivities produce a total transmissivity representative of the aquifer.

The discretization of the flow system incorporated 450 nodes and 812 elements. The rectangular nodal mesh consisted of 30 columns of 15 nodes arranged to produce a tight spacing near the drain. The nodal coordinates and corresponding simulated head values were used in a contouring subroutine to produce an equivalent isotropic scale model of the flow system with a hydraulic potential contour interval of 0.01 feet. The isotropic representation was obtained by transforming the horizontal coordinate of each node according to

$$x' = (K_y/K_x)^{\frac{1}{2}}x = x/1.5$$

where x and x' are the real and equivalent isotropic horizontal node coordinates respectively. Using a scale of 1 inch:6.4 feet, the resulting dimensions of the scale model were 10 inches vertically and 83.3 inches horizontally. Streamlines were then drawn on the model to produce a total of 18 stream tubes - 9 conveying equal amounts of irrigation recharge and 9 conveying equal amounts of regional recharge. A reproduction of this flow net is shown in Figure 4.2.2. The irrigation stream tube travel times and pore volumes required by the Bureau of Reclamation model were determined using the flow net. The upper layer effective porosity of 0.35 was used in the calculations of travel times along the nine streamlines defining the irrigation stream tubes. Each stream tube travel time was taken as the average of the bounding streamline travel times. The pore volume of each tube is found by multiplying the travel time by the volumetric recharge rate. The travel times and pore volumes of the irrigation stream tubes are given in Table 4.2.1.

Table 4.2.1: Irrigation Stream Tube Travel Times and Pore Volumes

Stream Tube*	Travel Time (yrs.)	Pore Volume (ft^3/ft drain)
1	.098	24.6
2	.333	83.6
3	.641	161.1
4	1.018	255.8
5	1.479	371.7
6	2.066	519.2
7	2.864	719.8
8	4.159	1045.2
9	8.985	2258.3

*Stream tubes are numbered starting nearest to the drain.

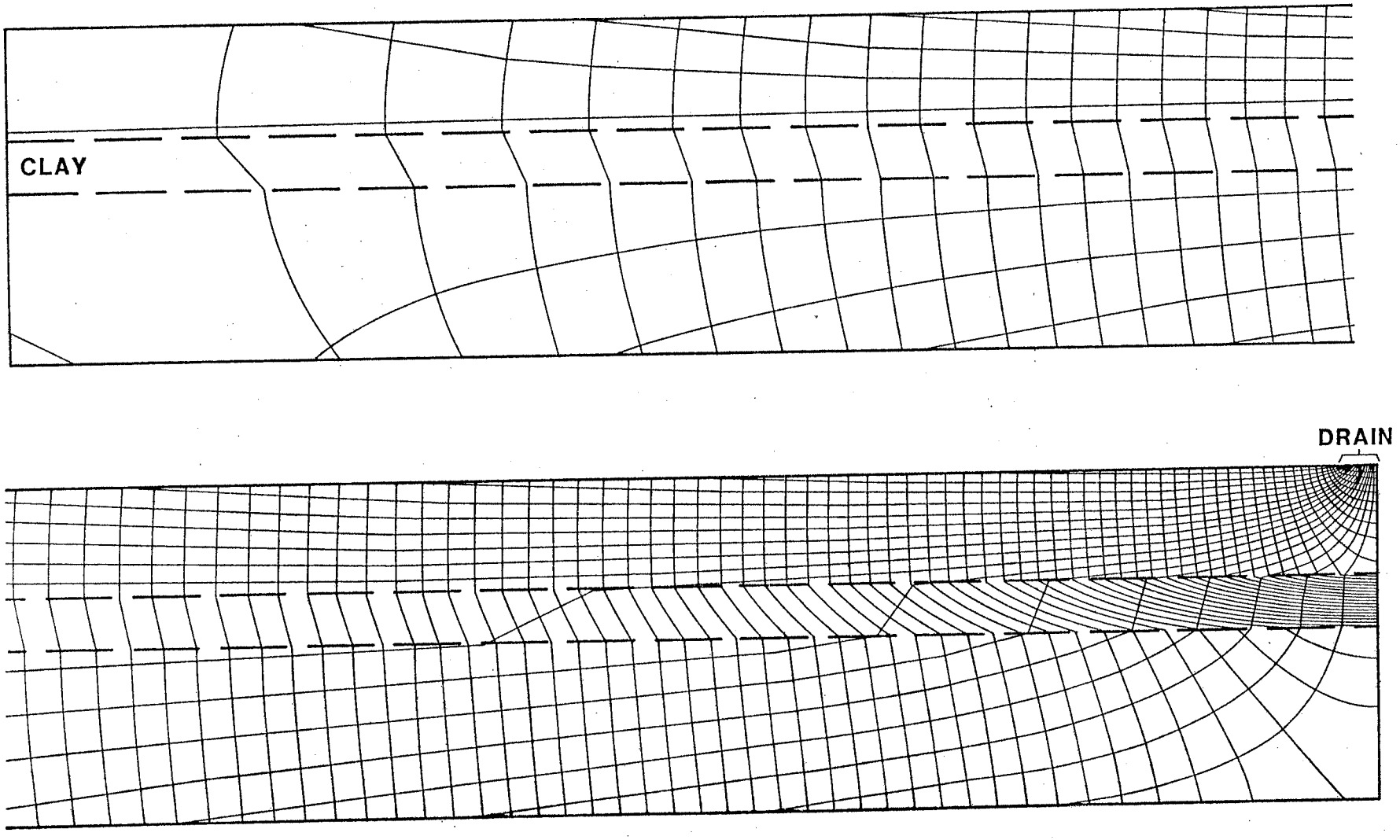

Figure 4.2.2: Simulated Steady-State Flow Net.

4.3 COUPLED MODEL APPLICATION

4.3.1 Steady-State Simulation

The 31 year period of 1950 through 1980 was considered in the steady-state simulations. The Saturated Chemistry and Drain Effluent Prediction programs were used to simulate the irrigation system as defined by the upper nine irrigation stream tubes. Yearly average drain concentrations were simulated by flow weighting the Drain Effluent Prediction program concentrations with the regional inflow concentrations according to

$$C_d = (Q_I C + Q_r C_r)/(Q_I + Q_r)$$

where Q_I = ε (780 ft) = 2262 ft^3/ft. drain/year, the volumetric irrigation recharge rate;

Q_r = q_r (800 ft) = 2320 ft^3/ft.drain/year, the volumetric regional recharge rate;

C = simulated yearly average irrigation system outflow concentration; and,

C_r = regional inflow concentration.

The regional inflow is assumed to possess the average concentrations observed in the three wells at depths of 50 to 65 feet (see Table 2.1.6).

Three model runs were performed to assess the importance of soil-water chemical reactions and the effect of differing initial soil analyses or groundwater compositions. Inputs to the Saturated Chemistry and Drain Effluent Prediction programs for these runs are listed in Table 4.3.1. The initial groundwater condition for run 1 was obtained from the analyses of soil samples from the borehole augered near the middle drain in 1979. The soil analysis concentrations were averaged over the depth

Table 4.3.1: Steady-State Coupled Model Input Data

Saturated Chemistry Program Inputs

Deep Percolation Data

Number of water applications per year	1
Date of application	1-18
Amount of applied water	6.44 ft.
Irrigation efficiency	0.55

Irrigation water analyses

Annual average concentrations for NO_3, Ca, Mg, NH_4, CO_3, Na, HCO_3, Cl and SO_4 obtained for the period 1950 through 1980 as follows:

- 1950-1956 - from analyses of Rio Grande at San Acacia in USGS Water Supply Papers
- 1957-1976 - regressed from analyses of Rio Grande conveyance channel at San Marcial in USGS Water Supply Papers
- 1977-1980 - analyses of irrigation water sampled at farm.

Stream Tube Data

Stream tube pore volumes	listed in Table 4.2.1
Width of each tube at water table	86.67 ft.
Volumetric moisture content at saturation	0.35
Number of divisions of each tube	10

Soil Analysis Data

Constituent	Run 1	Run 2*
	Initial soil conc. (meq/l)	
Ca	17.8	11.3
Mg	5.2	5.0
Na	22.0	24.2
NH_4	0	0
Cl	16.7	21.6
SO_4	26.2	16.2
HCO_3	3.5	3.4
CO_3	0.07	0.07
NO_3	0.02	0.02

*Regional inflow concentrations are identical to initial soil concentrations of Run 2.

Soil Analysis Data (cont.)

	Run 1	Run 2
Calcareous soil indicator	on	on
Gypseous soil indicator	off	off
Dry bulk density (g/cc)	1.72	1.72
Soil extract	0.2035	0.2035
Cation exchange capacity (meq/100g)	5.13	5.13
Partial pressure CO_2 (atm)	0.012	0.012

Drain Effluent Prediction Program Inputs

Monthly drain discharge (acre-ft/acre/month) 0.2417

Stream tube travel times listed in Table 4.2.1

Other inputs obtained from Saturated Chemistry program output.

interval of 30 to 67 feet, the zone assigned to the lower layer, and these averages were used to compute the initial groundwater concentrations assuming a lower layer porosity of 0.30. Run 2 was made using the average deep well (regional inflow) concentrations as the initial groundwater condition. To incorporate these initial conditions in the model, the groundwater concentrations are input as soil analysis concentrations along with a soil extract corresponding to saturation. Run 3 is identical to run 1 with the exception that the soil-water chemical reaction calculations in the Saturated Chemistry program were bypassed.

The simulated drain concentration histories for calcium, sodium, sulfate, bicarbonate, chloride and total dissolved solids (TDS) obtained from runs 1 and 2 with differing initial conditions are shown in Figures 4.3.1 through 4.3.3. The difference in initial conditions has no effect on simulated drain concentrations of the conservative constituents, chloride and sulfate, after complete displacement of the irrigation stream tubes in 1958. Simulated drain concentrations of the nonconservative constituents, calcium, sodium and bicarbonate, for the two runs display only minor differences after 1958.

Figures 4.3.4 and 4.3.5 are plots of simulated drain calcium, sodium, bicarbonate and TDS concentrations from runs 1 and 3. Simulated sodium concentrations increase and calcium and bicarbonate concentrations decrease with the inclusion of soil-water chemical reactions, possibly indicating replacement of sodium by calcium on the matrix surface and precipitation of calcium carbonate. The lower simulated TDS concentrations of the run including reactions is attributed mostly to the decrease in calcium and bicarbonate concentrations.

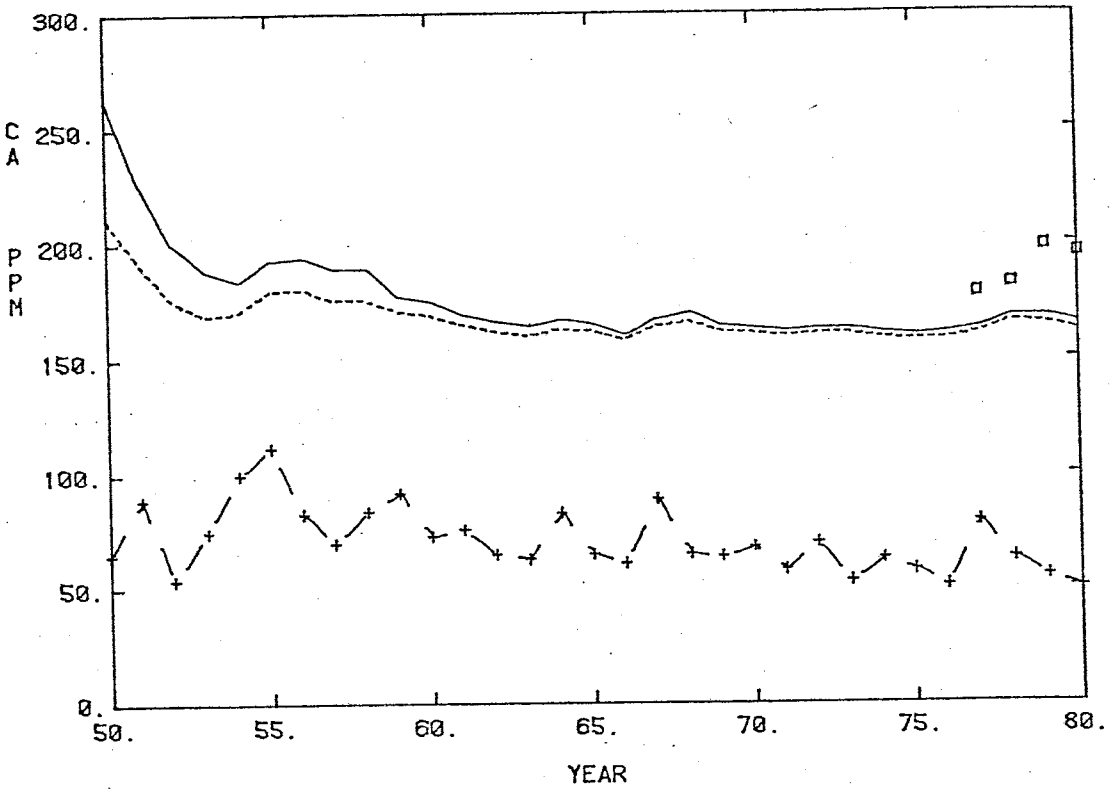

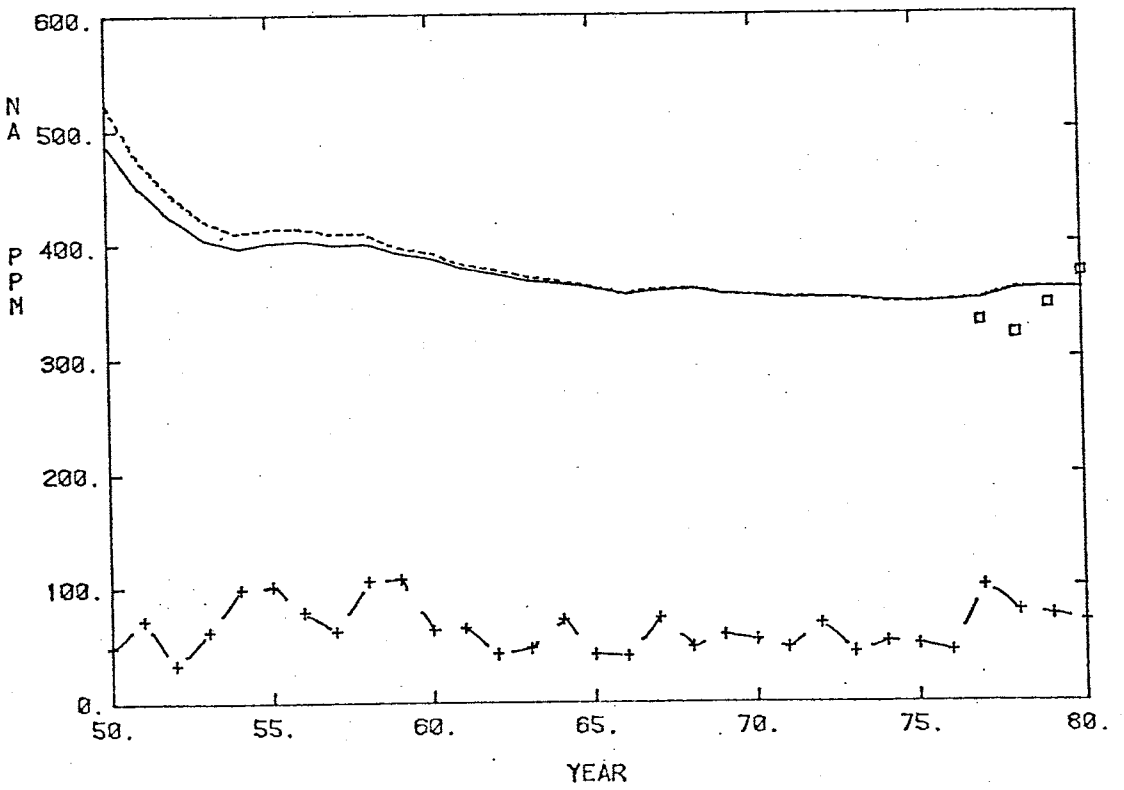

Figure 4.3.1: Simulated Drain Calcium and Sodium Concentrations for Soil Analysis (——) and Deep Well Concentrations (---) Initial Conditions; Observed Drain Concentrations (□); and, Irrigation Water Concentrations (-+-).

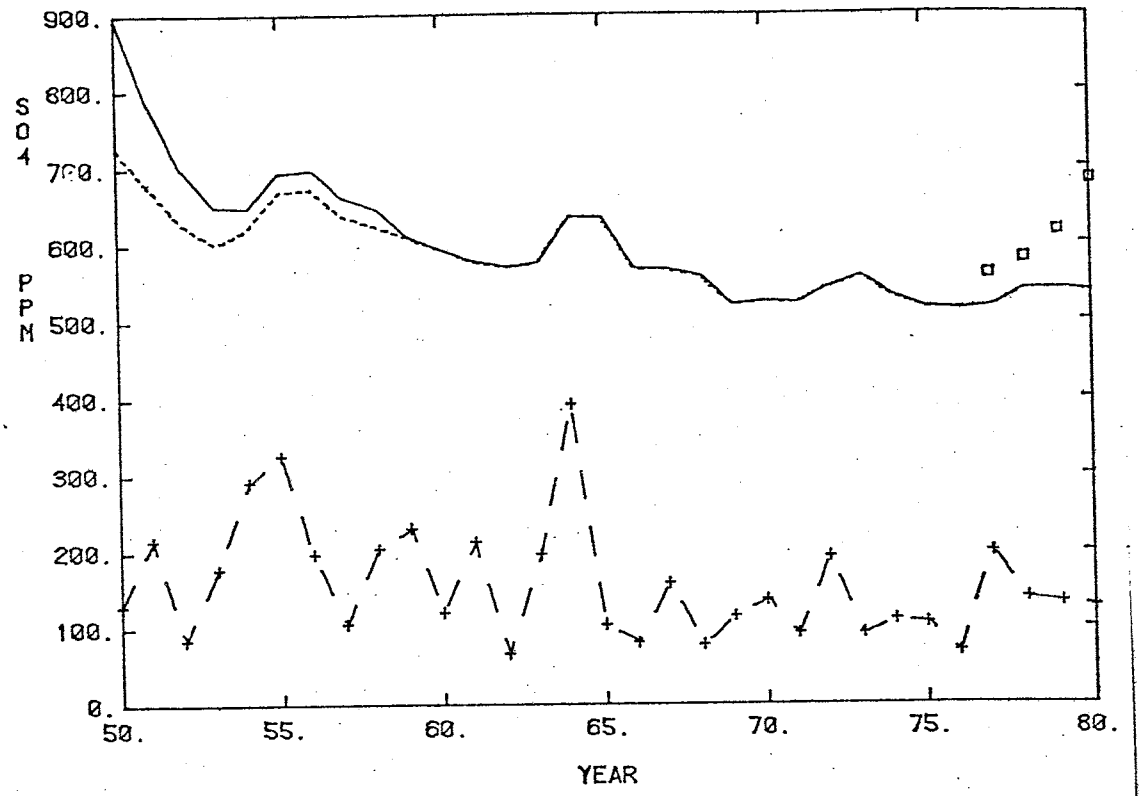

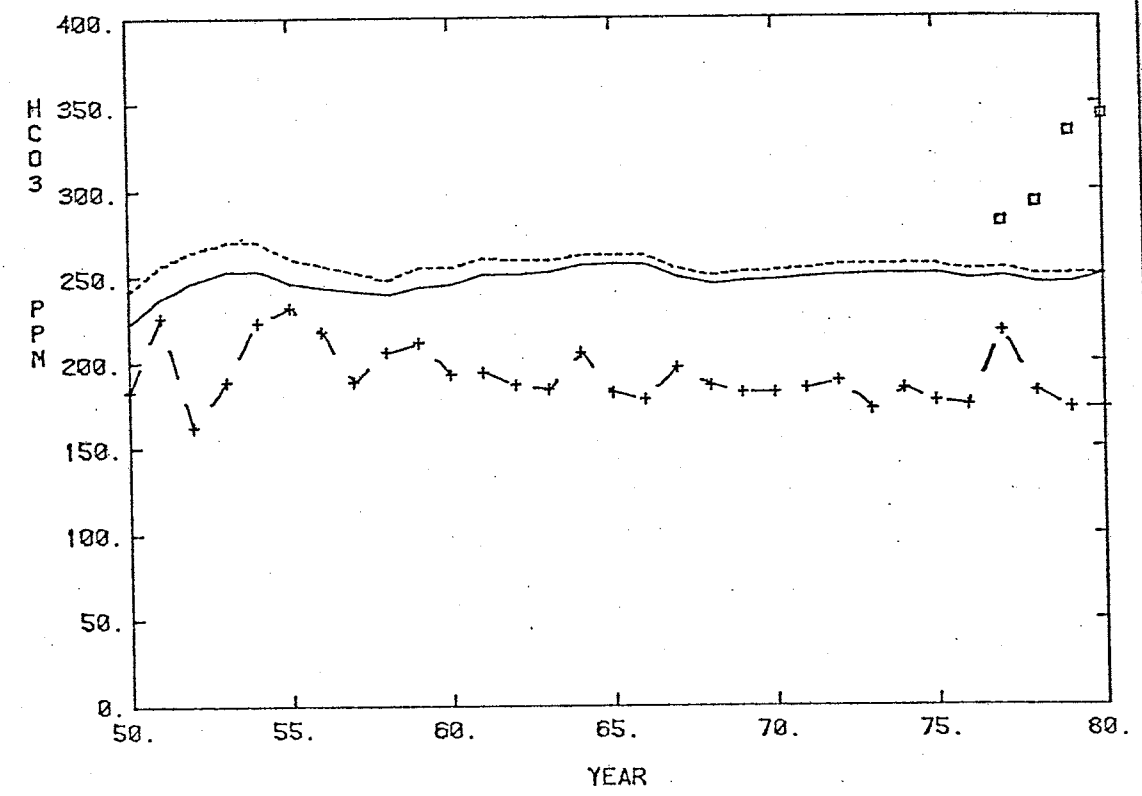

Figure 4.3.2: Simulated Drain Sulfate and Bicarbonate Concentrations for Soil Analysis (——) and Deep Well Concentrations (---) Initial Conditions; Observed Drain Concentrations (□); and, Irrigation Water Concentration (-+-).

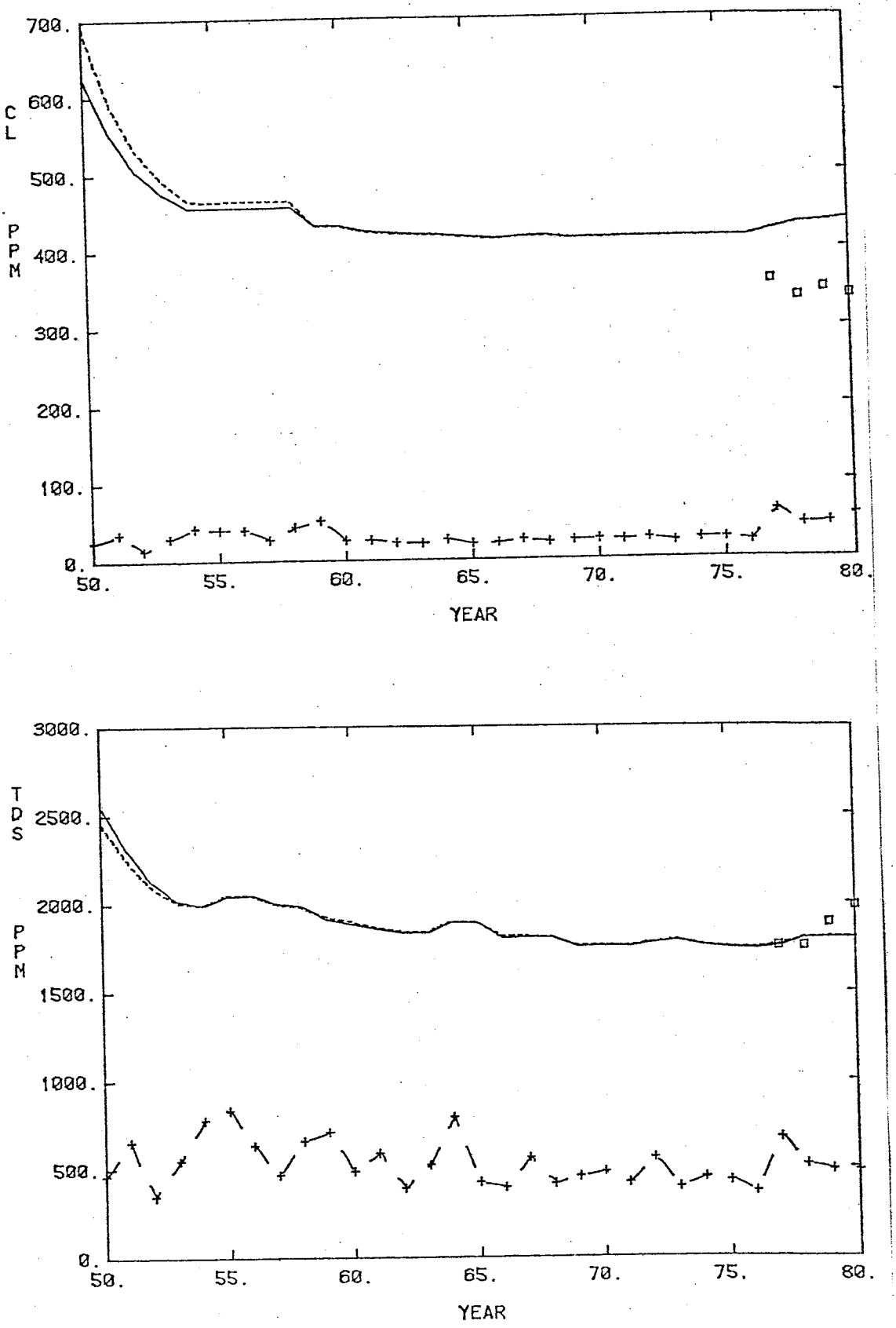

Figure 4.3.3: Simulated Drain Chloride and TDS Concentrations for Soil Analysis (——) and Deep Well Concentrations (---) Initial Conditions; Observed Drain Concentrations (□); and, Irrigation Water Concentrations (-+-).

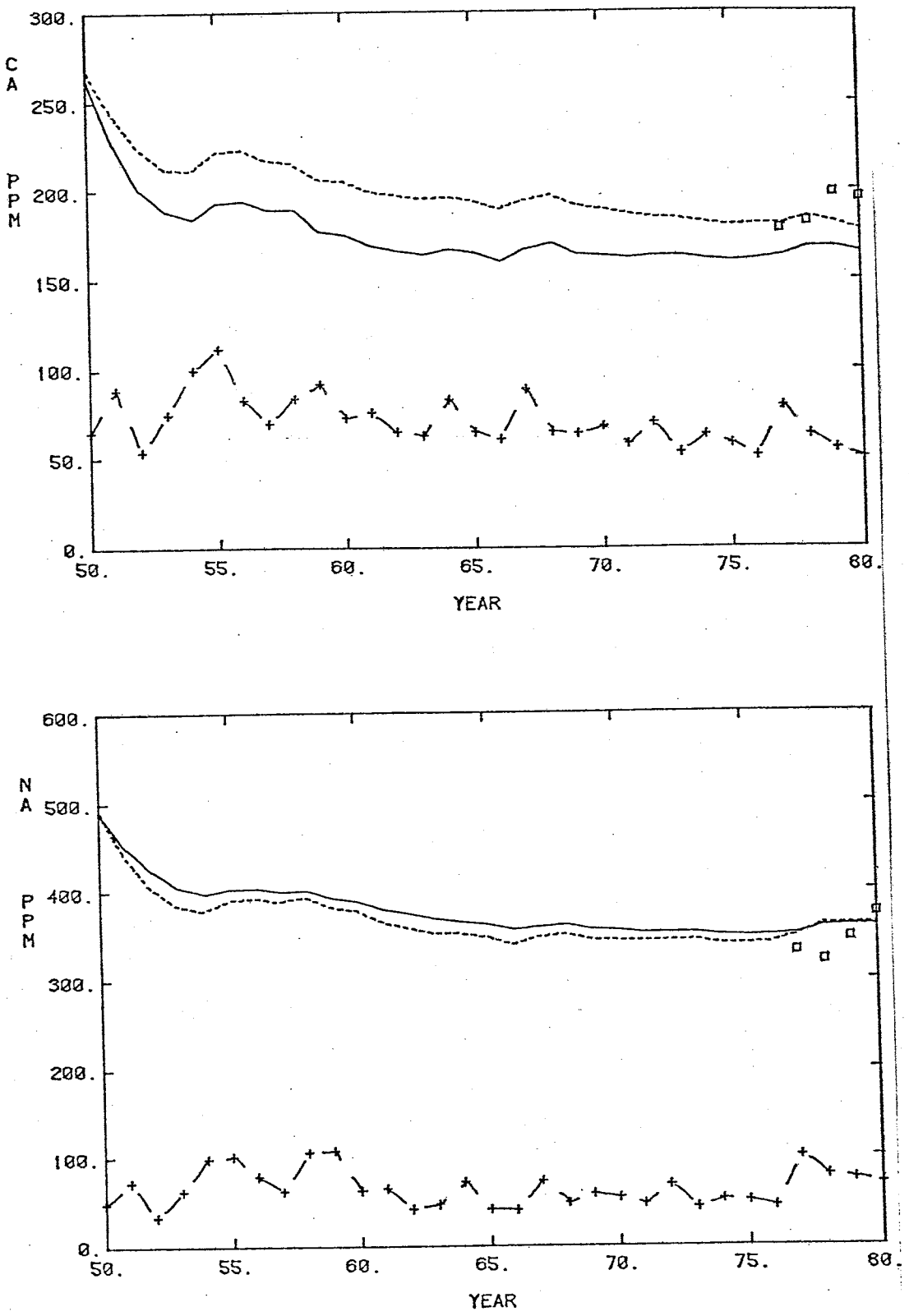

Figure 4.3.4: Simulated Drain Calcium and Sodium Concentrations with (——) and without (---) Chemical Reactions; Observed Drain Concentrations (□); and, Irrigation Water Concentration (-+-).

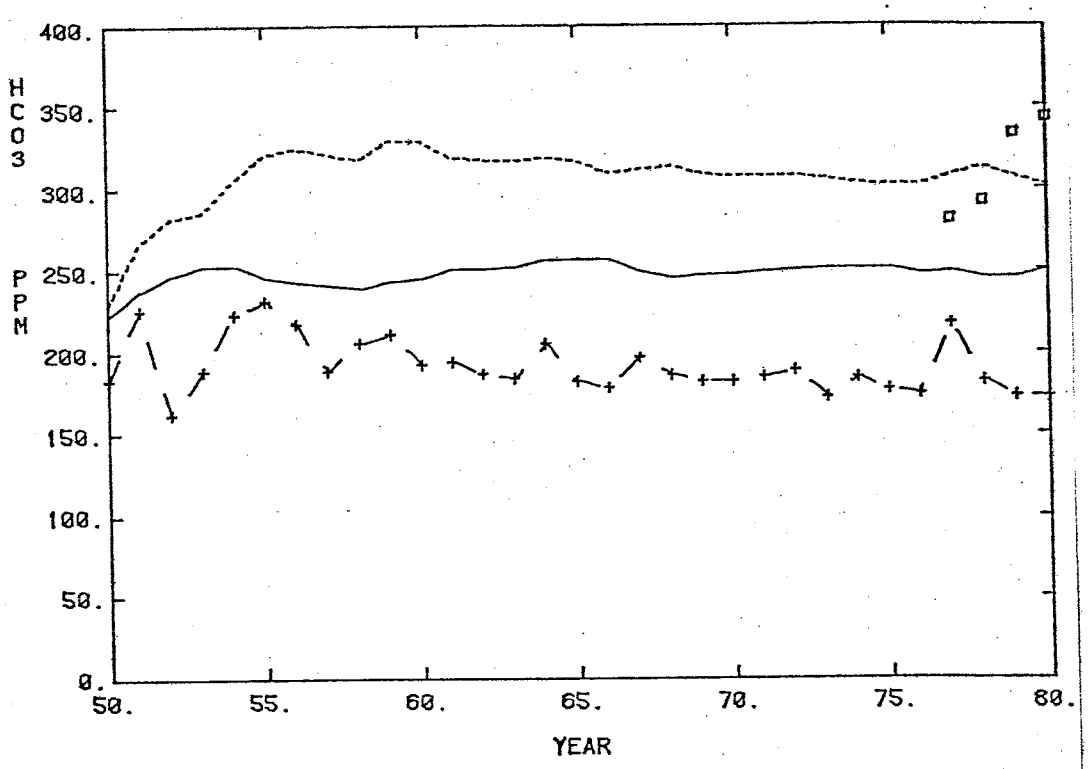

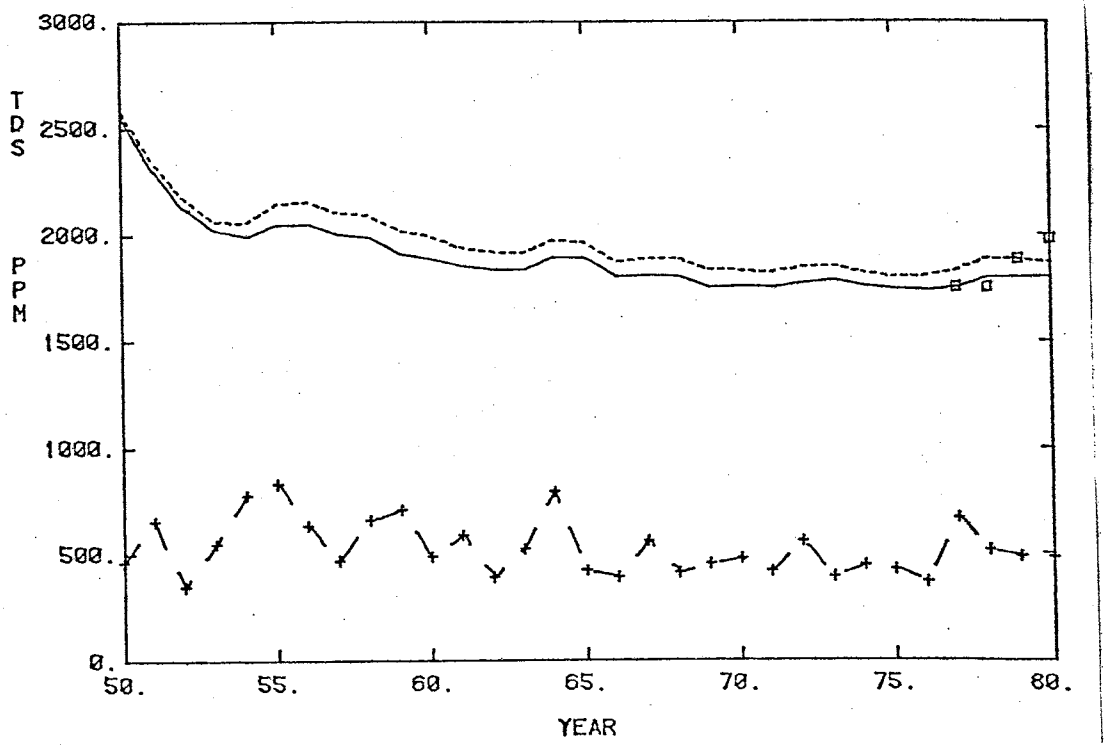

Figure 4.3.5: Simulated Drain Bicarbonate and TDS Concentrations with (——) and without (---) Chemical Reactions; Observed Drain Concentrations (▫); and, Irrigation Water Concentration (-+-).

4.3.2 Transient Simulation

The Saturated Chemistry and Drain Effluent Prediction programs are used here to simulate the transient irrigation system for the period of 1978 through 1980 using a monthly time increment. Drain concentrations are simulated by flow weighting the irrigation system outflow concentrations with regional inflow of the same constant magnitude and quality used in the steady-state simulation. The irrigation stream tube travel times and pore volumes obtained from the steady-state flow model are assumed to apply to the transient flow system as well.

Transient simulations were performed with and without the inclusion of soil-water chemical reactions. The inputs to the Saturated Chemistry and Drain Effluent Prediction programs used in the simulations are listed in Tables 4.3.2 and 4.3.3. The Deep Percolation Data is identical to that used in the transient lumped parameter model simulation, with the irrigation application dates taken as the midpoint of each four week period. The Soil Analysis Data represents the analyses of soil samples from the middle drain borehole averaged over the depth interval of 7 to 24 feet. The monthly irrigation system outflows required by the Drain Effluent Prediction program are assumed equivalent to the amount of irrigation recharge occurring in each month.

The effect of including chemical reactions on simulated drain calcium, sodium, bicarbonate and TDS concentrations is shown in Figures 4.3.6 and 4.3.7. The inclusion of reactions produces minor increases in simulated TDS concentrations due mostly to calcium, sodium and bicarbonate concentration increases.

Drain calcium, sodium, sulfate, bicarbonate, chloride and TDS concentration histories simulated with reactions included are plotted with

Table 4.3.2: Transient Coupled Model Input Data

Saturated Chemistry Program Inputs

Deep Percolation Data

	1978	1979	1980
Number of applications per year	13	12	11
Amount of applied water (ft)	6.59	5.82	5.10
Irrigation efficiency	0.55	0.55	0.50
Specific application data (dates, amounts, chemical analyses)	See Table 4.3.3		

Stream Tube Data

Stream tube pore volumes	listed in Table 4.2.1
Width of each tube at water table	86.67 ft.
Volumetric water content at saturation	0.35
Number of divisions of each tube	24

Soil Analysis Data

Initial soil concentrations (meq/l)

Ca	Mg	Na	NH_4	Cl	SO_4	HCO_3	CO_3	NO_3
6.8	1.3	12.4	0	4.4	14.2	1.9	0.07	0.02

Calcareous soil indicator	on
Gypseous soil indicator	off
Dry bulk density (g/cm^3)	1.72
Soil extract	0.230
Cation exchange capacity (meq/100g)	3.76
Partial pressure CO_2 (atm)	0.012

Table 4.3.2: Transient Coupled Model Input Data (cont.)

Drain Effluent Prediction Program Inputs

Monthly drain discharge data

Month	Drain discharge (acre-ft/acre/month) 1978	1979	1980
1	.007	.021	.011
2	.046	.020	.036
3	.007	0	0
4	.322	.447	.396
5	.414	.197	.133
6	.317	.405	.597
7	.781	.737	.822
8	.333	.302	.355
9	.370	.221	.182
10	.329	.233	0
11	.024	.021	.004
12	.015	.016	.017

Stream tube pore volumes listed in Table 4.2.1

Other inputs obtained from Saturated Chemistry program output.

Table 4.3.3: Specific Surface Application Data

Application Date	Depth (ft)	Applied Water Concentrations* (meq/l) Ca	Mg	Na	HCO_3	CO_3	Cl	SO_4
1-14-78	.016				- 0 -			
2-10-78	.103				- 0 -			
3-10-78	.015				- 0 -			
4-7-78	.715	3.06	0.97	3.72	3.10	0.40	1.49	3.20
5-5-78	.919	3.22	1.03	3.87	2.11	1.22	1.22	3.44
6-2-78	.705	2.46	0.77	2.65	2.20	0.22	0.91	1.83
7-1-78	.956	2.23	0.67	2.03	2.36	0	0.97	1.21
7-28-78	.780	3.78	1.22	4.32	3.60	0.30	1.25	4.27
8-25-78	.741	3.51	1.09	3.95	3.82	0	1.22	3.43
9-22-78	.823	3.27	1.05	3.25	3.15	0.43	1.34	3.18
10-20-78	.730	2.99	0.87	3.76	2.92	0.69	1.49	2.78
11-17-78	.053				- 0 -			
12-15-78	.033				- 0 -			
1-12-79	.046				- 0 -			
2-9-79	.045				- 0 -			
4-6-79	.994	2.32	0.71	2.94	2.96	0	1.10	2.27
5-4-79	.437	1.68	0.56	2.51	1.99	0	1.06	1.43
6-1-79	.900	2.26	0.71	3.00	2.58	0	1.22	2.39
7-1-79	.876	2.16	0.64	3.01	3.52	0	0.75	1.86
7-27-79	.761	1.95	0.57	2.41	2.40	0	1.29	1.80
8-24-79	.671	2.54	0.78	2.67	2.40	0	0.97	3.45
9-21-79	.491	2.98	0.84	2.59	1.19	0	0.85	2.82
10-19-79	.518	2.81	0.85	2.76	3.36	0	1.04	2.54
11-16-79	.047				- 0 -			
12-14-79	.035				- 0 -			
1-11-80	.021				- 0 -			
2-8-80	.072				- 0 -			
4-4-80	.791	3.02	0.92	3.47	2.96	0	1.49	2.99
5-2-80	.265	1.80	0.64	2.36	1.73	0	1.30	2.16
6-1-80	1.193	1.62	0.54	1.92	2.07	0	1.45	1.53
7-1-80	.711	2.04	0.62	2.42	2.46	0	0.85	2.04
7-25-80	.933	2.74	0.82	3.37	3.37	0	1.24	2.88
8-22-80	.709	2.14	0.89	3.10	2.42	0	0.92	2.46
9-19-80	.363	1.58	0.66	2.30	1.80	0	1.11	1.83
11-14-80	.008				- 0 -			
12-12-80	.033				- 0 -			

*Nitrate concentrations ranged from 0.01 to 0.06 meq/l, ammonium concentrations assumed zero.

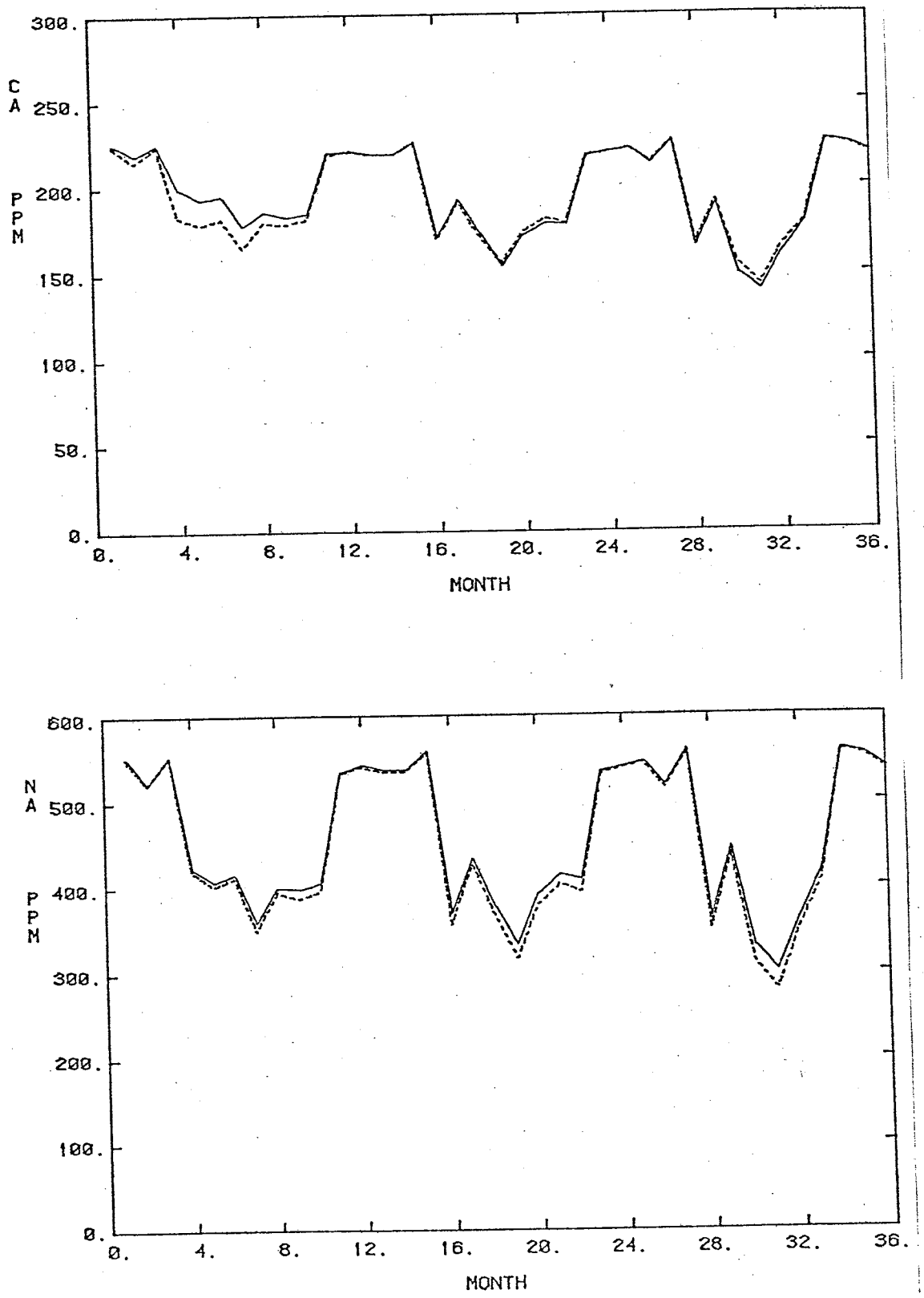

Figure 4.3.6: Simulated Drain Calcium and Sodium Concentrations with (——) and without (---) Chemical Reactions.

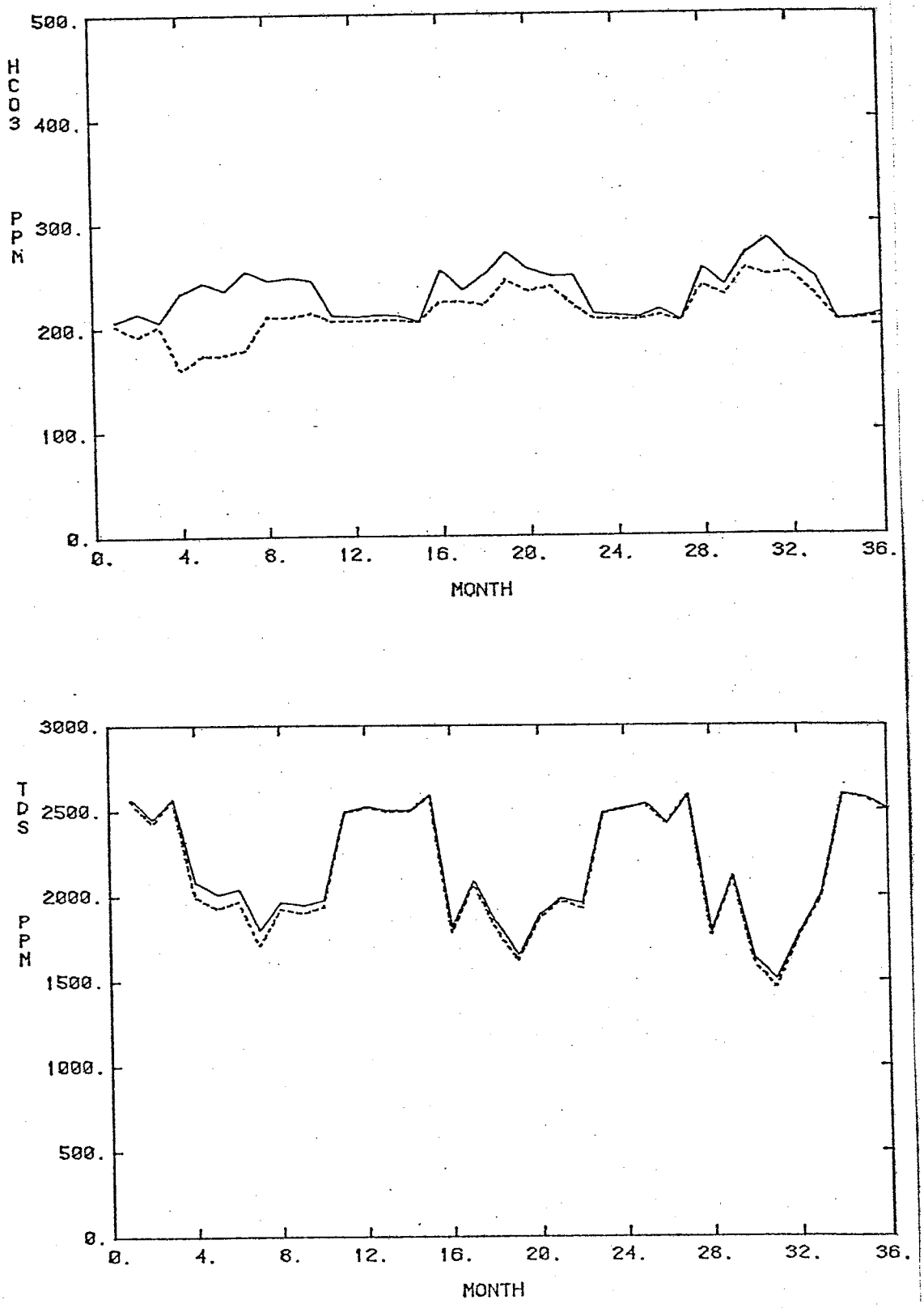

Figure 4.3.7: Simulated Drain Bicarbonate and TDS Concentrations with (——) and without (---) Chemical Reactions.

observed drain concentrations in Figures 4.3.8 through 4.3.10. In general, simulated drain concentrations display better agreement during irrigation seasons than during the winter months. This trend is also seen in the simulated mass output histories for these six constituents as shown in Figures 4.3.11 through 4.3.13. The winter month disagreement is due to the assumption that drain flow is composed mostly of high concentration regional inflow during the months of little surficial recharge. Regional flow was assumed to enter the aquifer through the base and flow to the drain without any change in concentration. In reality, regional flow probably enters the farm laterally and is partially intercepted by the drain. The application of irrigation water during summer months would suppress this lateral movement in the upper layer as depicted by the upper layer of the flow net in Figure 4.2.2. During winter months, lateral inflow would produce drain flow components of regional inflow quality from the lower layer and resident irrigation recharge quality from the upper layer. The relative magnitudes of the drain flow components would be dictated by the transmissivities of the layers.

To simulate lateral regional inflow during the winter months the aquifer will be considered to function as the two layered system defined in the transient lumped parameter model application (section 3.3.2). The drain concentration for this system is calculated by flow weighting the outflow concentrations of the two layers according to

$$C_d = \frac{T_1 q_r C_1 + T_2 q_r C_2}{(T_1 + T_2) q_r}$$

where T_1 and T_2 are the upper and lower layer transmissivities, C_1 and C_2 are the concentrations in the upper and lower layers, and q_r is the

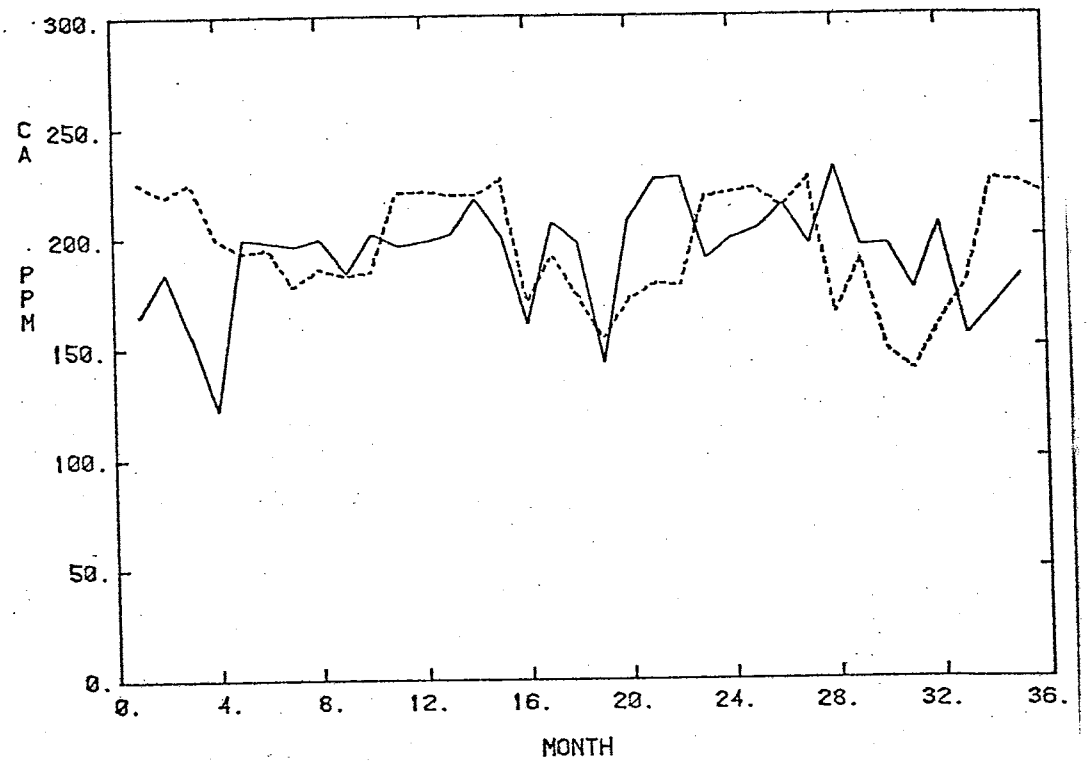

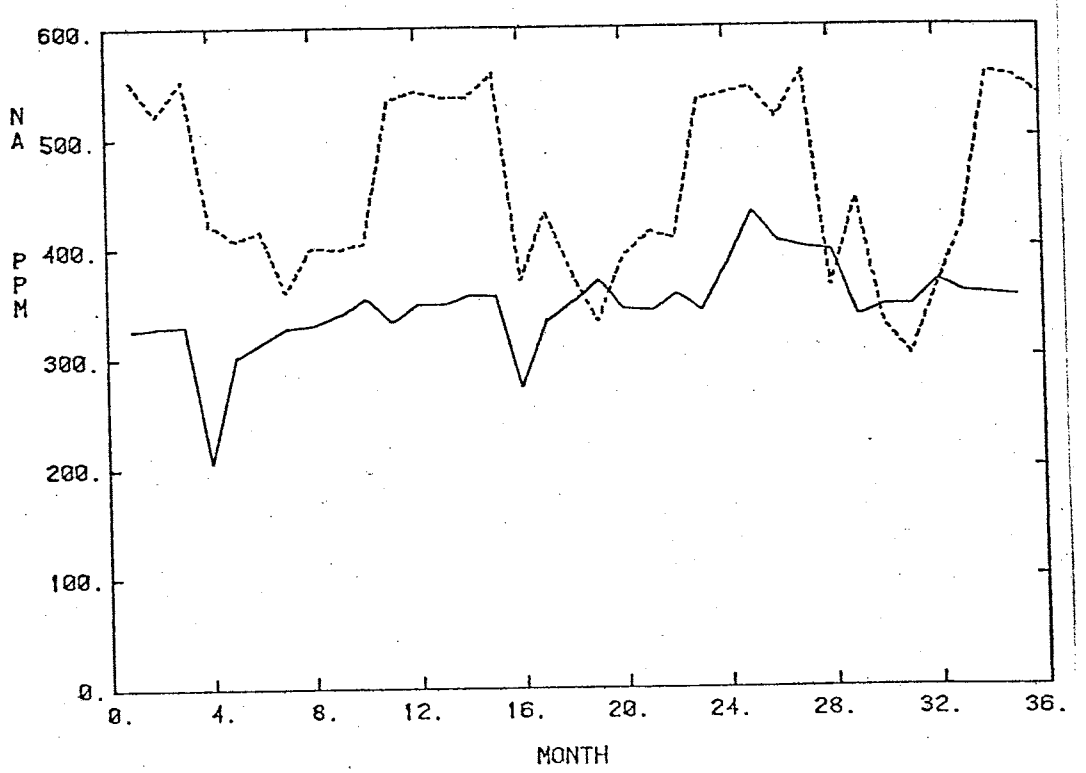

Figure 4.3.8: Simulated (---) and Observed (——) Drain Calcium and Sodium Concentrations.

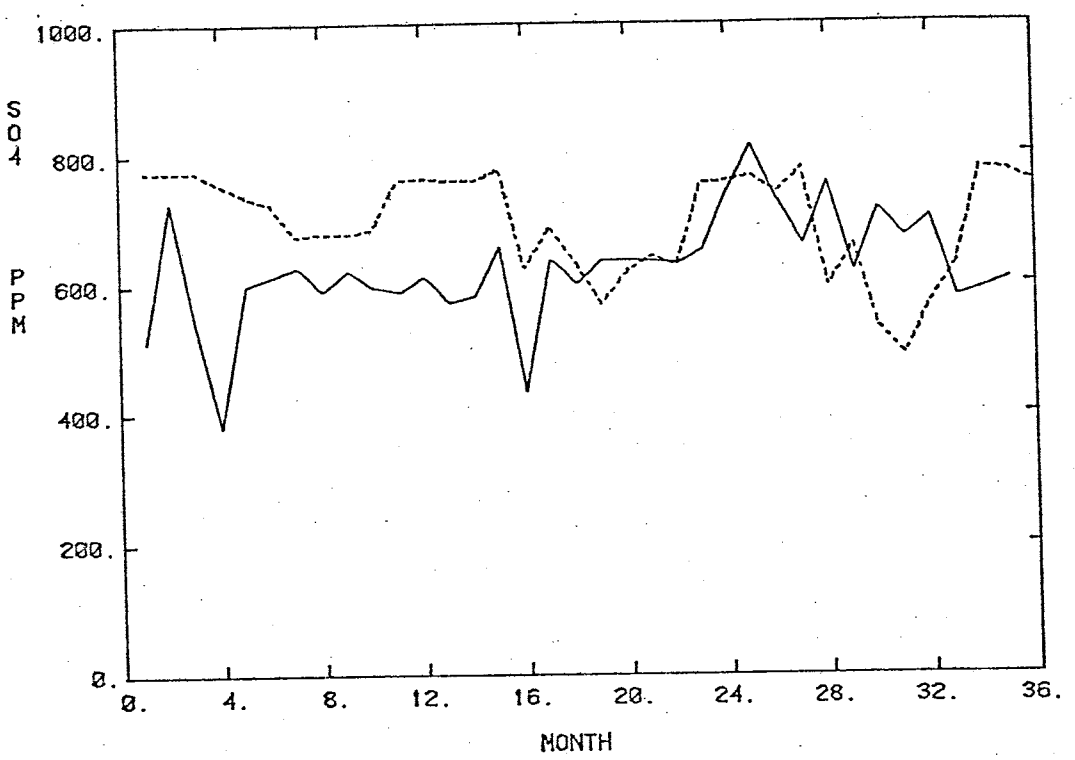

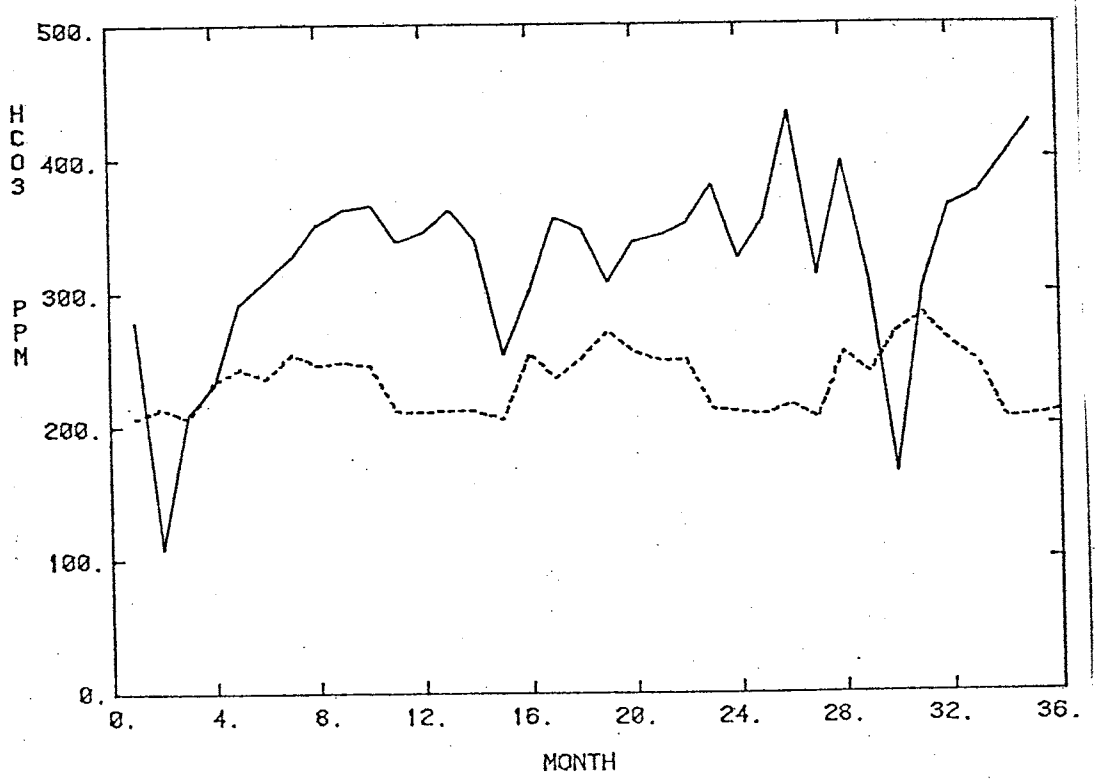

Figure 4.3.9: Simulated (---) and Observed (——) Drain Sulfate and Bicarbonate Concentrations.

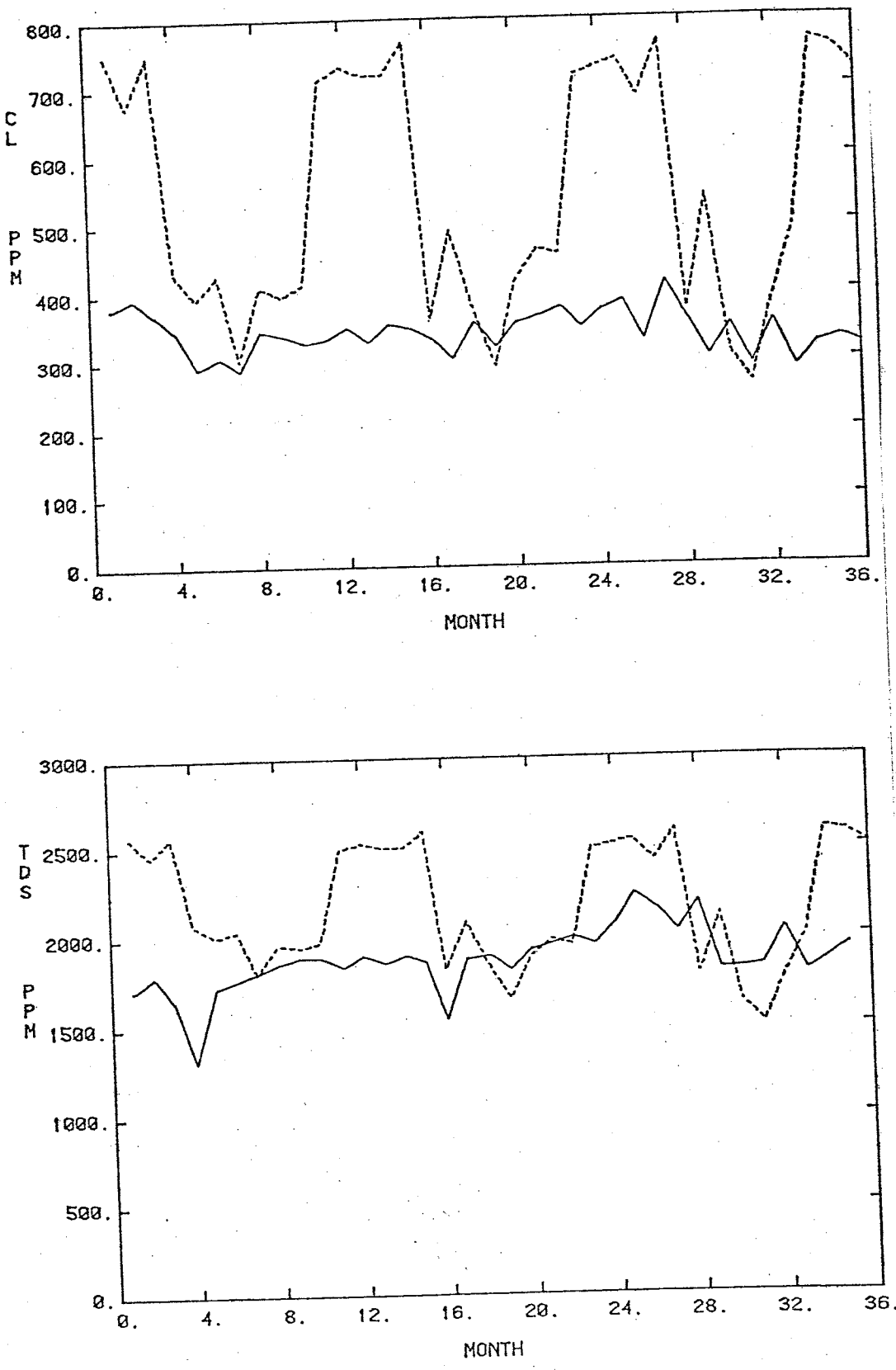

Figure 4.3.10: Simulated (---) and Observed (——) Drain Chloride and TDS Concentrations.

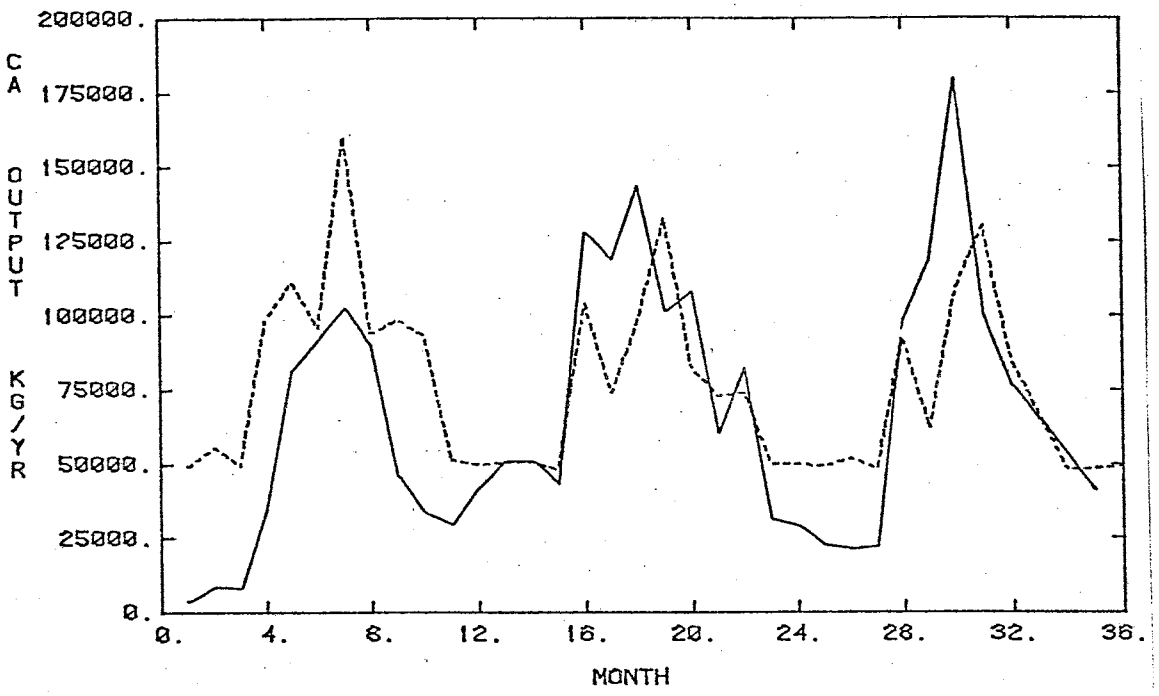

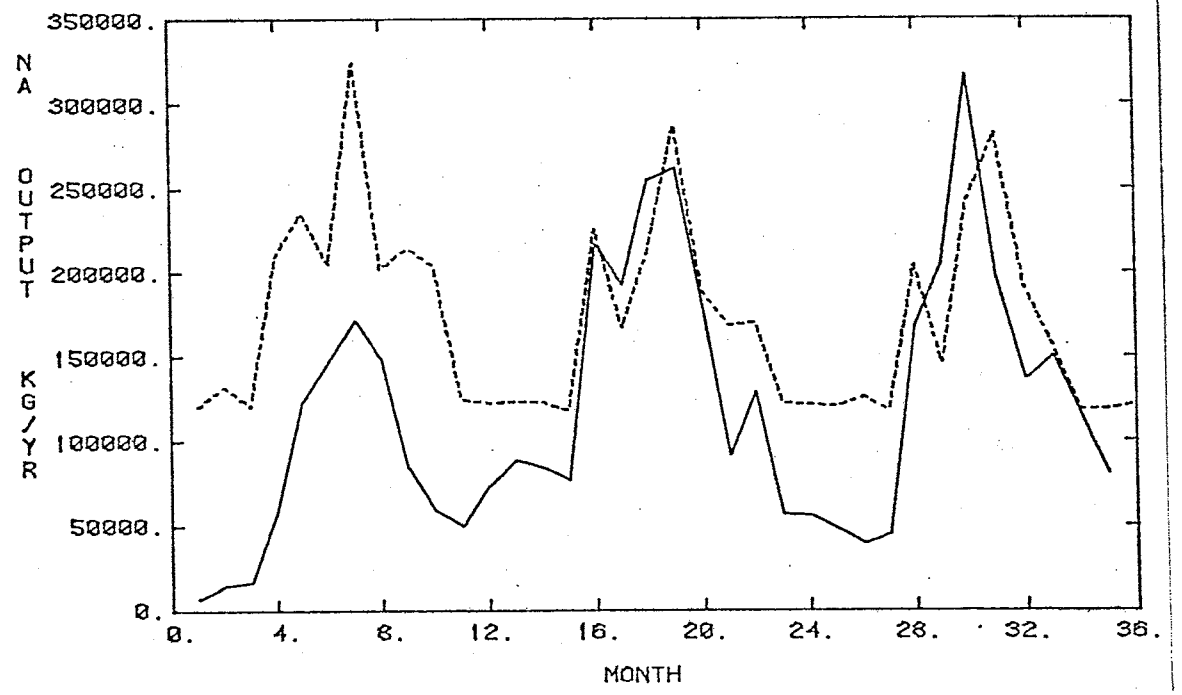

Figure 4.3.11: Simulated (---) and Observed (——) Mass Output of Calcium and Sodium.

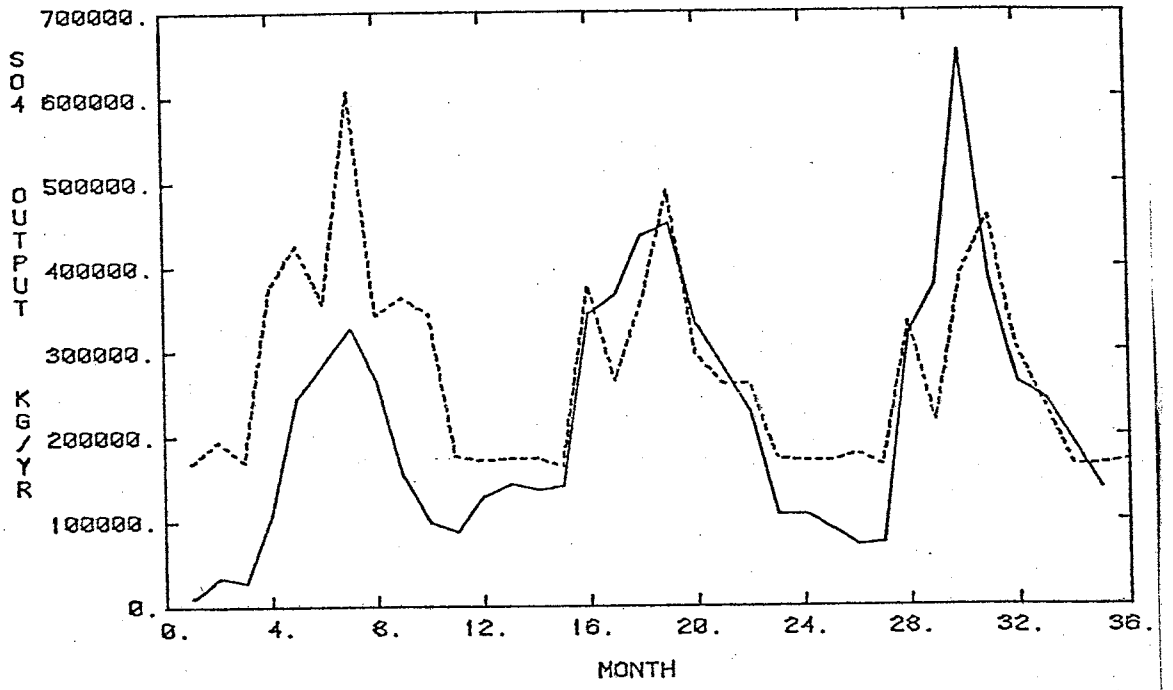

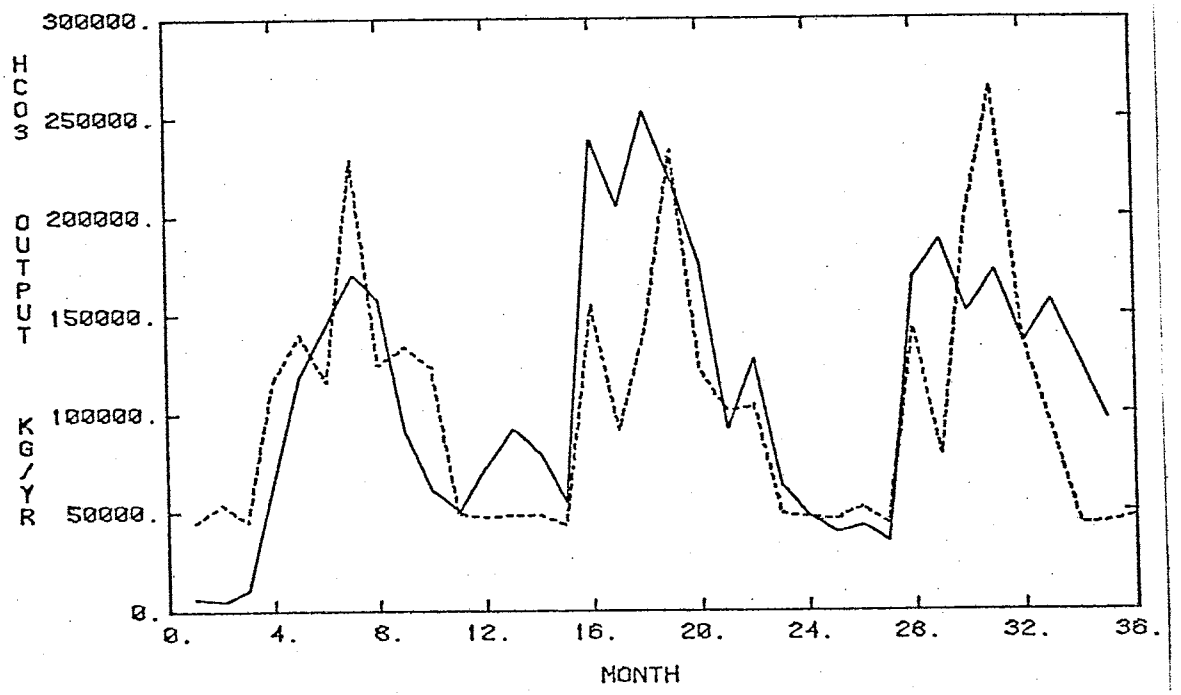

Figure 4.3.12: Simulated (---) and Observed (——) Mass Output of Sulfate and Bicarbonate.

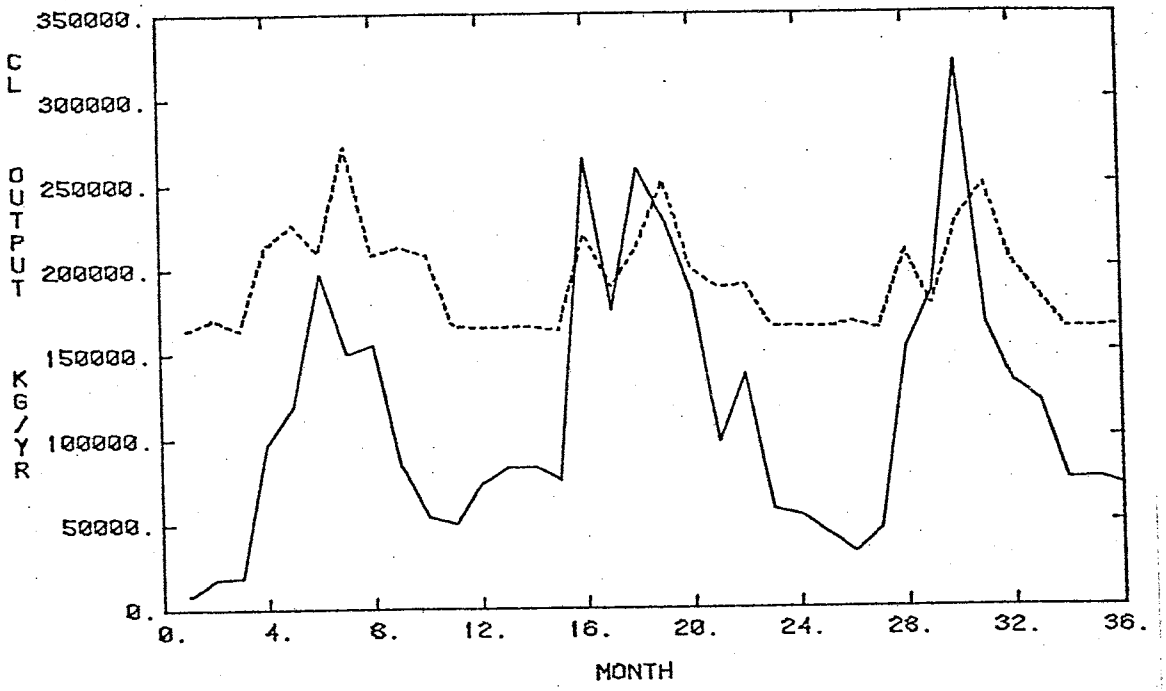

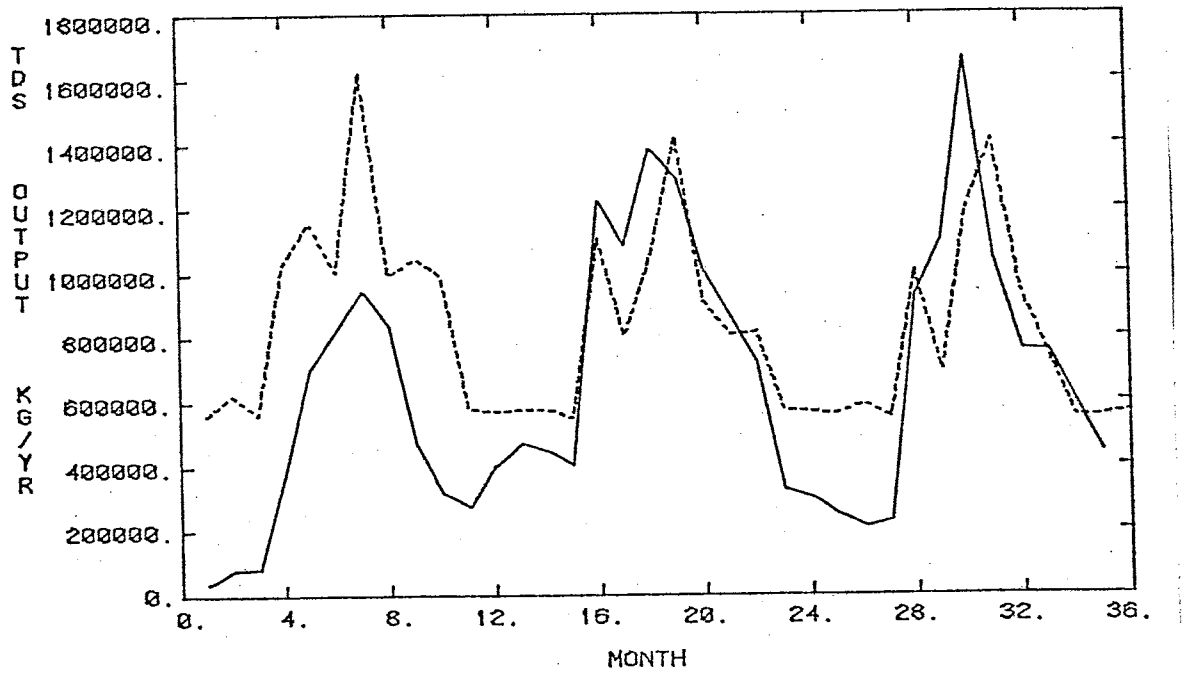

Figure 4.3.13: Simulated (---) and Observed (——) Mass Output of Chloride and TDS.

regional inflow rate. Recalling the upper to lower layer conductivity ratio of 10 and the upper and lower layer thicknesses of 20 and 45 feet used in the lumped parameter model, the equation above becomes

$$C_d = 0.82C_1 + 0.18C_2$$

The upper layer concentration for each winter month is assumed to be the irrigation system outflow concentration during the last month of the irrigation season as simulated by the Drain Effluent Prediction program. This produces the effect of displacing resident irrigation recharge laterally into the drain. The lower layer concentration is assumed equal to the regional inflow concentration. The simulated drain concentrations and mass output histories of chloride and TDS shown in Figures 4.3.14 and 4.3.15 were obtained using this method to compute winter drain concentrations. In this case it is noted that winter drain concentrations are lower than observed. However, the simulated and observed mass output histories display good winter month agreement indicating an overestimate of winter drain flow.

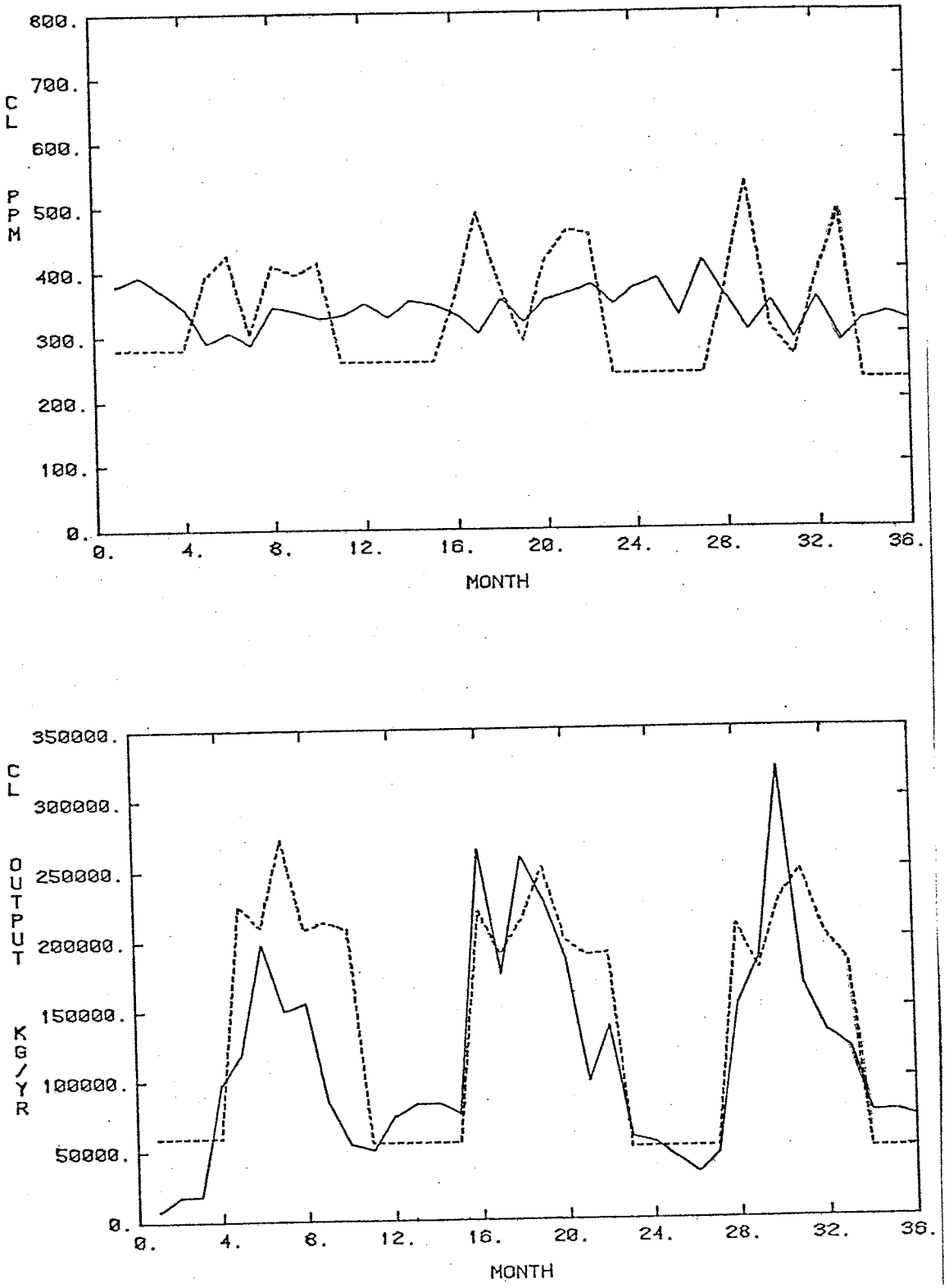

Figure 4.3.14: Observed (——) and Simulated (---) Chloride Concentration and Mass Output Histories with Lateral Winter Month Regional Inflow.

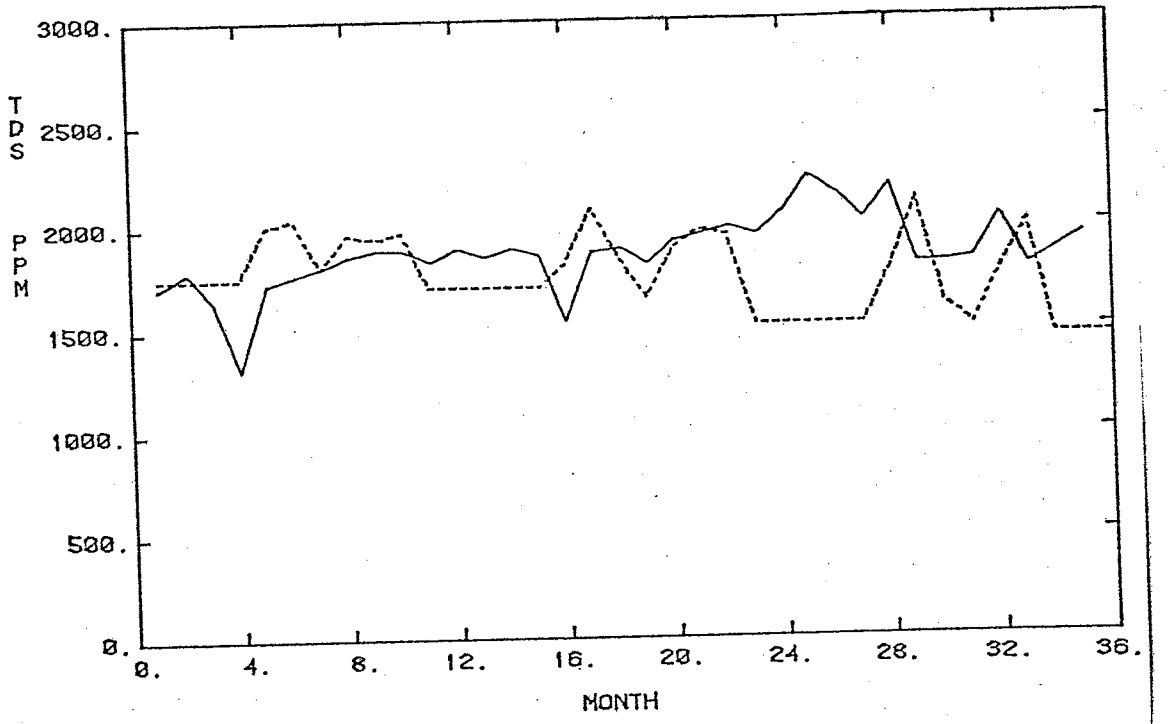

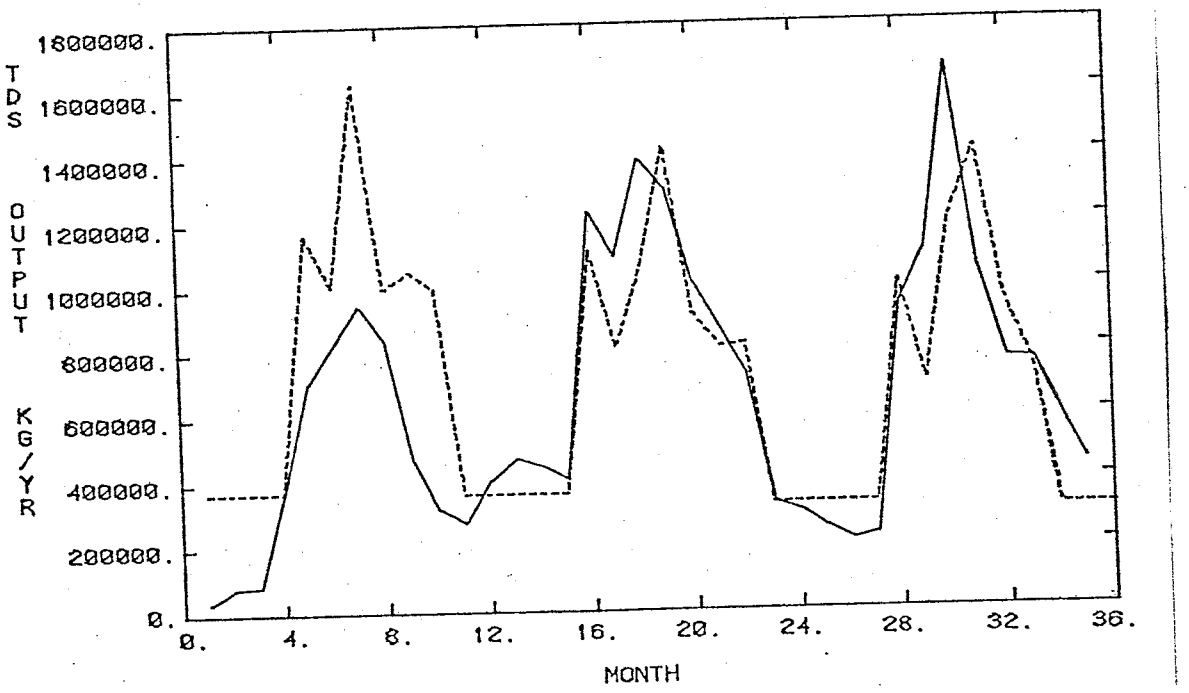

Figure 4.3.15: Observed (——) and Simulated (---) TDS Concentration and Mass Output Histories with Lateral Winter Month Regional Inflow.

4.4 DISCUSSION

The Bureau of Reclamation chemistry model is designed to simulate the outflow concentrations of an irrigated aquifer given an initial soil analysis and the nature of the irrigation water inputs. In order to apply this model to the San Acacia farm it was necessary to define a flushing irrigation system which behaves independently of the regional flow system. This was accomplished by constructing a steady-state flow net of the aquifer receiving equal regional and irrigation recharge, and assigning the irrigation system to the stream tubes conveying only irrigation recharge. Drain concentrations were simulated by mixing the predicted irrigation system outflow with the regional inflow.

Simulation results imply this modeling scheme does not accurately represent the dynamics of the transient system. Results obtained by assuming lateral regional inflow indicate the regional and irrigation flow systems do not behave independently. Rather, during periods of little surficial recharge, high concentration regional flow enters the irrigation system forcing resident irrigation recharge into the drain and violating the flushing irrigation system assumption. By virtue of design, the coupled model presented here is incapable of simulating this complex relation between the irrigation system and regional inflow. The assumption of a constant regional inflow rate is also inappropriate for the transient system as indicated by the water balance results of the lumped parameter model study (section 3.3.3). The constant regional inflow rate of 2.9 ft/yr used in the coupled model simulations overestimates the amount entering the farm during 1978 thus producing higher simulated mass output rates than observed during that year.

In both the transient and steady simulations, the inclusion of soil-

water chemical reactions only produced significant changes in simulated calcium and bicarbonate concentrations. It is difficult to determine whether these reactions are indicative of the real system since they are assumed to occur in a flushing irrigation system isolated from the regional inflow. The flow of poor quality regional water into the irrigation system during winter months is expected to effect the possible reactions involving nonconservative constituents. The transient behavior of the regional inflow may be ignored in the steady-state simulation of conservative constituents since yearly average drain concentrations are considered. Under steady flow conditions, the yearly average drain concentration of a conservative element is simply a mixture of the regional inflow and irrigation system outflow concentrations. Whether this mixing is considered to occur in the drain or seasonally within the aquifer is inconsequential.

The steady-state simulation results display fair agreement with observed drain concentrations when all constituents are treated as nonreactive. This agreement appears to be independent of the initial soil analysis or groundwater composition. The dominant factor controlling the simulated drain concentrations is the magnitude and quality of the regional inflow. If poor quality regional flow was not entering the system, simulated drain concentrations would fall to the level of the irrigation recharge concentrations after the year 1958. Based on the steady simulation results it was concluded that the average concentrations observed in the three wells at depths of 50 to 65 feet are somewhat indicative of the regional inflow quality. The average TDS concentration of about 2600 ppm observed in these wells was used as the regional inflow TDS concentration. The average irrigation water TDS concentration for the monitored

period is 543 ppm implying an irrigation recharge concentration of roughly 1100 ppm. The assumption of equal regional and irrigation recharge rates would thus imply regional inflow is responsible for about 70 percent of the total mass output from the system.

5. SUMMARY AND CONCLUSIONS

Two modeling approaches were used in this study to determine the characteristics of the middle drain flow system at the San Acacia farm. The first approach employed multiple celled lumped parameter models, and the second consisted of a profile finite element flow model coupled with the U. S. Bureau of Reclamation chemistry model. The results of the modeling studies indicate the mixing process producing observed drain concentrations involves a complex transient relationship between the irrigation recharge and a poor quality regional inflow.

The drain chloride concentrations and mass outputs simulated with the transient two cell lumped parameter model displayed good agreement with observed values. This model appears to adequately represent the middle drain flow system. The advantages of using the lumped parameter model are its ease of generalization, minor input requirements, and inexpensive computer simulation costs. The disadvantages of the model presented in this study include the inability to simulate soil-water chemical reactions involving nonconservative constituents, and limited predictive capabilities due to the required input of the transient drain flow.

To apply the coupled finite element flow- Bureau of Reclamation chemistry model it was necessary to divide the aquifer into separate irrigation and regional flow systems. Simulation results indicate this separate treatment of the regional and irrigation inflow components does not accurately represent the transient system. However, this approach does produce good agreement between observed simulated drain concentrations in the steady-state case. This is attributed to the assumption that the transient behavior of the regional and irrigation recharge does not influence yearly average drain concentrations.

The following general conclusions are drawn from this study of the middle drain flow system at the San Acacia farm:

(1) A transient regional inflow of poor quality water contributes to the flow of the middle drain.

   a) For the period of 1978 through 1980, the average regional inflow and irrigation recharge rates are nearly equal.

   b) The quality of the regional inflow is similar to that observed in the three wells at depths of 50 to 65 feet.

   c) The regional inflow component is responsible for roughly 70 percent of the total mass output from the system.

(2) Separation of the irrigation impact on water quality is difficult in this regionally dominated system.

(3) An effective porosity of 0.30 to 0.35 is representative of the alluvial aquifer at the San Acacia farm.

APPENDIX

Detailed Description of Effective Porosity Tests

A cross section of the apparatus used for the effective porosity determinations is shown in Figure A1. The sleeve (5 cm in diameter and 5.1 cm in length) and collar are part of the Eijkelkamp permeameter equipment, and the lucite base was designed specifically for the experiments. The total base storage was computed to be approximately 1 ml from the lucite base and release valve specifications.

After the base and collar are affixed, the sample is saturated by adding tap water through the release valve. The sample is then flushed with tap water until the electrical conductivity of the effluent is identical to the input water (between 330 and 350 μmhos). Electrical conductivities were measured with a portable HACH conductivity meter. Distilled water was used for flushing purposes in preliminary tests but was noted to have a corrosive effect on the sample as indicated by persistently higher effluent than input conductivities.

The tracer solution used in the tests possessed and electrical conductivity around 2000 μmhos, a level obtained by dissolving NaCl crystals in tap water. A 10 ml slug of the tracer is placed on top of the sample, afterwhich an equivalent volume is removed through the release valve to bring the slug into the sample. The slug is displaced through the sample by adding tap water at the top and releasing successive 2 ml effluent volumes. Due to the physical characteristics of the conductivity probe, 8 ml of tap water was added to each 2 ml effluent sample in order to obtain a sample of sufficient volume to be analyzed for electrical conductivity. The conductivity of each 2 ml sample, σ, is found from the relation

$$(10\ \text{ml})\ \sigma' = (2\ \text{ml})\ \sigma + (8\ \text{ml})\ \sigma_0$$

or

$$\sigma = 5\sigma' - 4\sigma_0$$

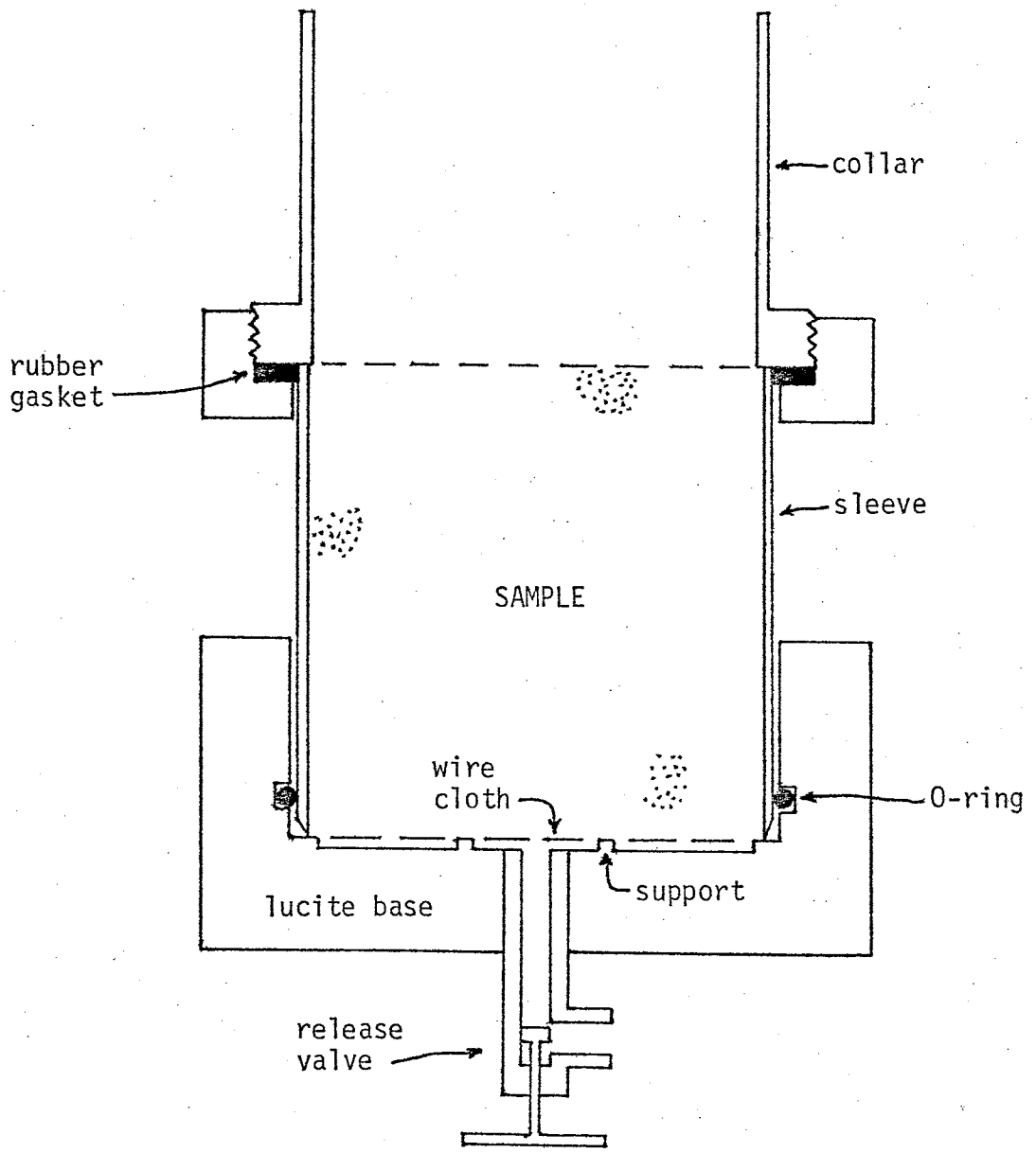

Figure A1: Effective Porosity Test Apparatus.

where σ_0 is the tap water conductivity and σ' is the measured conductivity of the 10 ml diluted sample. Assuming the peak conductivity occurs at the mean position of the tracer slug as it is displaced through the sample, the first moment of the conductivity versus eluted volume breakthrough curve represents the effective pore volume of the sample plus 6 cm^3 (one half the slug volume plus the base storage). The effective pore volume of the sample is thus computed as

$$V_p = \frac{\Sigma(\sigma_i-\sigma_0)V_i}{\Sigma(\sigma_i-\sigma_0)} - 6\ cm^3 \qquad (A.1)$$

where σ_i is the conductivity of sample i and V_i is the total eluted volume including sample i. The effective pore volume is equivalent to the effective porosity percentage since the sample bulk volume is 100 cm^3.

As a specific example, the effective porosity test data for sample number 3 is listed in Table A1 and the corresponding breakthrough curve is shown in Figure A2. The conductivity of the tracer slug was 1920 μmhos and the tap water used for flushing and dilution possessed a conductivity of 340 μmhos. The expected effective pore volume computed from equation (A.1) is 38.9 cm^3, and the effective pore volume indicated by the maximum conductivity is 38 ± 1 cm^3.

Table A1: Effective Porosity Test Data for Sample 3

Effluent Sample No.	Total Eluted Volume (cm^3)	Diluted Conductivity σ'(μmhos)	Sample Conductivity σ(μmhos)
1	10	340	340
2	12	340	340
3	14	340	340
4	16	340	340
5	18	340	340
6	20	345	365
7	22	350	390
8	24	350	390
9	26	355	415
10	28	360	440
11	30	360	440
12	32	375	515
13	34	400	640
14	36	430	790
15	38	460	940
16	40	480	1040
17	42	495	1115
18	44	500	1140
19	46	480	1040
20	48	460	940
21	50	440	840
22	52	420	740
23	54	400	640
24	56	380	540
25	58	375	515
26	60	375	515
27	62	360	440
28	64	355	415
29	66	350	390
30	68	350	390
31	70	350	390
32	72	350	390
33	74	350	390

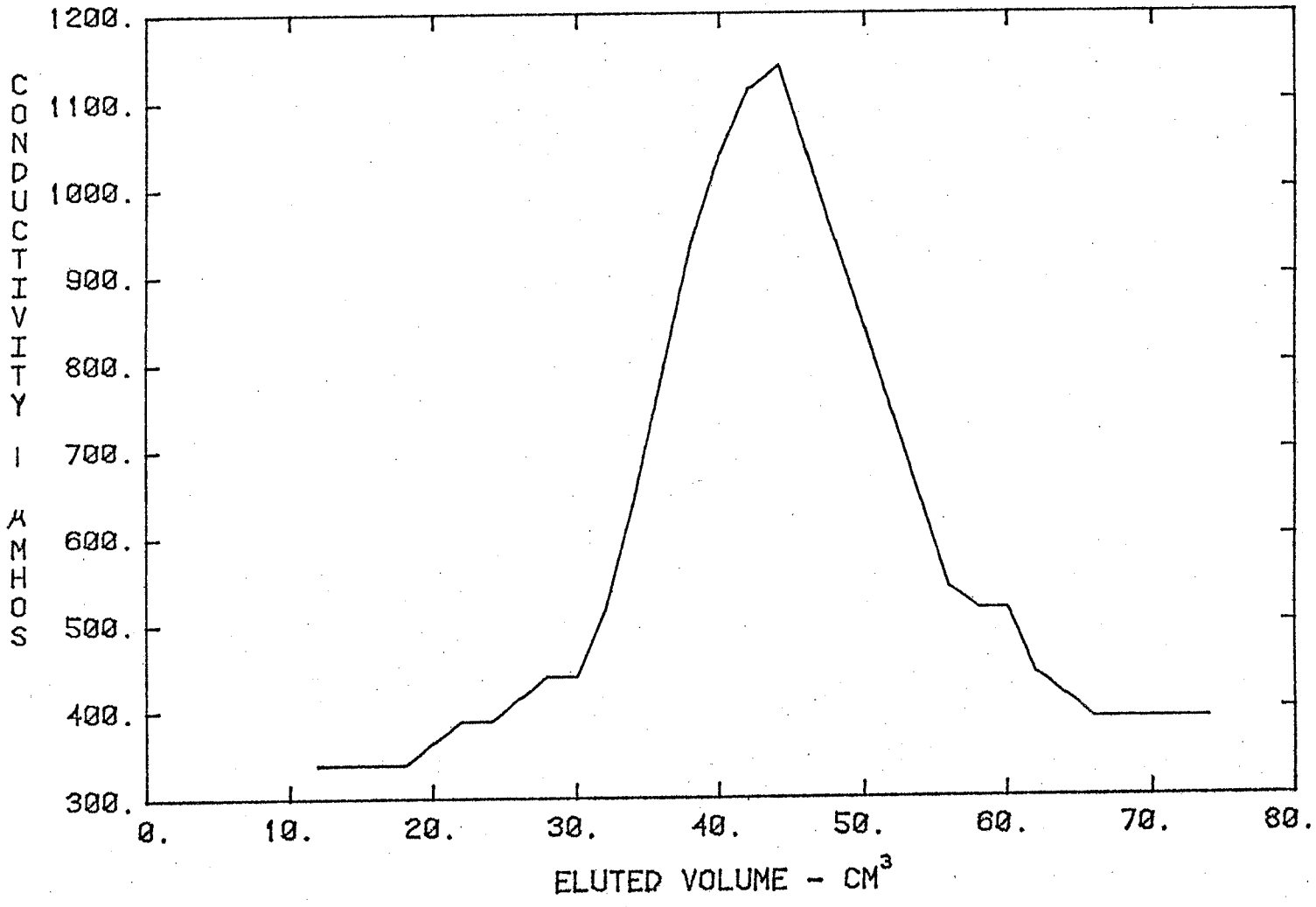

Figure A2: Conductivity Breakthrough Curve for Sample 3.

REFERENCES

Bear, J., 1972, Dynamics of Fluids in Porous Media: Elsevier, New York, 764p.

Fried, J. J., 1975, Groundwater Pollution: Elsevier, Amsterdam, 330p.

Gelhar, L. W., P. J. Wierenga, C. J. Duffy, K. R. Rehfeldt, R. B. Senn, M. Simonett, T-C. Yeh, A. L. Gutjahr, W. R. Strong, and A. Bustamante, 1980, Irrigation Return Flow Studies at San Acacia, New Mexico: Monitoring, Modeling and Variability: Hyd. Res. Program Tech. Progress Rpt., N.M.I.M.T.

Gelhar, L. W. and J. L. Wilson, 1974, Groundwater Quality Modeling: Ground Water, 12(6), p. 399-408.

Konikow, L. F., 1977, Modeling Chloride Movement in the Alluvial Aquifer at the Rocky Mountain Arsenal, Colorado: U.S.G.S. Water Supply Paper 2044.

Konikow, L. F. and J. D. Bredeheoft, 1974, Modeling Flow and Chemical Quality Changes in an Irrigated Stream-Aquifer System: Water Resour. Res., 10(3), p. 546-562.

McLin, S. G., 1981, Ph.D. dissertation in progress: N.M.I.M.T.

Meinzer, O. C., 1923, Outline of Ground-Water Hydrology, with Definition: U.S.G.S. Water Supply Paper 779.

Papadopulos, S. S. and S. P. Larson, 1978, Aquifer Storage of Heated Water, II. Numerical Simulation of Field Results: Ground Water, 16(4), p. 242-248.

Pinder, G. F., 1973, A Galerkin - Finite Element Simulation of Groundwater Contamination of Long Island: Water Resour. Res., 9(6), p. 1657-1669.

Pinder, G. F. and W. G. Gray, 1977, Finite Element Simulation in Surface and Subsurface Hydrology: Academic Press, New York, 295p., p. 123-124.

Robson, S. G., 1978, Application of Digital Profile Modeling Techniques to Ground-Water Solute Transport at Barstow, California: U.S.G.S. Water Supply Paper 2050.

Shaffer, M. J., R. W. Ribbens, and C. W. Huntley, 1977, Prediction of Mineral Quality of Irrigation Return Flow, Volume V, Detailed Return Flow Salinity and Nutrient Simulation Model: U.S. Environmental Protection Agency, Ada, Oklahoma, 400p.

Spiegel, Z., 1955, Geology and Ground- Water Resources of Northeastern Socorro County, New Mexico: N.M. Bureau of Mines and Mineral Resources Groundwater Rpt. 4.

Wierenga, P. J., C. J. Duffy, R. Kselik, R. Senn, and W. Strong, 1979, Impacts of Irrigated Agriculture on Water Quality in the Rio Grande Below Albuquerque: Eng. Exp. Station Rpt., N.M.S.U.